JOURNAL OF THE AERONAUTICAL SCIENCES

VOLUME 22 APRIL, 1955 NUMBER 4

CONTENTS

Aerodynamics of a Rectangular Plate with Vortex Separation in Supersonic Flow.....H. K. CHENG 217

The Difference Property of the Kernel of the Unsteady Lifting Surface Theory.....H. G. KUESSNER 227

The Generalized Shock-Expansion Method and Its Application to Bodies Traveling at High Supersonic Air Speeds.....A. J. EGGERS, JR., RAYMOND C. SAVIN, AND CLARENCE A. SYVERTSON 231

The Lift and Moment on a Ring Concentric to a Cylindrical Body in Supersonic Flow.....F. EDWARD EHLERS 239

The Application of Finite Difference Methods to Boundary-Layer Type Flows.....W. T. ROULEAU AND J. F. OSTERLE 249

A Provisional Analysis of Turbulent Boundary Layers with Injection.....JOSEPH H. CLARKE, HANS R. MENKES, AND PAUL A. LIBBY 255

On Supersonic Flow Past a Finite Wedge at the Crocco Mach Number.....KŌ TAMADA AND YOSHIO SHIBAOKA 261

Effect of Large Deflections and Initial Imperfections on the Buckling of Cylindrical Shells Subject to Hydrostatic Pressure.....WILLIAM A. NASH 264

Readers' Forum: "The Second-Order Thin Airfoil Theory for Compressible Flow," by Isao Imai; "Wedge Pressure Coefficients in Transonic Flow by Hydraulic Analogy," by Richard G. Fleddermann and Robert T. Stancil; "A Dust Method for Locating the Separation Point," by A. M. O. Smith and J. S. Murphy; "Equations for the Chordwise Center of Pressure for the Basic Twist Distributions on Triangular Wings Having Supersonic Leading and Trailing Edges," by R. N. Haskell, J. J. Hosek, and W. S. Johnson, Jr.; "Conditions for the Appearance of Shock Waves in Steady Flows," by Raymond Marchal; "Matrix Method of Coupling Shear Flexibility and Rotatory Inertia in Bending Vibration," by Marvin Stern; "Equations for Loading on Triangular Wings Having Subsonic Leading Edges Due to Various Basic Antisymmetric Twist Distributions," by R. N. Haskell and W. S. Johnson, Jr.; "Buckling Loads for Beams of Variable Cross Section Under Combined Loads," by B. E. Gatewood; "Further Comments on 'Note on Boundary-Layer Transition in Supersonic Flow,'" by A. H. Lange and R. E. Lee; "An Approximate Relationship Between Small Radius Ratio Turbine Passage Geometry and Radial Pressure Variation," by J. P. Fraser; "On the Determination of Local Heat-Transfer Coefficients for Bodies with Pressure Gradient in Supersonic Flow," by Irving Korobkin; "Second-Order Pressure Law for Two-Dimensional Compressible Flow," by Wallace D. Hayes; "Brachistocronic Maneuvers of a Constant Mass Aircraft in a Vertical Plane," by Placido Cicala and Angelo Miele.....270–288

Published by

INSTITUTE OF THE AERONAUTICAL SCIENCES, INC.

JOURNAL OF THE AERONAUTICAL SCIENCES

SUBSCRIPTION RATES

JOURNAL OF THE AERONAUTICAL SCIENCES, Published Monthly.—United States and Possessions: 1 Year, $12.00; Single Copies, $1.50. Foreign Countries Including Canada (American Currency Rates): 1 Year, $13.00; Single Copies, $1.50.

AERONAUTICAL ENGINEERING REVIEW, Published Monthly.—United States and Possessions: 1 Year, $3.00; Single Copies, $0.50. Foreign Countries Including Canada (American Currency Rates): 1 Year, $3.50; Single Copies, $0.50.

Notices of change of address should be sent to the Institute at least 30 days prior to actual change of address.

Manuscripts for publication, proofs, and all correspondence should be addressed to the Editorial Office of the JOURNAL.

Correspondence regarding subscriptions may be addressed to Publication Office, 20th and Northampton Sts., Easton, Pa., or to the Editorial Office of the JOURNAL OF THE AERONAUTICAL SCIENCES, 2 East 64th Street, New York 21, N.Y.

Entered as Second Class Matter at the Post Office, Easton, Pa., May 1, 1937. Acceptance for mailing at a special rate of Postage provided for in the Act of August 24, 1912. Authorized April 29, 1937.

JOURNAL OF THE AERONAUTICAL SCIENCES

VOLUME 22 APRIL, 1955 NUMBER 4

Aerodynamics of a Rectangular Plate with Vortex Separation in Supersonic Flow*

H. K. CHENG†

Bell Aircraft Corporation

ABSTRACT

A solution is obtained for the supersonic flow field in the tip region of a rectangular flat plate, in which the phenomenon of vortex separation from the side-edge is approximated by introducing into the analytic flow field a ray of singularity possessing the vortex behavior. The strength and the location of the vortex singularity, and thus the solution, are determined by imposing additional conditions to the problem, namely, (1) that the flow velocity around the edge be bounded, and (2) that the vortex system be dynamically free.

The mathematical model employed in describing the vortex separation phenomenon is essentially the same as that used in the treatment of the leading-edge separation from slender delta wings in references 6–9. The solution exhibits certain general characteristics of side-edge separation which have been observed at low speed for low-aspect-ratio airfoils.

INTRODUCTION

RECENT DEVELOPMENTS IN airplanes and missiles for high-speed flight have resulted in a trend toward using thin airfoils of short span. Consequently, it becomes necessary to obtain reasonable predictions for the aerodynamic load in the tip region and at moderate angle of attack. In this paper, a theoretical investigation of the supersonic flow field in the tip region of a rectangular plate based on a simplified model is made. The salient feature of this investigation is the introduction of the effect of vortex separation from the *side-edge* into the supersonic flow field considered—an effect which has long been recognized as being important in determining the aerodynamic characteristics of narrow rectangular airfoils at low speed.[1–4]

Validity of the assumption of a nonseparated continuous flow over an airfoil surface depends on the very existence of a "boundary layer." When this model leads to prediction of an infinite adverse pressure gradient along the boundary or an infinite flow velocity around a corner, the assumption of a smooth and thin boundary layer gives way to the phenomenon of "separation" which is well known in hydrodynamics (or low-speed aerodynamics). One of the most familiar examples is the shedding of vortices and the realization of the Kutta condition at the sharp trailing-edge of an airfoil.[1,2] Another typical example is the local leading-edge separation described by Betz, in that the real flow around a sharp leading-edge occurs with a small "vortex region" where flow separation takes place locally, rendering the velocity there finite.[5, 22] The influence of the vortex region resulting from the local separation should receive due attention in the treatment of slender airfoils, for its effect would be not as locally restricted as in the other cases. Theoretical investigations based on a simplified model have been made along this line in references 6 and 7. Adams in reference 6 shows that the nonlinear lift of a slender delta wing due to the leading-edge separation is of the order of $\alpha^{5/3}$ where α is the angle of attack. A certain ambiguity remains in Adams' results but this can be removed by modifying the equilibrium condition of the *free* vortex system with its surrounding stream. This was pointed out later by Edwards,[8] and by Brown and Michael.[9] However, Adams' remark regarding the order of magnitude of the nonlinear lift remains valid.

The formation of a vortex region in the neighborhood of a sharp *side-edge* of an airfoil is in essence a phenomenon of the same nature (and, perhaps, it is more basic in character in a certain sense). According to the ordinary linearized theory which assumes no separation from the side-edge, the transverse components of the

Received June 11, 1954.

* The author wishes to express his appreciation of the helpful discussion and criticism afforded him by Prof. N. Rott and Dr. M. C. Adams (now with Douglas Aircraft Company, Inc.) of Cornell University, A. H. Flax of Cornell Aeronautical Laboratory, Inc., and Dr. J. Isenberg of Bell Aircraft Corporation.

† Aerodynamics Section, Engineering Division.

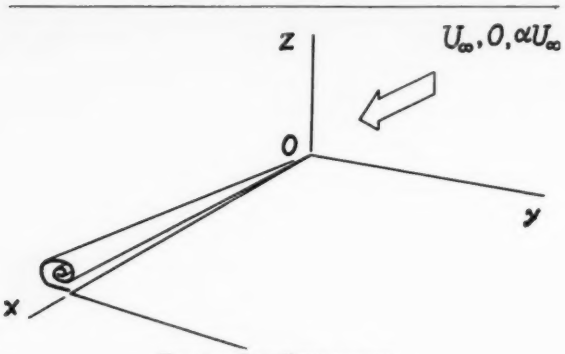

FIG. 1. Coordinate system.

velocity, $\partial\varphi/\partial y$ and $\partial\varphi/\partial z$, are infinite at the edge, although the "Kutta condition" may be thought of as being fulfilled in a certain sense.[10] Comparison of the theoretical predictions which are based on the "non-separated" flow model with the experimental results of Winter, for a series of narrow rectangular airfoils at *low speed*,[1] showed appreciable discrepancies. The data were for a combination of low aspect ratio and (sufficiently) high angle of attack. A nonlinear theory accounting for the separation effect from the side-edges has been given in a paper by Bollay;[11] and, recently, another approach to the problem parallel to the following investigation is presented in reference 14. Here, a simplified mathematical model is adopted to describe the vortex separation from the side-edge in a supersonic flow, which is similar to the one employed in references 6–9, in that the rolled up vortex sheet, or better the free vortex system arising from the separation, is idealized as a ray of concentrated vorticity in the cross-flow field near the edge, which increases in strength downstream from the apex. This representation in the analysis may be interpreted as an idealization of the external flow field of the free vortex system (which occupies a region of nonvanishing dimension in reality) by the "mean" in a certain sense suggested by the classical theory of vortex motion.[12, 13]

The present investigation was initiated from the study of yaw effects on the characteristics of thin airfoils with side-edges. The problem finds its analog in the problems of diffraction of a plane wave around sharp corners.[16, 17]

(1) Basic Assumptions and Model

The steady motion of a slightly disturbed flow of a nonviscous fluid is governed by a perturbation velocity potential φ which satisfies the linear Prandtl-Glauert differential equation

$$(M_\infty^2 - 1)\frac{\partial^2\varphi}{\partial x^2} - \frac{\partial^2\varphi}{\partial y^2} - \frac{\partial^2\varphi}{\partial^2 z} = 0 \qquad (1.1)$$

where x, y, and z are rectangular Cartesian coordinates, as in Fig. 1, the x-axis and the y-axis being, respectively, aligned with the side-edge and the leading-edge of the plate, and where M_∞ denotes the stream Mach Number. The boundary condition at upstream infinity is

$$\frac{\partial\varphi}{\partial x} = \frac{\partial\varphi}{\partial y} = \frac{\partial\varphi}{\partial z} = 0 \qquad (1.2)$$

and the boundary condition on the top and the bottom surfaces of the plate which lies in the plane $z = 0$ is

$$\frac{\partial\varphi}{\partial z} = -\alpha U_\infty \qquad (1.3)$$

where α is the angle of attack of the plate, and U_∞ the free stream velocity. While Eq. (1.1) neglects terms of the square of the perturbation velocity, the boundary conditions as stated from above are almost exact. We shall assume *a priori* that the contribution of the side-edge separation to the velocity potential belongs to an order lower (that is, larger in magnitude) than the square of the perturbation velocity, and the differential system, Eqs. (1.1)–(1.3), shall therefore suffice for the present purpose (refer to the coordinate system in Fig. 1).

The pressure is required to be continuous everywhere in the field except across the lifting surface—the wing, which may be expressed, for a plane wing, as

$$p - p_\infty = -\rho U_\infty \frac{\partial\varphi}{\partial x} \qquad (1.4)$$

where ρ is the stream density; whereas, it is known that when the problem involves a slender-body approximation, or one with a thin wing-slender body combination, a more appropriate formula for the local pressure may be used in place of Eq. (1.4), namely[18, 19]

$$p - p_\infty = -\rho U_\infty\left(\frac{\partial\varphi}{\partial x} + \alpha\frac{\partial\varphi}{\partial z}\right) - \frac{\rho}{2}\left[\left(\frac{\partial\varphi}{\partial y}\right)^2 + \left(\frac{\partial\varphi}{\partial z}\right)^2\right] \qquad (1.5)$$

In order to give a detailed pressure distribution over the plate in the present problem, especially in the vicinity of the side-edge, Eq. (1.5) might be more accurate than Eq. (1.4); however, in determining the resultant force (or the lift) and its center of pressure, Eq. (1.4) will be sufficient, as will be shown later.

Since the phenomenon of vortex separation from the side-edge arises from the local breakdown of the continuous flow around the edge, the role of the fluid viscosity does not enter into the solution in its first approximation. It is thus likely that the assumption of a conical irrotational field may still provide fruitful deductions for the present problem. Consequently, the vortex sheet or the vortex spiral may be visualized as a conical surface. Observation of real flow past a corner suggests that the free vortices may be regarded as being confined to a narrow (conical) region.[16, 28] Therefore, in order to simplify the analysis further, a crucial step is taken, which is mathematically the same as that employed in references 6–9, in that the total free vorticity in the narrow conical region close to the side-edge is replaced by a single concentrated

"vortex" which gathers strength downstream in the conical field. The location of this "vortex" must then coincide with one of the conical rays through the apex, which is to be determined, along with the unknown "circulation" or the unknown strength of the vortex, by two additional conditions: (1) that the flow velocity in the vicinity of the edge be bounded, which would otherwise tend to become infinite, (2) that the location of the axis of the concentrated vortex be compatible with its surrounding stream in such a way that the free vortex system becomes *dynamically free*.

If a small perturbation is maintained, the motion of the free vortices in the neighborhood of the side-edge, when viewed from downstream, will be seen as essentially the same as that which takes place in the neighborhood of a slender airfoil. Therefore, the second condition mentioned above reduces virtually to Eq. (2) of reference 14b; this point will be brought up again in Section (4).

We shall formulate in the next section the corresponding mathematical problem and obtain the solution thereof by the well-known method of conical field developed by Busemann and others.[19–24]

(2) Formulation of the Problem

Assumption of conical symmetry in the velocity field reduces the Prandtl-Glauert differential equation, which is satisfied also by the Cartesian velocity components $\partial\varphi/\partial x$, $\partial\varphi/\partial y$, and $\partial\varphi/\partial z$, to

$$\left[\rho^2(\rho^2-1)\frac{\partial^2}{\partial\rho^2}+\rho(2\rho^2-1)\frac{\partial}{\partial\rho}-\frac{\partial^2}{\partial\theta^2}\right]\times\left(\frac{\partial\varphi}{\partial x},\frac{\partial\varphi}{\partial y},\frac{\partial\varphi}{\partial z}\right)=0 \quad (2.1)$$

where

$$\left.\begin{aligned}\rho &= \beta\frac{\sqrt{y^2+z^2}}{x}\\ \theta &= \arctan(z/y)\end{aligned}\right\} \quad (2.2)$$

and $\beta=\sqrt{M_\infty{}^2-1}$.

Further transformation, due to Chaplygin, namely

$$s=\frac{\rho}{1+\sqrt{1-\rho^2}} \quad (2.3)$$

leads to

$$\left[\frac{\partial^2}{\partial s^2}+\frac{1}{s}\frac{\partial}{\partial s}+\frac{1}{s^2}\frac{\partial^2}{\partial\theta^2}\right]\left(\frac{\partial\varphi}{\partial x},\frac{\partial\varphi}{\partial y},\frac{\partial\varphi}{\partial z}\right)=0 \quad (2.4)$$

which is the Laplace equation in cylindrical coordinates. If one introduces the complex variable

$$\epsilon = se^{i\theta}$$

one sees that, within the unit circle in the ϵ-plane, the components $\partial\varphi/\partial x$, $\partial\varphi/\partial y$, and $\partial\varphi/\partial z$ may be represented by the real parts of three analytic functions, say U, V, and W, respectively.

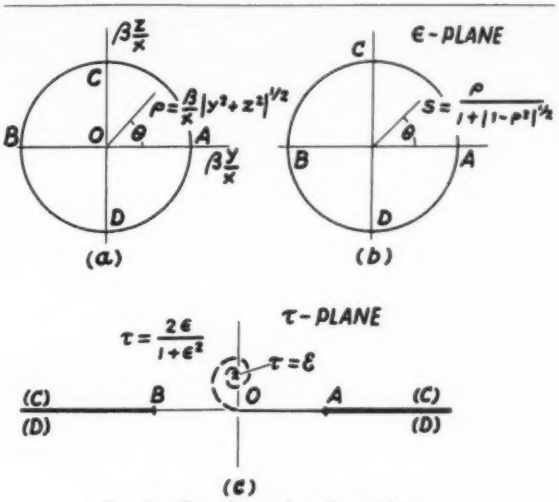

FIG. 2. Transformation of coordinates.

These functions are compatible with one another through relations provided by conditions of irrotationality and continuity. The usual conical wing problem may then be solved in a relatively assessable domain through the conformal transformation

$$\tau=\frac{2\epsilon}{1+\epsilon^2} \quad (2.5)$$

in that one encounters essentially a potential problem in the half-plane.[21, 24] The above transformation maps the Mach cone onto the left- and the right-hand branches of the real axis as shown in Fig. 2, and the interior of the upper and the lower halves of the Mach Cone from the apex into the upper and the lower halves of the entire τ-plane, respectively.† Through the transformations, Eqs. (2.2), (2.3), and (2.5), it is seen that on the portion of the real axis between $\tau=-1$ and $\tau=1$ the following relation holds

$$\tau=\beta(y/x) \quad (2.6)$$

and that the infinity of the τ-plane corresponds to the locations of the top and the bottom positions of the Mach Cone from the apex, the points C and D in Fig. 2. In the τ-plane, the compatibility relation reads[21, 24]

$$U'(\tau):V'(\tau):W'(\tau)=\frac{i\tau}{\beta\sqrt{1-\tau^2}}:-\frac{i}{\sqrt{1-\tau^2}}:1 \quad (2.7)$$

it is clear that if either one of the derivatives, say $W'(\tau)$, is determined, the solution system can be obtained by the integration of Eq. (2.7). A relation which provides much simplicity to the analysis is that in the vicinity of the x-axis, i.e., $\tau=0$ (which is the side-edge of the plate in the present problem),

$$\tau=\beta\frac{y+iz}{x}+0(\tau)^3 \quad (2.8)$$

† One may also solve the boundary value problem directly in the ϵ-plane.

It then follows from the last two relations, Eqs. (2.7) and (2.8), that there exists a flow region, downstream of the apex of the conical field, in which the motion reduces substantially to one that occurs in the slender-body theory.[30] That is,

$$\frac{\partial^2\varphi}{\partial y^2} + \frac{\partial^2\varphi}{\partial z^2} = 0(\tau)^2 \tag{2.9}$$

The boundary condition of the problem in the τ-plane is described as follows. Between the origin and the point on the plate, the boundary condition is clearly given by Eq. (1.3):

$$R.P.W(\tau) = -\alpha U_\infty$$

where $R.P.$ stands for the real part of the function involved. For $\tau > 1$ on the real axis, the boundary values take on the Ackeret results, namely,

$$\left.\begin{aligned} R.P.U(\tau) &= \pm(\alpha/\beta)U_\infty \\ R.P.V(\tau) &= 0 \\ R.P.W(\tau) &= -\alpha U_\infty \end{aligned}\right\} \tag{2.10}$$

where the positive and the negative signs in the first equation designate, respectively, boundary values on the top and the bottom surfaces of the plate. On the other branch of the transformed Mach Cone, that is, $\tau < -1$,

$$R.P.U(\tau) = R.P.V(\tau) = R.P.W(\tau) = 0 \tag{2.11}$$

In order to render the solution determined and acceptable to the physical problem, we specify the solution's behavior near each of the points $\tau = -1, 0, 1, \epsilon$, and at infinity, where ϵ denotes the location of the axis of the concentrated vortex in the τ-plane. Near that axis which is $\tau = \epsilon$ the vortex behavior requires

$$V'(\tau),\ W''(\tau) \sim \frac{1}{(\tau - \epsilon)^2} \tag{2.12}$$

As $|\tau|$ approaches infinity,

$$U'(\tau),\ W'(\tau) \sim \frac{1}{\tau} \tag{2.13}$$

which, in view of the transformation Eq. (2.5), accounts for the logarithmic singularities at the top and the bottom positions of the Mach Cone from the apex. The latter logarithmic singularities result from the jumps occurring in the boundary values prescribed on the Mach Cone.[23, 24] Also with reference to the boundary condition on the Mach Cone, the analytic functions are required to behave as[24]

$$\left.\begin{aligned} W'(\tau) &\sim \sqrt{\tau + 1} \text{ at } \tau = -1 \\ &\sim \text{regular at } \tau = 1 \\ U'(\tau),\ V'(\tau) &\sim \text{regular at } \tau = -1 \\ &\sim (1/\sqrt{\tau - 1}) \text{ at } \tau = 1 \end{aligned}\right\} \tag{2.14}$$

For the singular behavior of the solution at the side-edge, $\tau = 0$, the requirement of attaining a finite velocity leads to

$$V'(\tau),\ W'(\tau) \sim (1/\sqrt{\tau}) \tag{2.15}$$

It will be convenient to regard the solution system desired (U, V, W) as the sum of a system (U^*, V^*, W^*) and a system that assumes continuous flow around the edge (U_0, V_0, W_0) which is readily known as[19, 21, 23–27]

$$\left.\begin{aligned} U_0(\tau) &= \frac{\alpha}{\pi\beta} U_\infty \left[\frac{\pi}{2} - \arcsin(1 - 2\tau)\right] \\ V_0(\tau) &= 2\frac{\alpha}{\pi} U_\infty \frac{\sqrt{1 - \tau}}{\sqrt{\tau}} \\ W_0(\tau) &= i\frac{2\alpha}{\pi} U_\infty \left[\frac{\sqrt{1 + \tau}}{\sqrt{\tau}} - \log(\sqrt{\tau} + \sqrt{1 + \tau})\right] - \alpha U_\infty \end{aligned}\right\} \tag{2.16}$$

The star-system (U^*, V^*, W^*) shall then comply with the following conditions: On the real axis,

$$\left.\begin{aligned} R.P.U^* &= R.P.V^* = 0, \text{ except } |\tau| < 1 \\ R.P.W^* &= 0, \text{ except } -1 < \tau < 0 \end{aligned}\right\} \tag{2.17}$$

and as τ approaches ϵ, -1, 1, 0 and infinity, respectively,

$$\frac{dW^*}{d\tau} \sim \frac{B}{(\tau - \epsilon)^2},\ \sqrt{\tau + 1},\ \text{regular},\ \frac{1}{\tau^{3/2}} \text{ and } \frac{1}{\tau^2} \tag{2.18}$$

It is noted in the above equation that the constant B must be real and positive, so that the phenomenon of the vortex separation may be assured, the singularity of the type $\tau^{-3/2}$ at the edge $\tau = 0$ is required in order to cancel the infinity of the same type in W_0', and the behavior τ^{-2} at infinity is necessary to provide no further jump in the boundary values on the Mach Cone.

(3) Solution in Terms of the Vortex Strength and the Location of the Vortex

The analytic function fulfilling conditions of Eq. (2.17) as well as (2.18) for $dW^*/d\tau$ is

$$\frac{dW^*}{d\tau} = \frac{B}{2}\left[\frac{1}{(\tau - \epsilon)^2} - \frac{1}{(\tau - \bar{\epsilon})^2}\right] + \frac{B}{2F(\tau)}\left[\frac{\partial}{\partial\epsilon}\frac{F(\epsilon)}{\tau - \epsilon} + \frac{\partial}{\partial\bar{\epsilon}}\frac{F(\bar{\epsilon})}{\tau - \bar{\epsilon}}\right] \tag{3.1}$$

where the function $F(\tau)$ is $\tau^{3/2}(\tau + 1)^{-1/2}$, and B a real constant directly proportional to the circulation around the vortex core, Γ. (Details on the derivation of the above result can be found in Appendix I of reference 15. The derivation follows the approach of reference 29, in that the multivalued functions, such as $\tau^{1/2}$, $(\tau + 1)^{1/3}$, and $(\tau - 1)^{1/2}$, have to be carefully defined and their definitions strictly followed.) The functions $dU^*/d\tau$ and $dV^*/d\tau$ are obtained readily through the relation Eq. (2.7). We shall examine presently whether conditions (2.17) and (2.18) can indeed be fulfilled by the above function.

First, we shall show that the function given in Eq. (3.1), which is supposed to be the derivative of W^*, is analytic everywhere in the τ-plane except at the site of the vortex, $\tau = \epsilon$, and at the singular points along the real axis where the conditions imposed by Eq. (2.18) are to be observed. In view of the special branches chosen for the functions involved in $F(\tau)$, it may be seen that the function of Eq. (3.1) is analytic across the gap spanning between $\tau = -1$ and $\tau = 0$ along the real axis. The behavior of the function in approaching the points $\tau = -1, 0$, and 1 is determined virtually by the reciprocal of the function $F(\tau)$, which fulfills the requirements given by Eq. (2.18). As τ approaches the site of the vortex, $\tau = \epsilon$, the first term on the right-hand side of Eq. (3.1) stands out predominantly and the third term gives rise to three distinct singular parts, one of which contributes to the other half of the vortex strength while the other two cancel each other, leaving

$$\frac{dW^*}{d\tau} \sim \frac{B}{(\tau - \epsilon)^2} + 0(1)$$

which is the behavior desired. It appears from Eq. (3.1) that some singularity of the pole type may exist at the conjugate point of the vortex site, namely $\tau = \bar{\epsilon}$. However, careful inspection shows that they actually cancel one another out leaving the function of Eq. (3.1) finite and regular there. Furthermore, the reciprocal of $F(\tau)$ behaves as the reciprocal τ for large value of $|\tau|$; therefore the function given possesses also the desired property for large $|\tau|$, that is

$$\frac{dW^*}{d\tau} \sim \frac{1}{\tau^2}$$

It can therefore be seen that the conditions imposed by (2.18) are completely fulfilled.

Next, we examine the fulfillment of the boundary condition (2.17) on both the top and the bottom of the real axis. The function given by Eq. (3.1) may be written as

$$\frac{dW^*}{d\tau} = iB\left[I.P.\ \frac{1}{(\tau - \epsilon)^2} + \frac{1}{F(\tau)}\ I.P.\ \frac{\partial}{\partial \epsilon}\ \frac{F(\epsilon)}{\tau - \epsilon}\right]$$

where $I.P.$ stands for the imaginary part of the function involved, and the second term under the bracket sign results from the fact that, in view of the definitions adopted,

$$\overline{F(\tau)} = -F(\bar{\tau}),$$

where the bar sign stands for the complex conjugate of the function involved.

On either the left-hand branch of the Mach Cone ($\tau < -1$), or the right-hand branch of the Mach Cone together with the wing ($\tau > 0$), the above expression of $dW^*/d\tau$ on the real axis yields a purely imaginary value, thus the real part is zero. We conclude therefore that the function given by Eq. (3.1) can be taken as the derivative of the solution desired for $W^*(\tau)$. Similar steps of verification may also be carried out for the corresponding functions $dU^*/d\tau$ and $dV^*/d\tau$.

With due precaution on the multivalued functions mentioned above, the "star-system": (U^*, V^*, W^*) can now be obtained by direct integration. These integrals will not be presented here; however, one may refer to Appendix II of reference 15 for details. The constants B and ϵ appearing in Eq. (3.1) remain arbitrary up to this stage (it is worth noticing, in view of the boundary condition, Eq. (2.17), that the "starred system" (U^*, V^*, W^*) obtained above in terms of the arbitrary constant B and ϵ is valid not only for a rectangular flat plate, but also for *a class of plan forms*).

(4) Determination of the Vortex Strength and Its Location

It is seen from Eqs. (2.16) and (3.1) that in the neighborhood of $\tau = 0$

$$\left.\begin{aligned} \frac{dW_0}{d\tau} &\sim -\,i\,\frac{\alpha}{\pi}\,U_\infty\,\tau^{-3/2}, \\ \frac{dW^*}{d\tau} &\sim -\,\frac{B}{2}\left[\frac{d}{d\epsilon}\,\frac{F(\epsilon)}{\epsilon} + \frac{d}{d\bar{\epsilon}}\,\frac{F(\bar{\epsilon})}{\bar{\epsilon}}\right]\tau^{-3/2} \end{aligned}\right\} \tag{4.1}$$

in order to render the velocity finite in the vicinity of the side-edge, the constant B shall be taken as

$$B = -\,i\,\frac{2\alpha}{\pi}\,\frac{U_\infty}{\left[\dfrac{d}{d\epsilon}\,\dfrac{F(\epsilon)}{\epsilon} + \dfrac{d}{d\bar{\epsilon}}\,\dfrac{F(\bar{\epsilon})}{\bar{\epsilon}}\right]} \tag{4.2}$$

which, according to the property of the function $F(\tau)$ mentioned in the previous section, yields a real value for B. For small values of ϵ, the above equation may be written in its first order as

$$B \approx i\,\frac{4\alpha}{\pi}\,U_\infty\,\frac{\mu\bar{\mu}}{(\mu - \bar{\mu})} \tag{4.3}$$

where $\mu = \epsilon^{1/2}$. The use of Eq. (4.3) in place of Eq. (4.2) implies an error of the order of $\alpha\epsilon^{3/2}$.

A condition in addition to Eq. (4.2) or (4.3) is now necessary in order to determine both B and ϵ. Since the exact boundary condition requires continuity of the pressure across the free vortex sheet, the equivalent condition in the simplified model shall then be the vanishing of the total force on the vortex system, which is in reality the fulfillment of the exact boundary condition by the *mean value*. This force-free condition is of particular importance in the present analysis. As a result of the vortex type singularity incorporated in the simplified solution in the present analysis, which is given by Eq. (3.1), a pressure jump will occur somewhere in the field, which can be observed quite easily from the "compatibility relation" Eq. (2.7) and the local pressure formula Eq. (1.5). This pressure jump may be interpreted as the force acting on the "vortex feedlines" of the simplified model,[6] the mathematical detail about which will be given briefly in Section (5). In order to render the vortex system *dynamically free*, this force shall be balanced by the one acting on the vortex core at $\tau = \epsilon$, which is essentially a "Joukowski Force." Both forces (per unit depth of x) mentioned

above belong to the same order as $\Gamma \cdot \epsilon$, which will be seen later as α^2; cancellation of these two forces in their first order results in

$$U_\infty \frac{d}{dx}(\Gamma \bar{\zeta}_0) \approx \rho \Gamma \overline{V_m'} \tag{4.4}$$

where Γ is the circulation around the vortex center, ζ_0 the *relative* position of the vortex center to the edge in a complex plane *normal* to the edge, and $\overline{V_m'}$ the conjugate of the complex-vortex-velocity (at the vortex center) in the same plane. Therefore, the left-hand member is seen to arise from the pressure jump across the diaphragm or the "feedlines," and the right-hand member is simply the "Joukowski-force." Since in the present case, $\zeta_0 = x\epsilon/\beta$ and $\Gamma = 2\pi x B/\beta$, and the plane normal to the edge coincides with the y, z-plane, application of Eq. (4.4) yields the additional equation

$$2\frac{U_\infty}{\beta}\bar{\epsilon} \approx -i \lim_{\tau \to \epsilon} \left[W(\tau) + \alpha U_\infty + \frac{B}{\tau - \epsilon} \right] \tag{4.5}$$

where the limit on the right-hand side is the complex-velocity "at" the vortex center, that is, the complex-velocity *prescribed* by the *surrounding fluid* in the cross-flow plane.

An alternative way of obtaining the above relation can in fact be made, based essentially on the Kelvin (or Helmholtz) Vortex Conservation Theorem. From Kelvin's theorem, one may deduce that *each vortex filament* set free from the side-edge must *move in a way prescribed by the motion of the surrounding fluid* in order to remain force-free. However, this state of affairs, as pointed out already in reference 8, can be true only when applied to each individual vortex filament or bundle of filaments whose total *circulation remains unchanged*, whereas, the total strength or the circulation of the vortex system in the conical field keeps *changing* linearly downstream. Nevertheless, application of the above rule deduced from the Kelvin theorem is still possible, for one can determine from the knowledge of strength and the vortex-center of the vortex system, B and ϵ, the *instantaneous* rate of motion of the free vortices (in the cross-flow plane) and equate this instantaneous velocity to the one prescribed by the surrounding stream. With the above understanding, one then arrives at Eq. (4.4) which can be identified as Eq. (2) of reference 14b, and thus Eq. (4.5), the details can be found in references 8 and 14. The left-hand member of Eq. (4.5) is therefore seen to be the "instantaneous complex-velocity" of the free vortex system, which differs from the rate of motion of the vortex-center in the cross-flow plane by a factor of two. Substituting the integral of the function given by Eq. (3.1) for $W(\tau)$, and neglecting terms of the square of ϵ, one arrives through Eq. (4.5) at an algebraic equation for ϵ (refer to Appendix III of reference 15 for detail)

$$2\frac{U_\infty}{\beta}\bar{\epsilon} \approx 2\frac{U_\infty \alpha}{\pi}\frac{1}{\mu} - iB\left[\frac{1}{4\mu^2} - \frac{1}{2\mu\bar{\mu}} + \frac{1}{2\bar{\mu}(\bar{\mu} - \bar{\mu})}\right] \tag{4.6}$$

where $\mu = \epsilon^{1/2}$ and B is given by Eq. (4.3).

The last equation yields,

$$\epsilon \approx \pm\frac{i}{2}\left(\pm\frac{\beta\alpha}{\pi}\right)^{2/3} \tag{4.7}$$

Here the positive and negative signs correspond, respectively, to the positive and the negative angles of attack. The above result signifies the fact that the vortex-center locates *directly above* the side-edge (at approximately the "12 o'clock position") and on the *suction side* which seemingly agrees well with some of the observations recorded in reference 16.† The equation of the "vortex core" in space, as deduced directly from the last equation, is

$$x:y:z \approx 1:0:\frac{1}{2\beta}\left(\frac{\beta\alpha}{\pi}\right)^{2/3} \tag{4.8}$$

and the circulation round the "vortex core," according to Eq. (4.3), is

$$\Gamma = 2\pi\frac{x}{\beta}B \approx 4U_\infty \frac{x}{\beta}\left(\frac{\beta\alpha}{\pi}\right)^{1/3} \cdot \alpha \tag{4.9}$$

which is a positive real constant, giving a clockwise circulatory motion as anticipated. The above results which characterize the side-edge separation are consistent with those obtained in the corresponding problems of slender airfoils.[14] The error introduced by using Eqs. (4.3) and (4.6), instead of their more "exact" forms, Eqs. (4.2) and (4.5), is of the order of $\alpha^{4/3}$ in ϵ, and of the order of α^2 in B.

From the above results, it can be seen that the nonlinear effect on the velocity field belongs to an order varying from $\alpha^{4/3}$ (at points away from the vortex free region) to $\alpha^{2/3}$ (at points within the immediate vicinity of free vortex region or the side-edge) which is of lower order (larger in magnitude) than the square of the perturbation. The use of the linearized system of differential equation and boundary condition, Eqs. (1.1)–(1.3), is thus seen justified.

As to the determination of the pressure difference across the wing, the linearized formula, Eq. (1.4), can also be seen to be sufficient for examination of the solution system obtained after substitution of Eqs. (4.7) and (4.9) shows that the nonlinear effect of the side-edge separation is of the order of $\alpha^{4/3}$ in $\Gamma(\tau)$ and $W(\tau)$, and of $\alpha^{5/3}$ in $U(\tau)$, thus the difference between Eqs. (1.4) and (1.5) belongs to an order of $\alpha^{2/3}$. However, somewhere at the immediate vicinity of the side-edge, say for $\tau = 0(\epsilon)$ or smaller, the order of magnitude of both $\Gamma(\tau)$ and $W(\tau)$ are seen to become as large as $\Gamma/\epsilon = 0(\alpha)^{2/3}$. It appears that Eq. (1.5) could have been more accurate than Eq. (1.4), but it

† The agreement of the theoretical prediction based on a similar model with some actual observations has been checked by Rott.[17]

is noted that some error has already been anticipated at the immediate neighborhood of the side-edge because of the adaptation of the concentrated vortex in place of a continuous vortex sheet. The use of Eq. (1.5) does not seem to warrant the effort. In fact, it can be shown that the contribution of the higher order term contained in the pressure formula of Eq. (1.5) to the *integrated aerodynamic forces* can be at most of the order of $\alpha^{7/2} \log \alpha$ for the *present case* (which can be ignored in comparison with $\alpha^{3/2}$).

(5) The Nonlinear Effect on the Load Distribution Over the Tip Region

As pointed out in the last section it may be sufficient to use the linearized formula Eq. (1.4) for load prediction, in which the streamwise perturbation velocity $\partial\varphi/\partial x$ can be obtained from Eq. (3.1) by direct integration of Eq. (2.7).

In view of the behavior of the solution at $\tau = \epsilon$ it is clear from Eq. (2.7) that a singularity of the logarithmic type shall exist in the function $U(\tau)$ at the point $\tau = \epsilon$. This logarithmic singularity causes the function $U(\tau)$ to become multivalued in its real part, but in order to render the analytic flow field unique, a special cut-line in the τ-plane for the singularity is necessary. Consequently, a jump in the pressure will be found across the cut-line, whose magnitude is proportional to the strength of the "vortex" [note that those higher order terms in Eq. (1.5) do not contribute to the jump]. Although the shape of the cut-line can be arbitrarily chosen, it does, however, connect the point $\tau = \epsilon$ and infinity. It then passes through the side-edge $\tau = 0$ and the wings proper, such as the dotted curve in Fig. 2c. For, the assumption of vortex separation at the side-edge implies continuity in fluid pressure and velocity *along* the wing surfaces up to the side-edge $\tau = 0$.

Since vortex filaments do not terminate themselves within an irrotational field, this cut-line may be thought of, after reference 6, as being composed of the "vortex feedlines" joining the bound-vortices on the wing and the concentrated vortex.

The loading on the wing may be written in the form of load coefficient

$$\Delta C_p \equiv \frac{p^- - p^+}{{}^1/_2 \rho U_\infty{}^2} \approx 2 \cdot \frac{(\partial\varphi^+/\partial x) - (\partial\varphi/\partial x)}{U_\infty} \tag{5.1}$$

Upon substituting $R.P.\{U(\tau + i0) - U(\tau - i0)\}$ for the difference in $\partial\varphi/\partial x$ across the wing, and retaining terms of orders ϵ^2 and lower, the wing load in the tip region can be expressed as

$$\frac{\Delta C_p}{4(\alpha/\beta)} \approx \frac{1}{2}\left[1 - \frac{2}{\pi} \arcsin(1 - 2\tau)\right] + \frac{2\sqrt{2}}{\pi} |\epsilon|^{1/2}\left[-\arg.\frac{R(\epsilon, \tau)}{\tau - \epsilon} + \tau^{1/2}(1 - \tau)^{1/2} I.P.\frac{\epsilon^{1/2}}{R(\epsilon, \tau)} - (1 - 2\tau) I.P.\frac{\epsilon}{R(\epsilon, \tau)} - I.P.\frac{\epsilon}{\tau - \epsilon}\right] \tag{5.2}$$

where

$$R(\epsilon, \tau) = \epsilon + (1 - 2\epsilon)\tau - 2\epsilon^{1/2}(1 - \epsilon)^{1/2}\tau^{1/2}(1 - \tau)^{1/2}$$

In evaluation of the *argument* of the complex function $R(\epsilon, \tau)/(\tau - \epsilon)$ for points on the wing, it should be noted that the branch for the argument is to be chosen such that arg. $(-1) = -\pi$; this is evident from the fact that the pressure difference at the side edge of the wing, $\tau = 0$, must be equal to that across the cut-line, which is determined entirely by the potential jump around the vortex center and given by $2\sqrt{2}\,|\epsilon|^{1/2}$. The terms under the first bracket sign in the above equation are obviously the linearized results which are well known. The nonlinear part of the load coefficient is accordingly of the order of $\alpha^{4/3}$ at the edge $\tau = 0$, which is given by the pressure jump across the "feedlines." However, it drops off rapidly away from the side-edge, providing an increase in lift of the order of $\alpha^{2/3}$ over most of the tip region. The expression given in Eq. (5.2), which is the ratio of the pressure difference across the plate to the pressure difference across a flat plate of infinite span, depends only on two variables, namely, $\beta y/x$ and $\beta\alpha$. The distributions are presented in Fig. 3 for two particular values of the "reduced angle of attack," $\beta\alpha = 4°$ and $10°$ which correspond, respectively, to $|\epsilon| = 0.0397$ and 0.0730 and are presumably small enough to render the present first order (in ϵ) theory consistent.

The increasing trend in the lift distribution toward the side-edge is of some interest, the same behavior has also been noted in the solution of the narrow rectangular

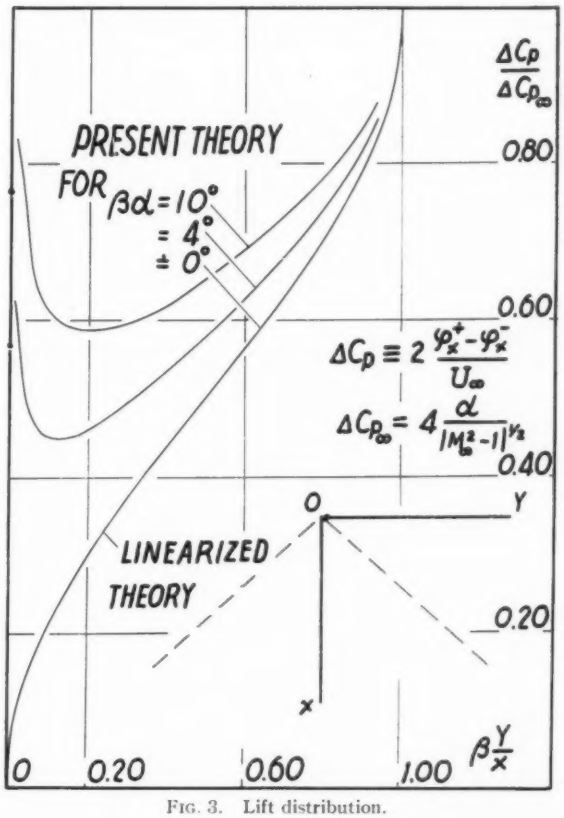

Fig. 3. Lift distribution.

wing problem.[14] Except in the *very* close neighborhood of the edge, this rising trend toward the edge in the wing loading seems to agree with the actual measurements.[1] The general increase in lift over most parts of the tip region could have been anticipated from the consideration of the spatial distribution of the vortex filaments, as illustrated by Fig. 4, in that the occurrence of vortex separation from the side-edge causes a portion of the bound vortex filaments to leave the lifting surface at the side-edge, instead of bending backward into the free-stream direction before being set free at the trailing edge. Since deficiency in lift of a lifting surface could be thought of as having resulted from the backward bending of the bound vortex filaments into the free-stream direction, one naturally expects that this drop in the tip loading in the event of the side-edge separation will be considerably reduced.

(6) The Total Force on the Tip Region

The nonlinear effect on the total force and its moments may be sufficiently determined by integrating directly over the tip region ($0 \leq \tau \leq 1$) the corresponding part of the function provided by Eq. (5.2). A simple way in handling this integration by the use of Cauchy's integral theorem can be effected and the detail is given in reference 15. The resultant force on the free vortex system vanishes, since the contribution of the pressure difference across the cut-line is canceled by the "Joukowski Force" on the core, which is of the order of α^2.

The nonlinear part of the lift coefficient is then found to be

$$C_L^* \approx \frac{12}{\beta} |\epsilon| \cdot \alpha \tag{6.1}$$

which is based on the wing area intercepted by the Mach Cone from the tip apex, hence the lift coefficient of the tip region is given by the sum

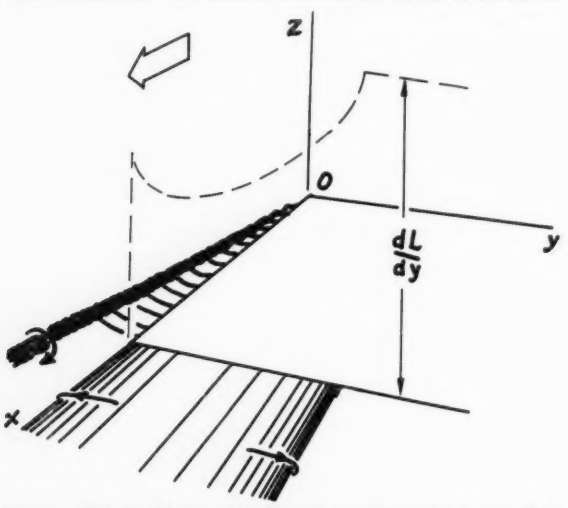

Fig. 4. Sketch of free vortex filaments as interpreted according to Fig. 3.

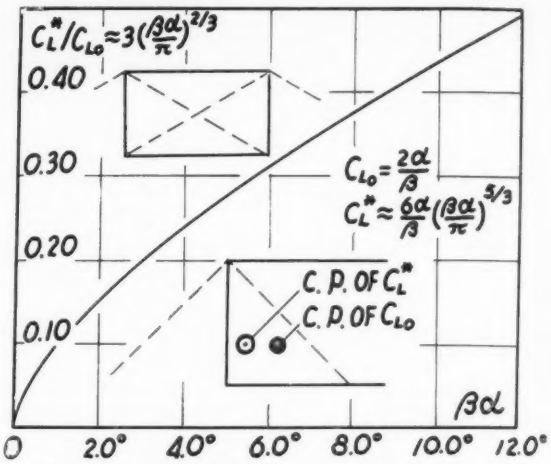

Fig. 5. Nonlinear effect of tip vortex separation on lift.

$$C_L \approx \frac{2\alpha}{\beta} + \frac{6\alpha}{\beta}\left(\frac{\beta\alpha}{\pi}\right)^{2/3} \tag{6.2}$$

It is noted that the above lift formula is possibly correct up to an order higher (smaller in magnitude) than α^2, provided the error introduced by replacing the free vortex sheet with a concentrated vortex does not invalidate the solution system and its result to the same order or lower.

The result presented in Fig. 5 shows that at the reduced angle of attack $\beta\alpha = 1°$ the nonlinear effect may be as high as 10 per cent of the value predicted by the linearized theory; and at $\beta\alpha = 4°$ it becomes 24 per cent. This suggests an explanation of the apparent discrepancy between theory and experiment in the value of the lift curve slope at $\alpha = 0$ for low aspect ratio airfoils. (This point has also been discussed in reference 4, pp. 373–374.[31]) For, according to the present result, Eq. (6.2), or Fig. 5, the rate of change of the lift curve slope with respect to the angle of attack is infinitely large at $\alpha = 0$ for an idealized sharp edge. The same figure, Fig. 5, provides also the value of C_D^*/C_{D_0} as a function of $\beta\alpha$.

It is worthy of notice that the lift coefficient given in Eq. (6.2) based on the area intercepted by the tip Mach Cone may also be taken as the lift coefficient for a complete rectangular plate of aspect ratio $AR = 1/\beta$, as shown in the upper left-hand corner of Fig. 5.

By obtaining the moment of force about the side-edge in a similar manner, the c.p. of the nonlinear lift can be determined, which is found located at the intersection of the two-third chord line $x = 2C/3$ and the ray

$$\beta(y/x) \approx (1/4) \tag{6.3}$$

to the first approximation. Whereas, the c.p. of the linear part of the lift is known acting at the intersection of the two-third chord line and the ray $\beta(y/x) = 5/8$. Eq. (6.3) signifies the fact that the nonlinear lift corresponding to Eq. (6.1) is not simply a result of local concentration of lift near the side-edge but, rather, a

contribution of the pressure difference over a considerably extended area.

At higher Mach Number, in view of Eq. (6.2), the nonlinear term may become important in determining the tip effect.

It is believed that the present analysis provides reasonable information on the flow field within the Mach Cone from the apex (except in the *immediate vicinity* of the tip, $\tau = 0$). In the neighborhood of the *tip Mach Cone*, $\tau = 1$, the solution is, however, subject to an error of the order of α^2 as a consequence of the differential shifts of the true "characteristic cone" (which is a shock wave in reality) on the top and the bottom of the wing. A detailed investigation on the lift distribution in the neighborhood of the tip Mach Cone seems lacking in literature,[32] but its effect on the total lift is believed to remain at an order higher (smaller in magnitude) than α^2, provided the *thickness* and the *boundary-layer* effects remain sufficiently small, or at least innocuous.

(7) Concluding Remarks

The results characterizing the solution obtained above can be given in terms of the strength or the circulation of the free vortex system, the equation of the vortex core in space, and the nonlinear lift as well as its center of pressure. The foregoing are given respectively in Eqs. (4.8), (4.7), (6.1), and (6.3). The load distribution over the tip region, as illustrated in Fig. 3, may also be taken as one of the salient features characterizing the phenomenon.

As remarked at the end of Section (3), solutions of the same type can also be obtained without difficulty for a class of plan forms such as that illustrated in Fig. 6, for which the variation in configuration only leads to a different determination of the free vortex strength and its location, i.e., B and ϵ.

Comparison of the features mentioned with the solutions in the other cases has been made in a previous note,[14] however an additional remark concerning the equilibrium condition of the free vortex system will be given here. Close examinations of all these solutions reveal that there exists a moment of *couple* left unbalanced in the vortex system, although the resultant *force* has been made vanished to the appropriate order. This error shall certainly remain harmless; in fact, if this moment of the couple, together with other "moments of the higher order," could be made identically zero, the simplified model itself would become the exact model. But the order of magnitude of this unbalanced couple can serve, perhaps, as a reference measuring the error introduced by the simplification, that is, the error caused by the replacement of the free vortex sheet with the concentrated vortex. This order of magnitude is found to be $\alpha^{5/2}$ in the case of side-edge separation, and of $\alpha^{7/2}$ in the case of the leading-edge separation. It is hoped that the question of this type of error can be satisfactorily settled in the future, when some of the "exact solutions" to the continuous-vortex-sheet models become available.[28, 33]

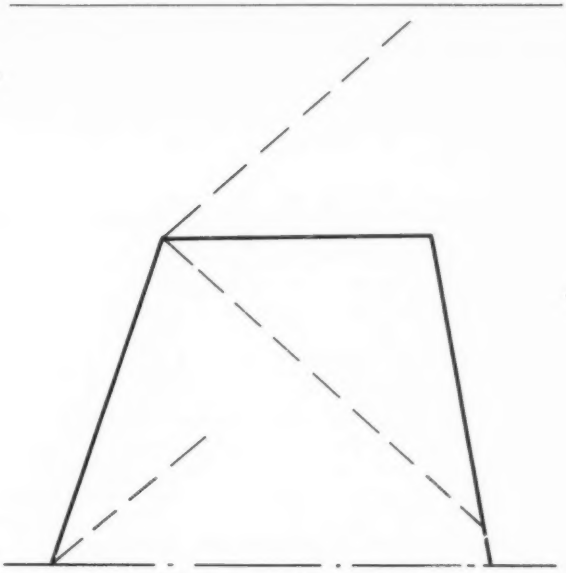

Fig. 6. Plan form for which Eq. (3.1) is valid.

References

[1] Winter, H., *Flow Phenomena on Plates and Airfoils of Short Span*, NACA TM 798, 1936. (Translated from *Strömungsvorgänge an Platten und Profilierten Körpern bei kleinen Spannweiten*, VDI, 1936.)

[2] Zimmermann, C. H., *Characteristics of Clark Y Airfoils of Small Aspect Ratios*, NACA TR 431, 1932.

[3] Tosti, L. P., *Low Speed Static Stability and Damping-in-Roll Characteristics of Some Swept and Unswept Low Aspect Ratio Wings*, NACA TN 1468, 1947.

[4] Flax, A. L., and Lawrence, H. R., *The Aerodynamics of Low Aspect Ratio Wings and Wing-Body Combinations*, The Transactions of the Third Anglo-American Aeronautical Conference 1951, pp. 363–398J.

[5] Betz, A., *Aerodynamic Theory*, Vol. IV (W. F. Durand, Ed.), Div. J, Chapter II, Sec. 1; Springer, Berlin, 1935.

[6] Adams, M. C., *Leading-Edge Separation from Delta Wing at Supersonic Speeds*, Readers' Forum, Journal of the Aeronautical Sciences, Vol. 20, No. 6, p. 430, June, 1953.

[7] Legendre, R., *Écoulement au voisinage de la pointe avant d'une aile à forte fleche aux incidences moyennes*, La Recherche Aéronautique, Bulletin Bimetriel, De L'Office National D'Études Et De Recherches Aéronautiques, November-December, 1952, and January-February, 1953.

[8] Edwards, R. H., *Leading-Edge Separation from Slender Delta Wing*, Readers' Forum, Journal of the Aeronautical Sciences, Vol. 21, No. 2, pp. 134–135, February, 1954.

[9] Brown, C. E., and Michael, W. H., *Effect of Leading-Edge Separation on the lift of a Delta Wing*. Paper presented at the 22nd Annual Meeting of IAS, January, 1954 (available as Reprint No. 437).

[10] von Kármán, T., *Supersonic Aerodynamics—Principles and Applications*, Journal of the Aeronautical Sciences, Vol. 14, No. 7, pp. 373–402, July, 1947.

[11] Bollay, W., *A Theory for Rectangular Wings of Small Aspect Ratio*, Journal of the Aeronautical Sciences, Vol. 4, pp. 294–296, 1936.

[12] Prandtl, L., *The Essentials of Fluid Dynamics*; Hafner Publishing Co., New York, 1952, pp. 50–53 and 72–76.

[13] Milne-Thomson, L. M., *Theoretical Hydrodynamics*, 2nd Edition; Macmillan Co., New York, 1950, pp. 313–350.

[14](a) Cheng, H. K., *An Approximate Solution to a Problem of Vortex Separation with Application to the Prediction of Nonlinear Lift*, Bell Aircraft Corporation Aerodynamics Section, Theoretical Research Note No. 2. (b) Also see *Remarks on Nonlinear Lift and Vortex Separation*, Readers' Forum, Journal of the Aeronautical Sciences, Vol. 21, No. 3, pp. 212–214, March, 1954.

[15] Cheng, H. K., *Aerodynamics of a Rectangular Plate with Vortex Separation in Supersonic Flow*, Bell Aircraft Corporation Aerodynamics Section, Theorectical Research Note 1.

[16] Uhlenbeck, G., *Diffraction of Shock Waves Around Various Obstacles*, Project M 720-4, University of Michigan, Ann Arbor (Office of Naval Research, Contract No. N6-ONR-232 TOIV), March, 1950.

[17] Rott, N., private communication.

[18] Adams, M. C., and Sears, W. R., *Slender-Body Theory—Review and Extension*, Journal of the Aeronautical Sciences, Vol. 20, No. 2, pp. 85–98, February, 1953.

[19] Busemann, A., *Infinitesimale Kegelige Überschallströmung*, Deutschen Akademie der Luftfahrtforschung, 1942–43, p. 455. English translation available as NACA TM 1100, March, 1947.

[20] Stewart, H. J., *The Lift of a Delta Wing at Supersonic Speeds*, Quarterly Applied Mathematics, Vol. IV, No. 3, October, 1946.

[21] Hays, W. D., *Linearized Supersonic Flow*, North American Aviation, Inc., Report No. A1-222.

[22] Brown, C. E., *Theoretical Lift and Drag of Thin Triangular Wings at Supersonic Speeds*, NACA TN 1183, December, 1946.

[23] Lagerstrom, P. A., *Linearized Supersonic Theory of Conical Wings*, NACA TN 1685, January, 1950.

[24] Golstein, A., and Ward, G. N., *The Linearized Theory of Conical Fields in Supersonic Flow, with Application to Plane Airfoils*, Aeronautical Quarterly, Vol. II, Pt. 1, May, 1950.

[25] Schlichting, H., Deutsche Luftfahrforschung, Jahrbuch, 1937.

[26] Lighthill, M. J., *The Supersonic Theory of Wings of Finite Span*, ARCR & M 2001, 1944.

[27] Evvard, J. C., *Distribution of Wave Drag and Lift in the Vicinity of Wing Tips at Supersonic Speeds*, NACA TN 1382, 1947.

[28] Goldstein, S., *Modern Development in Fluid Dynamics;* Oxford at the Clarendon Press, 1938, pp. 39–40, 62–65, and 552.

[29] Cheng, H. K., and Rott, N., *Generalizations of the Inversion Formula of Thin Airfoil Theory*, Journal of Rational Mechanics and Analysis, May, 1954.

[30] Jones, R. T., *Properties of Low Aspect Ratio Pointed Wings at Speeds Below and Above the Speed of Sound*, NACA TR 835, 1946.

[31] Vincenti, W. G., *Comparison between Theory and Experiment for Wings at Supersonic Speeds*, NACA TR 2100, June, 1950.

[32] Lighthill, J. M., *The Shock Strength in Supersonic "Conical Fields,"* Philosophical Magazine, Vol. 40, Ser. 17, No. 311, pp. 1202–1223, December, 1949.

[33] Prandtl, L., *Vorträge aus dem Gebiete der Hydro- und Aerodynamik;* Innsbruck, 1922 (Berlin 1924), pp. 18–33.

The Difference Property of the Kernel of the Unsteady Lifting Surface Theory

H. G. KUESSNER*

Max Planck-Institut fuer Stroemungsforschung, Goettingen, Germany

SUMMARY

The kernel of the integral representation of the general solution of the linearized lifting surface theory has the difference property. This leads to two corresponding forms of solution which give the unsteady reverse-flow theorem. From the difference property a condition of compatibility is obtained for the characteristic function G of the kernel of the harmonic three-dimensional subsonic case. By this the pressure is obtained in close analogy to the two-dimensional incompressible case.

(1) Difference Property of the Kernel

In order to represent the solutions of the unsteady lifting surface theory in the simplest possible manner, the integral representation is used with a Green function as kernel of the integral. The velocity potential of disturbance is expressed by

$$\phi(s, x, y, z) = \iint_{(a)} dx'\,dy' \int_{s'=0}^{s} dw(s', x', y', 0) \times K(s, x, y, z; s', x', y', 0) \quad (1)$$

where x, y, z are Cartesian coordinates in a system moving with the lifting surface and s is the straight flight path of the zero point of the coordinate system, starting from rest $s = 0$. The lifting surface (a) is assumed in the plane $z = 0$. The given downwash of the lifting surface

$$w(s, x, y, 0) = \phi_z(s, x, y, 0) \quad (2)$$

is contained in a Stieltjes integral with the parameter s. The velocity potential must satisfy the wave equation

$$D\phi \equiv \left\{\nabla^2 - \left[\frac{v(s)}{c_0}\left(\frac{\partial}{\partial s} + \frac{\partial}{\partial x}\right)\right]^2\right\}\phi(s, x, y, z) = 0 \quad (3)$$

The pressure of disturbance is given by Euler's equation

$$p(s, x, y, z) = -\rho_0 v(s)\left(\frac{\partial}{\partial s} + \frac{\partial}{\partial x}\right)\phi(s, x, y, z) \quad (4)$$

where ρ_0 is the density and c_0 the velocity of sound of the undisturbed fluid, $v(s)$ is the variable velocity of flight of the lifting surface.

Because $D\phi = 0$, we have according to Eq. (1) also $DK = 0$. If $v(s)$ = constant or $c_0 = \infty$, we may replace

$$s \to s - s'; \quad x \to x - x'; \quad y \to y - y'; \quad z \to z - z'$$

without changing the differential operator D of Eq. (3). Therefore we have also $D'K = 0$. By this the composition of the kernel K is simplified because it has the difference property

$$K(s, x, y, z; s', x', y', z') \equiv K(s - s', x - x', y - y', z - z') \quad (5)$$

This difference-kernel property of the linearized lifting surface theory is well known. It enables one to understand thoroughly the lifting surface theory, as will be shown in the following.

(2) Reverse-Flow Theorem

From Eqs. (1) and (5) we obtain the corresponding formula

$$\phi(-s', -x', -y', z) = \iint_{(a)} dx\,dy \times \int_{s=0}^{-s'} dw\,(-s, -x, -y, 0)\,K(s - s', x - x', y - y', z) \quad (6)$$

The lifting surface may attain a final rest point after a flight path s_0. Then we can add to Eq. (6) an integral with the limits $-s_0$ to 0, without changing ϕ. Because $\phi(z) = -\phi(-z)$, we can write Eq. (6) also

$$\overline{\phi(s', x', y', z)} = \iint_{(a)} dx\,dy \times \overline{\int_{s=0}^{s'} dw(s, x, y, 0)\,K(s - s', x - x', y - y', z)} \quad (7)$$

where the bar denotes reverse flow. If we multiply Eq. (6) by

$$\iint_{(a)} dx'\,dy' \int_{s'=0}^{s} dw(s', x', y', 0)$$

and apply Eqs. (1) and (5), we obtain the general reverse-flow theorem for $v(s)$ = constant or $c_0 = \infty$:

$$\iint_{(a)} dx\,dy \int_{s=0}^{s} dw(s, x, y, 0)\,\overline{\phi(s, x, y, z)} = \iint_{(a)} dx\,dy \overline{\int_{s=0}^{s} dw(s, x, y, 0)\phi(s, x, y, z)} \quad (8)$$

Received June 16, 1954.

* Professor Dr. Ingr.

If we apply first the operator (4) to Eq. (6) and then repeat the same procedure, we obtain the corresponding theorem for the pressure

$$\iint_{(a)} dx\,dy \int_{s=0}^{s} dw(s, x, y, 0)\; \overline{p(s, x, y, z)} = \iint_{(a)} dx\,dy\, \overline{\int_{s=0}^{s} dw(s, x, y, 0)}\; p(s, x, y, z) \quad (9)$$

For harmonic oscillations the functions of s and of x, y, z are separated. Therefore we may drop s in Eqs. (8) and (9) and obtain the reverse-flow theorem, stated by Flax[1] for harmonic oscillations:

$$\iint_{(a)} dx\,dy\, w(x, y, 0)\cdot\overline{p(x, y, z)} = \iint_{(a)} dx\,dy\, \overline{w(x, y, 0)}\; p(x, y, z) \quad (10)$$

Eqs. (6) to (10) are useful, if the kernel K is not known explicitly or known only in a complicated form. They hold for every Mach Number.

(3) Singularity of Kernel

The difference property of the kernel K is evident in the supersonic case. But in the subsonic case the kernel is composed of a regular part and of a singular part which do not have this property singly. Only their sum has it, as will be proved in the following.

We assume a harmonic downwash

$$w(s, x, y, 0) = w(x, y, 0)\exp(iks) \quad (11)$$

By a general nonorthogonal Lorentz transformation of the coordinates we transform the wave Eq. (3) at rest (compare references 2 and 3). With the corresponding reduced coordinates x, y, z and reduced quantities ϕ^*, p^* we have

$$(\nabla^2 + \kappa^2)\phi^*(x, y, z) = 0 \quad (12)$$

$$-[\omega + (\partial/\partial x)]\phi^*(x, y, z) = p^*(x, y, z) \quad (13)$$

where

$$\omega = \frac{ikl}{1-\beta^2}; \qquad \kappa = \frac{kl\beta}{1-\beta^2}; \qquad \beta = \frac{v}{c_0} \quad (14)$$

The reduced velocity potential is expressed by

$$\phi^*(x, y, z) = \iint_{(a)} dx'\,dy'\, w^*(x', y', 0) \times K(x - x', y - y', z) \quad (15)$$

In the author's published lecture[2] and paper[3] a characteristic function for the subsonic case has been introduced:

$$G(u, v, w; v', w') = \sum_{1}^{\infty} \frac{R_n(u)}{R_n'(0)}\, S_n(v, w)\, S_n(v', w') \quad (16)$$

being a regular solution of the wave Eq. (12). u, v, n are orthogonal single-valued coordinates depending on x, y, z. u = constant is a convex surface; $u = 0$ denotes the lifting surface. $w = 0$ denotes the plane of symmetry normal to the lifting surface. R_n is a wave function vanishing at infinity. S_n is a surface harmonics for u = constant.

The kernel K must have singular points on the boundary of the lifting surface

$$u = 0; \qquad v = 0; \qquad \text{and} \qquad v = \pi \quad (17)$$

$v = 0$ may be the leading edge and $v = \pi$ the trailing edge of the lifting surface. Therefore, according to the former stated conditions, we assume the general kernel*

$$K = \Lambda_1 \int_{-\infty+i\pi/2}^{\infty-i\pi/2} F(\alpha, \omega)\, d\alpha \begin{vmatrix} G(u, v, w; v', w'), & G_v(\alpha, 0, 0; v', w') \\ G_{v'}(u, v, w; 0, 0), & G_{vv'}(\alpha, 0, 0; 0, 0) \end{vmatrix} + \Lambda_2 \int_{-\infty+i\pi/2}^{\infty-i\pi/2} F(\alpha, \omega)\, d\alpha \begin{vmatrix} G(u, v, w; v', w'), & G_v(\alpha, \pi, 0; v', w') \\ G_{v'}(u, v, w; \pi, 0), & G_{vv'}(\alpha, \pi, 0; \pi, 0) \end{vmatrix} \quad (18)$$

$$F(u, \omega) = \frac{V(u, 0, 0)}{U(u, 0, 0)} \exp \omega x(u, 0, 0) \quad (19)$$

U and V are the usual auxiliary functions of orthogonal coordinates. The constants Λ_1 and Λ_2 have to satisfy the condition that on the lifting surface the given downwash is reproduced:

$$\iint_{(a)} dx'\,dy' \lim_{z=0} \frac{\partial}{\partial z} K(x - x', y - y', z) = 1 \quad \text{for } x, y \text{ inside } (a) \quad (20)$$

But we need a second condition in order to determine Λ_1 and Λ_2. If we assume $\Lambda_1 = \Lambda_2$, we obtain a solution giving only the Kelvin momentum and no steady lift. This was a paradox of hydrodynamics during the 19th century. If we assume $\Lambda_2 = 0$, we obtain the Kutta condition, giving smooth flow on the trailing edge $v = \pi$ and the usual lifting forces. It is of course possible to compose solutions with $\Lambda_1 > \Lambda_2 > 0$, giving forces

* This is a modification of the author's Eqs. (44) and (53) of reference 3. Both assumptions are admissible as it is easy to see, but the present one is more convenient for surface harmonics $S_n(v, w)$.

between the Kelvin and the Kutta case, and this general case seems to be more realistic. An additional condition for Λ_2/Λ_1 may be obtained by the boundary-layer theory or by measurements of the aerodynamic derivatives.

We introduce the differential operators

$$D_x = \partial/\partial x + \partial/\partial x'; \qquad D_y = \partial/\partial y + \partial/\partial y'$$

According to the difference property Eq. (5) of the kernel K we have

$$D_x K = D_y K = 0 \tag{21}$$

Eqs. (18) and (21) are compatible only by the condition

$$C_1 D_x G = C_2 D_y G = \begin{vmatrix} G_v(0, \pi, 0; v', w'), & G_{v'}(u, v, w; 0, 0) \\ G_v(0, 0, 0; v', w'), & G_{v'}(u, v, w; \pi, 0) \end{vmatrix} \tag{22}$$

C_1 and C_2 are constants. If we apply the operator D_x to Eq. (18) and replace it by Eq. (22), we obtain for the first determinant of Eq. (18)

$$\begin{vmatrix} G_v(0, \pi, 0; v', w'), & G_{v'}(u, v, w; 0, 0), & G_v(0, \pi, 0; v', w'), & G_{vv'}(\alpha, 0, 0; 0, 0) \\ G_v(0, 0, 0; v', w'), & G_{v'}(u, v, w; \pi, 0), & G_v(0, 0, 0; v', w'), & G_{vv'}(\alpha, 0, 0; \pi, 0) \\ G_{vv'}(0, \pi, 0; 0, 0), & G_{v'}(u, v, w; 0, 0), & G_{vv'}(0, \pi, 0; 0, 0), & G_{vv'}(\alpha, 0, 0; 0, 0) \\ G_{vv'}(0, 0, 0; 0, 0), & G_{v'}(u, v, w; \pi, 0), & G_{vv'}(0, 0, 0; 0, 0), & G_{vv'}(\alpha, 0, 0; \pi, 0) \end{vmatrix} = 0 \tag{23}$$

A similar equation holds for the second determinant of Eq. (18). Therefore $D_x K = 0$. By this it is proved that the kernel K given by Eq. (18) has the required difference property if and only if Eq. (22) is valid. Therefore, every characteristic function G suitable for our basic assumption Eq. (18) must satisfy the condition of compatibility Eq. (22). This the author has proved for the two-dimensional case for which the characteristic function is known explicitly:

$$G(u, v; v') = \sum_1^\infty \frac{Ne_n^{(2)}(\kappa, u)}{Ne_n^{(2)\prime}(\kappa, 0)}\, se_n(\kappa, v)\, se_n(\kappa, v') \tag{24}$$

Ne_n and se_n are Mathieu functions.

The condition of compatibility was first given by the author in a special integral form in a lecture[2] and in private communications since January, 1953. He has discovered it by comparison of solutions of the two-dimensional case obtained in two different ways, after the introduction of the characteristic function G. Recently Timman[4] has given another special integral form of this condition. But the connection with the difference-kernel property is not remarked until now.

(4) Integral Representation of Pressure

Furthermore, Eq. (22) is useful for the integral representation of the pressure of the three-dimensional subsonic case. According to Eqs. (13) and (15) we have the reduced pressure

$$p^*(x, y, z) = \iint_{(a)} dx'\, dy'\, w^*(x', y', 0) \times K_1(x - x', y - y', z) \tag{25}$$

$$K_1 = -[\omega + (\partial/\partial x)]K = -[\omega - (\partial/\partial x')]K \tag{26}$$

Because

$$\lim_{u = \pm\infty} G(u, v, w; v', w') = 0 \tag{27}$$

we obtain from Eqs. (18), (26), and (27) by integration by part and applying Kutta's condition $\Lambda_2 = 0$:

$$K_1 = -\Lambda_1 \left\{ \left(\omega - \frac{\partial}{\partial x'}\right) G(u, v, w; v', w') + G_{v'}(u, v, w; 0, 0) \times \frac{\int_{-\infty + i\pi/2}^{\infty - i\pi/2} F(u, \omega)\, du \lim_{v=0} \dfrac{\partial}{\partial v} D_x G(u, v, 0; v', w')}{\int_{-\infty + i\pi/2}^{\infty - i\pi/2} F(u, \omega)\, du\, G_{vv'}(u, 0, 0; 0, 0)} \right\} \tag{28}$$

If we normalize the characteristic function G such that $C_1 = 1$, we finally obtain from Eqs. (22) and (28) the kernel of the reduced pressure:

$$K_1 = -\Lambda_1 \left\{ [\omega - (\partial/\partial x')]\, G(u, v, w; v', w') + G_v'(u, v, w; 0, 0)\, [G_v(0, \pi, 0; v', w') T(\kappa, \omega) - G_v(0, 0, 0; v', w')] \right\} \tag{29}$$

$$T(\kappa, \omega) = \frac{\int_{-\infty + i\pi/2}^{\infty - i\pi/2} F(u, \omega) G_{vv}'(u, 0, 0; \pi, 0)\, du}{\int_{-\infty + i\pi/2}^{\infty - i\pi/2} F(u, \omega) G_{vv}'(u, 0, 0; 0, 0)\, du} \tag{30}$$

By specialization we obtain from Eqs. (25), (29), and (30) the reduced pressure of the two-dimensional subsonic case

$$p^*(u, v) = -\frac{2}{\pi} \oint_0^\pi w^*(0, v') \sin v'\, dv' \left\{ \left(\omega - \frac{1}{\sin v'} \frac{\partial}{\partial v'} \right) G(u, v; v') + G_v'(u, v; 0) \left[G_v(0, \pi; v') T(\kappa, \omega) - G_v(0, 0; v') \right] \right\} \tag{31}$$

$$T(\kappa, \omega) = \frac{\int_{-\infty + i\pi/2}^{\infty - i\pi/2} \exp(-\omega \cosh u)\, G_{vv}'(u, 0, \pi)\, du}{\int_{-\infty + i\pi/2}^{\infty - i\pi/2} \exp(-\omega \cosh u) G_{vv}'(u, 0, 0)\, du} \tag{32}$$

This result the author has already proved in his former papers in several ways. It is the simplest possible representation of the solution because it transforms term by term into the known solution for incompressible fluid. This would not be if the integration path in Eqs. (18), (28), (30), and (32) had to remain on the real half-axis. In this case the integral representation of the solutions and also their computation would be complicated considerably.

References

[1] Flax, A. H., *Reverse-Flow and Variational Theorems for Lifting Surfaces in Nonstationary Compressible Flow*, Journal of the Aeronautical Sciences, Vol. 20, No. 2, pp. 120–126, February, 1953.

[2] Kuessner, H. G., *A Review of the Two-Dimensional Problem of Unsteady Lifting Surface Theory During the Last Thirty Years*, The Institute for Fluid Dynamics and Applied Mathematics, University of Maryland, Lecture Series No. 23, April, 1953.

[3] Kuessner, H. G., *A General Method for Solving Problems of the Unsteady Lifting Surface Theory in the Subsonic Range*, Journal of the Aeronautical Sciences, Vol. 21, No. 1, pp. 17–27, January, 1954.

[4] Timman, R., *Linearized Theory of the Oscillating Airfoil in Compressible Subsonic Flow*, Journal of the Aeronautical Sciences, Vol. 21, No. 4, pp. 230–236, April, 1954.

The Generalized Shock-Expansion Method and Its Application to Bodies Traveling at High Supersonic Air Speeds

A. J. EGGERS, JR.,* RAYMOND C. SAVIN,* AND CLARENCE A. SYVERTSON*

Ames Aeronautical Laboratory, NACA

SUMMARY

It is demonstrated that the shock-expansion method can be generalized to treat a large class of hypersonic flows, only one of which is flow about airfoils. This generalized method predicts the whole flow field, including shock-wave curvatures and resulting vorticity, providing that (1) disturbances originating on the surface of an object are largely absorbed in shock waves with which they interact and (2) disturbances associated with the divergence of stream lines in tangent planes to the surface are of secondary importance compared to those associated with the curvature of stream lines in planes normal to the surface. It is shown that these conditions may be met in three-dimensional as well as two-dimensional hypersonic flows. When they are met, surface streamlines may be taken as geodesics, which, in turn, may be related to the geometry of the surface.

The validity of the generalized shock-expansion method for three-dimensional hypersonic flows is checked by comparing predictions of theory with experiment for the surface pressures and bow shock waves of bodies of revolution. The bodies treated are two ogives having fineness ratios of 3 and 5. Tests were conducted at Mach Numbers from 2.7 to 6.3 and angles of attack up to 15 degrees in the 10- by 14-in. supersonic wind tunnel of the Ames Aeronautical Laboratory. At the lower angles of attack, theory and experiment approach agreement when the ratio of Mach Number to fineness ratio—that is, the hypersonic similarity parameter—exceeds 1. At the larger angles of attack, theory tends to break down, as would be expected, on the leeward sides of the bodies.

As a final point, it is inquired if the two-dimensionality of inviscid hypersonic flows has any counterpart in hypersonic boundary-layer flows. The question is answered in the affirmative, and results of experiment are employed to provide a partial check of this conclusion.

INTRODUCTION

THE SHOCK-EXPANSION METHOD has been widely and, for the most part, successfully used in calculating flow about airfoils traveling at moderate supersonic speeds. This method is, of course, a synthesis of two basic mathematical tools for treating supersonic flows—namely, the oblique shock equations of Rankine and Hugoniot and the corner expansion equations of Prandtl and Meyer. As was early observed by Epstein,[1] the method has the inherent advantage (over potential flow theories) of accounting for changes in entropy through strong shock waves. In this respect, then, the shock-expansion method is especially well suited for treating hypersonic flows about airfoils, inasmuch as these flows are usually characterized by strong shock waves.

The leading-edge shock wave interacts strongly, however, with Mach waves originating at the surface of an airfoil in hypersonic flight. This phenomenon can appreciably alter the shape of the shock wave and the flow downstream thereof, especially in the case of curved airfoils. Evidently, then, shock-wave - Mach-wave interaction must be investigated to determine the extent of applicability of the shock-expansion method to two-dimensional hypersonic flows.

The interaction phenomenon has, in fact, been studied by numerous investigators including Lighthill,[2] Pai,[3] and the present authors.[4]† Unfortunately these studies yield widely different answers for hypersonic flow, with the result that the applicability of the shock-expansion method remains in doubt. It is therefore undertaken as the first objective of this paper to resolve these differences, and it is demonstrated, as originally proposed by the authors,[4] that the major effects of the interaction phenomenon can be accounted for with the shock-expansion method when it is properly generalized.

Studies of more complex two- and three-dimensional flows have led to the discovery[5, 9] that flow about airfoils is only one of a large class of hypersonic flows that can be treated by the generalized shock-expansion method. It is undertaken, therefore, as the second objective of this paper to describe how this method can be employed to predict a complete three-dimensional flow field, including shock-wave curvatures and resulting vorticity. The validity of the method for three-dimensional hypersonic flows is checked by comparing the predictions of theory with experimental results for the surface pressures and bow shock waves of lifting and nonlifting bodies of revolution at Mach Numbers from 2.7 to 6.3.

As a final point, we inquire if the two-dimensional character of inviscid hypersonic flows has any counterpart in hypersonic boundary-layer flows. It is concluded that such a counterpart does exist, and recourse

Presented at the Aerodynamics Session, National Summer Meeting, IAS, Los Angeles, June 21–24, 1954.

* Aeronautical Research Scientist.

† Crocco[5] and Munk and Prim[6] treated the subject in connection with their investigations of flow at the nose of an airfoil. Boa-Teh Chu[7] considered the general problem; however, through a misinterpretation of his results, he arrived at erroneous conclusions regarding the strength of reflected disturbances.

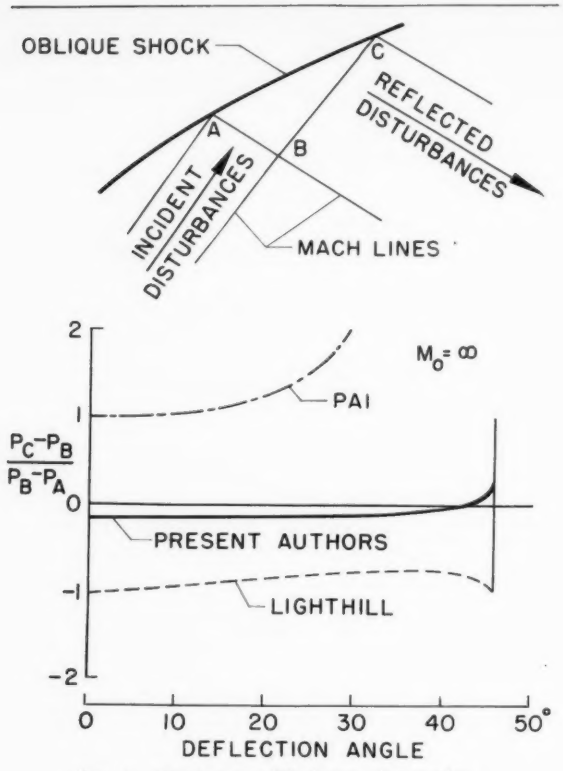

FIG. 1. Shock-wave - Mach-wave interaction.

is made to the experimental pressure-distribution data to obtain a partial check on this observation.

SHOCK-WAVE - MACH-WAVE INTERACTION AND THE GENERALIZED SHOCK-EXPANSION METHOD

The interaction problem may, for our purposes, be reduced to the determination of how large a fraction of a disturbance incident on a shock wave is reflected from the wave. To aid in our discussion of this problem, attention is called to Fig. 1. The sketch in the upper part of this figure shows an element of a curved oblique shock wave. The disturbances incident on this wave are propagated along the upward sloping Mach lines, while those reflected from the wave are propagated along the downward sloping Mach lines. We see that a measure of the strength of the disturbances incident on the wave is given by the change in pressure along the line AB, while a measure of the strength of the disturbances reflected from the wave is given by the change in pressure along the line BC. The ratio of the change along BC to that along AB is, then, a measure of the degree to which disturbances are reflected from the oblique shock wave. This ratio can be calculated by considering an infinitesimal element of the shock wave and by employing the compatibility relations for fluid properties along characteristic or Mach lines in combination with the oblique shock equations. It was precisely this method that was used by the present authors[4] in studying shock-wave - Mach-wave interaction, and the results obtained at a free-stream Mach Number, M_0, of infinity are shown in the lower part of Fig. 1. It is seen that the ratio is small compared to 1, except at extremely large deflection angles (close to those for shock detachment). The methods of Lighthill and Pai are not intrinsically different from that employed by the present authors, and yet we observe that Lighthill's equations give negative values of this ratio which are in the neighborhood of -1, while according to Pai, correspondingly large positive values are obtained. Lighthill's values are found to be inordinately large (negatively) as a result of an algebraic error made in his analysis. When this error is corrected, his results agree with those of the present authors.* The large positive values due to Pai result from partially neglecting entropy gradients in the flow downstream of the curved shock wave. When Pai's analysis is corrected, results are obtained which also agree with those of the present authors. It is concluded, therefore, that disturbances are, in general, only weakly reflected from shock waves in the flow. The fact that the shock-expansion method ignores these reflected disturbances should not, then, appreciably affect its applicability to the calculation of flow at the surface of an airfoil in hypersonic flight.

Now it is natural to inquire if, in the case of two-dimensional flow, the shock-expansion method can be generalized to give, in addition to surface conditions, fluid properties throughout the whole flow field. Our studies of shock-wave - Mach-wave interaction strongly suggest that such a generalization can be achieved inasmuch as it was found that disturbances are almost entirely absorbed in shock waves with which they interact. Thus, let us assume that they are, in fact, entirely absorbed, and let us see what this means in terms of the construction of the flow field. For this purpose, attention is called to Fig. 2 where flow about an airfoil is shown schematically. Mach Number and pressure at the surface are calculated employing the oblique shock equations and the isentropic expansion equations in the usual fashion. Several points on the surface of the

* Professor Lighthill has concurred in this matter in a private communication to the senior author.

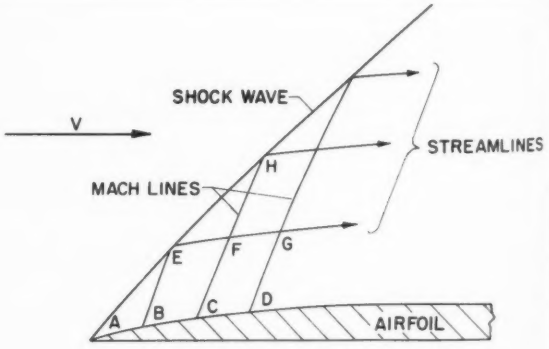

FIG. 2. Calculation of flow about an airfoil.

airfoil are chosen to start the construction of the flow. For purposes of simplicity we assume that the initial element of the oblique shock wave emanating from the leading edge is straight. The intersection of this element with the Mach line emanating from point B on the surface is then calculated by simple trigonometry. At the point of intersection it is assumed that the Mach wave is entirely absorbed in the shock wave. This is tantamount to requiring that flow conditions downstream of the shock wave (beyond point E) conform in terms of pressure* to those along the Mach line BE. The inclination of the shock wave at point E is thus fixed. Let us proceed to construct the Mach line emanating from the airfoil surface at point C. The intersection of this line with the stream line passing through point E is determined trigonometrically. Now, as this Mach line propagates beyond point F, it enters a flow field of slightly different Mach Number, and its inclination must be changed accordingly. With the new slope of this Mach line, we calculate its intersection at point H with the segment of shock wave extending beyond point E. At the intersection of these waves the attitude of the shock wave is again changed to satisfy the requirement that flow downstream of the wave (beyond point H) must have the same pressure as exists on the Mach line at point H. We proceed then to construct the whole flow field about the airfoil in this manner, and it is observed that the calculation is greatly simplified by comparison to the method of characteristics which requires that corrections be continuously made for disturbances propagated along the family of Mach lines proceeding from the shock toward the surface.†

In order to check some of these observations, shock-wave shapes and surface pressures were calculated with the generalized shock-expansion method and with the method of characteristics for a 10 per cent thick biconvex airfoil at zero incidence and a free-stream Mach Number of infinity. The calculations were made for an ideal diatomic gas, and the results are presented in Fig. 3. The shock waves are shown in the upper part of the figure, and it is seen that they are in rather close agreement. Due to the interaction phenomenon, both waves curve well away from the straight shock wave, having the correct slope at the leading edge. Shown on the lower part of Fig. 3 are the pressure distributions given by the two methods, and it is seen that they differ only slightly. As a final point, it should be emphasized that these results at a Mach Number of infinity represent a severe test of the generalized shock-expansion method. Comparable studies of flow about curved

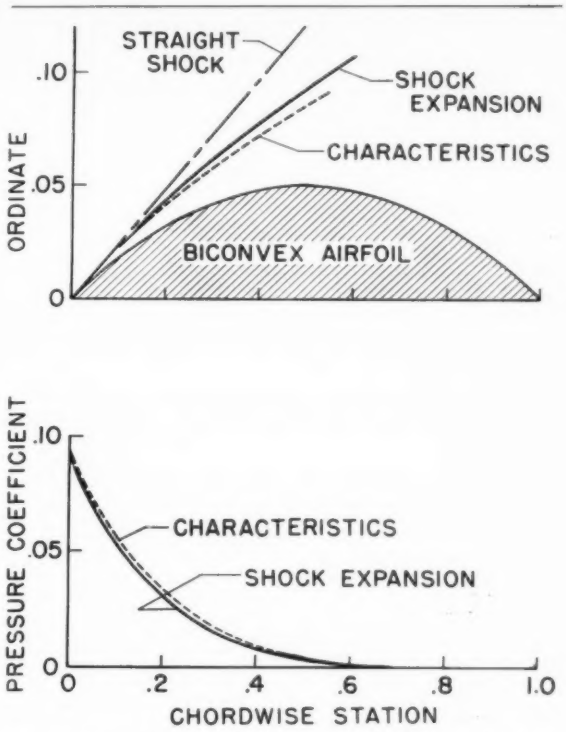

FIG. 3. Shock wave and pressures for a 10-per cent-thick biconvex airfoil at $M_\infty = \infty$.

airfoils at Mach Numbers from 3.5 to 15 show even smaller departures of the predictions of this method from those of the characteristics method.[4] Evidently, then, the generalized method is capable of predicting the disturbed flow field about airfoils in hypersonic flight.

We inquire next about the applicability of the method to three-dimensional hypersonic flows.

Application of the Generalized Shock-Expansion Method to Three-Dimensional Hypersonic Flows

In this study the specific questions asked are *when* and *how* can the generalized shock-expansion method be employed to calculate three-dimensional hypersonic flows? In order to answer these questions, we use the fact that the disturbed flow field extends only a short distance away from the surface of a body—that is to say, shock waves lie close to the surface. Thus it is reasonable to assume that the disturbed flow can be treated approximately by confining our attention to the immediate neighborhood of the surface. It is convenient then to consider the equations defining the steady adiabatic flow of a continuous fluid with reference to a local coordinate system. In particular, a rectangular coordinate system is chosen in which the X axis is tangent to a stream line at a point on the surface of a body. The Z axis is taken normal to the surface at the point of tangency, while the Y axis is tangent to the surface at the origin of coordinate system. Stream lines in the X-Z and X-Y planes would appear

* To the accuracy of this analysis they also then conform in terms of flow inclination.

† It has been our experience, for example, that the time required to construct a two-dimensional flow field by the generalized shock-expansion method is, at most, about 20 per cent of that required for the characteristics method. Surface pressures can, of course, be obtained in a matter of minutes with the shock-expansion method.

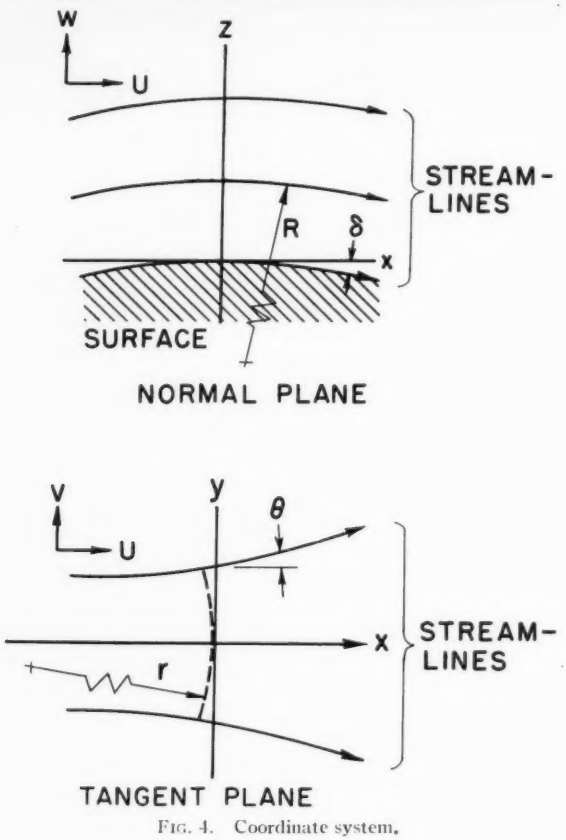

FIG. 4. Coordinate system.

something like those shown in Fig. 4. If we take U, V, and W as the components of velocity in the directions of the X, Y, and Z axes, respectively, the continuity equation becomes near the origin of the coordinate system

$$[\partial(\rho U)/\partial X] + \rho[(\partial V/\partial Y) + (\partial W/\partial Z)] = 0 \quad (1)$$

where ρ is the local density. Similarly, the momentum equations may be written

$$[U(\partial U/\partial X)] + [(1/\rho)\ (\partial P/\partial X)] = 0 \quad (2)$$

$$[U(\partial V/\partial X)] + [(1/\rho)\ (\partial P/\partial Y)] = 0 \quad (3)$$

$$[U(\partial W/\partial X)] + [(1/\rho)\ (\partial P/\partial Z)] = 0 \quad (4)$$

where P is the local static pressure. Now, if a strictly three-dimensional flow is to be calculated with the generalized shock-expansion method, then this flow must be at least locally two-dimensional. Intuitively one guesses* that this two-dimensionality occurs in planes normal to the surface of a body—that is, the X-Z planes. In this event we deduce from the continuity equation that

$$|\partial W/\partial Z| \gg |\partial V/\partial Y| \quad (5)$$

* This guess can be substantiated with mathematical reasoning.[9]

Noting that the velocities V and W are proportional to the flow inclination angles θ and δ, respectively (see Fig. 4), and using the transformation†

$$\partial\delta/\partial Z \cong -\sqrt{M^2 - 1}(\partial\delta/\partial X)$$

where M is the local Mach Number, Eq. (5) becomes

$$|\partial\delta/\partial X| \gg (1/\sqrt{M^2 - 1})|\partial\theta/\partial Y| \quad (6)$$

This expression determines *when* the generalized shock-expansion method can be employed to calculate three-dimensional hypersonic flows.‡ Physically, it may be interpreted to mean that disturbances associated with the divergence of stream lines in planes tangent to a surface must be of secondary importance compared to those associated with the curvature of stream lines in planes normal to the surface.

It is evident from Eq. (6) that increasing the Mach Number of the flow tends to make it appear locally more two-dimensional and, by the same token, more amenable to solution with the generalized shock-expansion method. Obviously, too, how high the Mach Number must be is determined by the shape of the body.** It follows, then, that the hypersonic similarity parameter relating body shape and Mach Number is a significant index to when the method can be employed for a particular class of bodies.

The remaining question to be answered is how can the generalized method be employed? Part of the answer to this question is self-evident; when Eq. (6) is satisfied, flow in planes tangent to surface stream lines and normal to the surface of three-dimensional bodies can be constructed with the generalized shock-expansion method after the manner developed for airfoils (see Fig. 2). The real problem, then, is to locate the surface stream lines. For this purpose it is observed that pressure gradients transverse to planes of essentially two-dimensional flow must be small by comparison to gradients in these planes. Hence, it follows from the

† The complete transformation is

$$\partial\delta/\partial z = -\sqrt{M^2 - 1}(\partial\delta/\partial X) + [M(\partial\delta/\partial C_1)]$$

where C_1 is a first-family Mach line (positively inclined with respect to a stream line). In flows of interest here, however, disturbances emanating from the surface are large compared to those reflected back to the surface (see discussion of shock-wave-Mach-wave interaction) and hence

$$|\partial\delta/\partial C_1| << (\sqrt{M^2 - 1}/M)|\partial\delta/\partial X|$$

‡ This observation is easily verified by combining Eqs. (1), (2), and (6) with the energy equation $\partial S/\partial X = 0$ and the state equation $\rho = \rho(P, S)$, where S is entropy, to obtain the differential equation of Prandtl and Meyer for flow along a stream line—namely,

$$dP/d\delta \cong \rho U^2/\sqrt{M^2 - 1}$$

** There are shapes, of course, like the right circular cone, for which the flow does not become strictly two-dimensional, irrespective of the magnitude of the Mach Number.[8]

momentum Eqs. (3) and (4) that (replacing velocities with flow inclination angles)

$$\left|\partial\theta/\partial X\right| \ll \left|\partial\delta/\partial X\right| \tag{7}$$

This equation states, in effect, that surface stream lines may be taken as geodesics; thus it establishes *how* the generalized method can be employed.

Geodesics are functions of the geometry of a surface and are perhaps most often identified as lines of shortest distance between two points.[10] They are also uniquely defined if their directions are known at a point. This is a useful property in many cases because stream-line directions can often be determined at the leading edge, or edges, of an object in hypersonic flow, independent of how complex its general shape may be.

We are now in a position to apply the generalized shock-expansion method to the calculation of three-dimensional hypersonic flow* about particular shapes. Bodies of revolution are of interest, so it will be undertaken to apply the theory to these shapes, and further, the results of theory will be compared with experiment.

Comparison of Theory and Experiment for Bodies of Revolution

It was suggested in the previous discussion that the hypersonic similarity parameter is a significant index to when the generalized shock-expansion method can be applied to three-dimensional flows. For bodies of revolution, this parameter, K, may be defined as the ratio of free-stream Mach Number, M_0, to fineness ratio, l/d; thus $K = M_0/(l/d)$. An analysis,[8] based primarily on Eq. (6), indicates that the generalized method is applicable to such bodies when K is greater than about 1.

The next problem is to determine the geodesics of a body which may be taken as surface stream lines. We know that these stream lines originate at the vertex. The only pertinent geodesics passing through the vertex are the meridian lines; hence the meridian lines are, to the accuracy of this analysis, the surface stream lines. This result is exactly true for noninclined bodies of revolution but can only be considered an approximation for inclined bodies. The calculation of flow about a body proceeds then as follows: Flow at the vertex is assumed known either from cone theory or from experiment. Flow downstream of the vertex along the surface stream lines is determined with the Prandtl-Meyer expansion equations in the same manner as for airfoils. The flow field between the body and the shock is constructed in meridian planes by assuming the pressure is essentially constant along Mach lines emanating from the surface—the construction in each plane parallels that for an airfoil.

The theory of when and how to apply the generalized shock-expansion method to bodies of revolution is now established. It remains then to determine if the method really works. For this purpose, experiments were conducted in the Ames 10- by 14-in. supersonic wind tunnel[11] on two ogives having fineness ratios of 3 and 5 and base diameters of 1.5 in. These bodies were tested at angles of attack of 0°, 5°, 10°, and 15°. The test Mach Numbers and Reynolds Numbers were as follows:

Mach Number	Reynolds Number (based on body diameter)
2.73	1.06 million
4.25	1.09 million
5.05	0.52 million
6.30	0.22 million

Surface pressures were measured in all cases (usually with McLeod gages), and bow shock waves were photographed with the aid of a schlieren apparatus. These data were also obtained for two cones having the same vertex angles as the ogives.

It is appropriate first to compare theoretical and experimental pressures acting on the bodies at zero angle of attack. The results for the fineness ratio 3 ogive demonstrate the important points, as we can see from a study of Fig. 5. Here, predictions of both the shock-expansion method† and characteristics theory[13] are shown along with experimental data. Corresponding to the Mach Number range of 2.73 to 6.30, the range of the hypersonic similarity parameter is from 0.91 to 2.10.

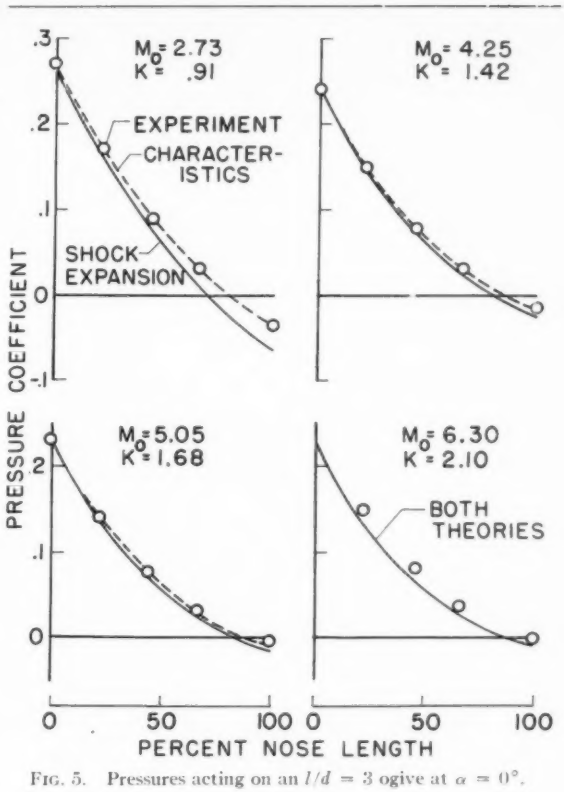

FIG. 5. Pressures acting on an $l/d = 3$ ogive at $\alpha = 0°$.

* It should be noted that the previous discussion of steady flows can be extended over to nonsteady flows about slender shapes.[9]

† In this case reliable theoretical results for the conical flow at the vertex are available[12] and have been employed.

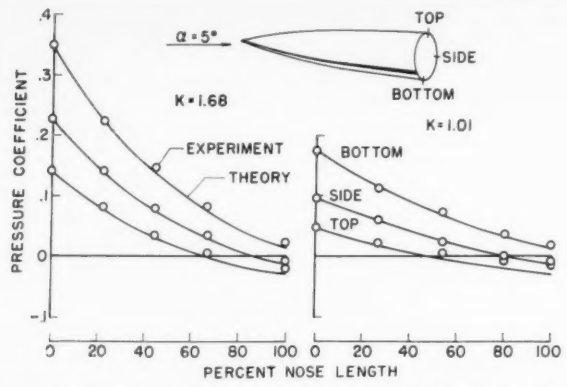

FIG. 6. Pressures acting on ogives at $M_0 = 5.05$ and $\alpha = 5°$.

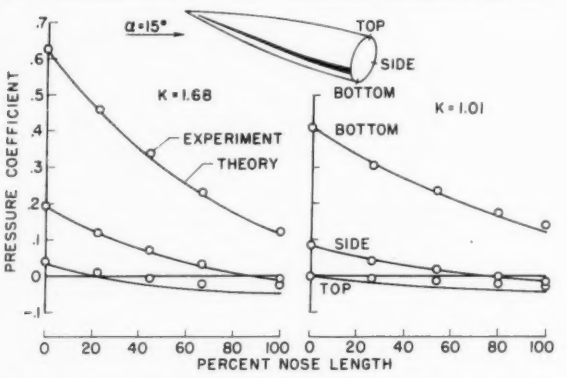

FIG. 7. Pressures acting on ogives at $M_0 = 5.05$ and $\alpha = 15°$.

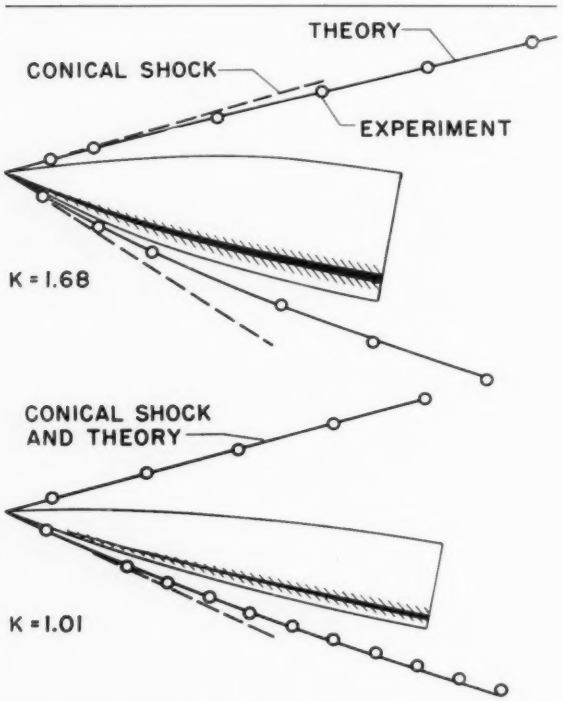

FIG. 8. Shock waves for ogives at $M_0 = 5.05$ and $\alpha = 10°$.

We observe that, in accordance with theory, the generalized shock-expansion method predicts surface pressure coefficients close to those obtained experimentally at values of the similarity parameter greater than 1. As would be expected, too, the agreement between these predicted coefficients and experiment tends to improve up to a Mach Number of 5. At the highest Mach Number of 6.30, we observe, however, that both the generalized method and characteristics theory give pressure coefficients that, although in agreement, are appreciably lower than experiment. There is no particular reason, on the basis of past experience or otherwise, to doubt the accuracy of the characteristics theory for this body. In this connection we note that the theory is in good agreement with experiment at all the lower Mach Numbers. It seems logical, therefore, to suspect that the departure of theory from experiment at $M_0 = 6.3$ is caused by viscous effects in the flow. More specifically, it is suggested that this departure may be traced to a substantial increase in thickness of the laminar boundary layer on the ogive. The low Reynolds Number of the tests and, to a somewhat lesser extent, the high Mach Number could produce such an increase. This matter will be considered further in connection with our study of the hypersonic boundary layer later in the paper.

Attention is now turned to flow about the inclined bodies. We will first concern ourselves with the surface pressures on the fineness ratio 3 and 5 ogives at a Mach Number of 5.05. Fig. 6 shows the pressure distributions according to the generalized shock-expansion method and experiment for three meridian planes corresponding to the bottom, the side, and the top of each body. In the application of the generalized method, the flow at the vertex was determined from the experimental results obtained with the cones that were tested.* The angle of attack is 5 degrees. Values of the hypersonic similarity parameter, K, for each body are also shown. For the fineness ratio 3 ogive, K is 1.68, while for the fineness ratio 5 ogive, K is 1.01. As would be expected, the agreement between theory and experiment is good for the fineness ratio 3 ogive. With the fineness ratio 5 ogive, nearly the same agreement is obtained except on the top or leeward side of the body where the generalized method gives too low pressures. The pressure distributions for these same two bodies inclined 15° are shown in Fig. 7. Here we observe that the agreement between theory and experiment is much the same as it was at 5° angle of attack. The tendency of the generalized method to give too low pressures on the top of a body has also become evident, however, in the case of the fineness ratio 3 ogive ($K = 1.68$).

* Experimental results for the conical flow at the vertex are also used in all other comparisons between theory and experiment (both for pressures and shock-wave shapes) made for the inclined bodies. This procedure was employed, rather than using theory as in the noninclined case, since reliable theoretical results for inclined cones, such as the second-order solutions of Stone-Kopal,[14] are not available at the high Mach Numbers of interest here.

The method is, of course, strictly applicable only at small angles of attack; hence the appearance of this error is not surprising. Nevertheless, it may be expected too that at 15° angle of attack viscous cross-flow effects[15] are influencing surface pressures, especially on the extreme leeward side of the body.

Surface pressures provide, of course, only a partial check of the generalized shock-expansion method—a check, so to speak, only at the inner boundary of the disturbed flow field. It is of interest, then, to check the method at the outer boundary of the disturbed flow—that is, at the bow shock wave. For this purpose, the bow waves for the fineness ratio 3 and 5 ogives at a Mach Number of 5.05 and 10° angle of attack were calculated in the plane of symmetry with the generalized method, and they are compared in Fig. 8 with those obtained experimentally. The conical shock waves created by the cones having the same vertex angles as the ogives are also shown for contrast. We observe in the case of the fineness ratio 3 ogive that theory and experiment are in excellent agreement. In the case of the fineness ratio 5 ogive, much the same observation can be made. This latter result would, in view of the marginal value of the similarity parameter ($K = 1.01$), seem somewhat fortuitous.

As an overall check on the generalized shock-expansion method, it is appropriate to consider the forces experienced by the ogives. To this end the normal-force coefficients were obtained by integration of the theoretical and experimental pressure distributions.* The results are shown in Fig. 9, and we observe again that the agreement between theory and experiment is better at the higher value of the similarity parameter. Axial forces have also been obtained for these ogives, and the shock-expansion method is found to apply with essentially the same accuracy.

Up to now we have considered only inviscid flow at high supersonic air speeds. In the treatment of bodies of revolution just completed, we noted, however, what appeared to be an indirect effect of viscosity—namely, an appreciable alteration of surface pressures by boundary-layer growth at the highest test Mach Number. We are reminded, therefore, of the important role played by viscosity in hypersonic flows, and we are led to inquire if the two-dimensionality of inviscid hypersonic flows has any counterpart in the hypersonic boundary layer. This matter is the final topic of discussion.

Hypersonic Boundary-Layer Flows

The arguments presented here are concerned with the steady hypersonic boundary layer, and they will

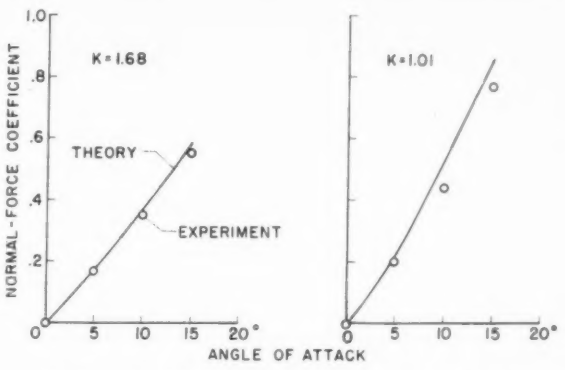

FIG. 9. Normal forces acting on ogives at $M_0 = 5.05$.

be, for the most part, physical.† Furthermore, they will appear as natural extensions of conclusions reached in our study of inviscid hypersonic flow. Let us reconsider, then, the motion of the inviscid fluid. We have established that this motion is, under certain well-defined circumstances, confined locally to planes normal to the surface of a body and tangent to surface stream lines. Correspondingly, there is no sensible momentum transfer across these planes. Now if viscous forces are set up in the flow bounding the surface, we recognize that they will act to resist the motion of the fluid—that is, the motion in the normal planes. Evidently, then, these forces act in the same planes of local two-dimensional flow as the pressure forces, and it must follow, of course, that resultant changes in momentum of the fluid also occur in these planes.

Consider now the changes in energy of the disturbed fluid. These changes can be brought about by viscous or dissipative work, pressure work, heat convection, and heat conduction.‡ It was just found, however, that the forces doing work act in the normal planes; hence we conclude that the corresponding changes in energy occur in these planes. Similarly, heat is convected in the normal planes, since mass is convected in these planes. Finally, we conclude also that heat is conducted locally in the normal planes inasmuch as the temperature gradients set up by the action of viscous forces are confined primarily to these planes.** Evidently, then, changes in energy of the fluid can be

* This integration was performed using pressure distributions obtained in the five equally spaced meridian planes between the bottom and the top of the body.

† Although not presented, corresponding mathematical arguments have been pursued using the Navier-Stokes and energy equations, and the final results confirm those obtained here. It is indicated too that these results *may* apply also to nonsteady boundary-layer flows.

‡ Radiation and absorption may, of course, also contribute to energy changes; however, it is beyond the scope of this paper to consider these phenomena.

** One might conceive of severe temperature gradients being imposed at the wall boundary by, for example, extremely nonuniform surface cooling. Such gradients, if transverse to stream lines, would naturally invalidate this argument.

treated locally as a two-dimensional phenomenon in planes normal to the surface of a body.

Thus far we have been concerned mainly with forces and their relation to the momentum and energy of the fluid. The question of conserving mass remains to be investigated. It will be recalled that the requirement of conservation of mass determined *when* the generalized shock-expansion method could be employed to calculate three-dimensional flows. This requirement is physically (and mathematically) the same, independent of whether or not viscous forces come into play. We conclude then that for the purposes of this study Eq. (6) can be used to determine *when* the three-dimensional boundary layer can be calculated with two-dimensional equations. From Eq. (6) it is indicated that the boundary layer must be largely hypersonic if this calculation is to be permissible. It is not to be implied, however, that the boundary layer always becomes two-dimensional, as on an airfoil, if the stream Mach Number is made extremely large. For example, in the case of axial flow about the right circular cone, Eq. (6) is violated independent of Mach Number,* and we must use something like the Mangler transformation[16] to obtain the boundary layer. On the other hand, if the body, instead of being conical, is curved in the stream direction, then it is indicated that the boundary-layer flow should approach the two-dimensional type with increasing Mach Number.

To check these observations experimentally in any detail is beyond the scope of the present paper; however, we can obtain a partial check with relative ease. This was done by using simple two-dimensional theory[17] to calculate the laminar boundary layer on the fineness ratio 3 ogive at zero incidence and a Mach Number of 6.3.† The body ordinates were increased by an amount equal to the displacement thickness of the boundary layer. The pressure distribution about the distorted body was then obtained with the generalized shock-expansion method. This corrected pressure distribution and the original uncorrected distribution are presented in Fig. 10 along with experiment. We observe that while uncorrected pressures are definitely low, the corrected pressures are in good agreement with experiment. In this case, then, the relatively simple methods of correcting airfoil pressure distributions for boundary-layer growth are, as indicated by theory, suitable for application to the body of revolution.

* Recall that this violation was also encountered in the case of inviscid flow about the cone (see footnote† on p. 234).

† The theory breaks down at the vertex of the body, much as at the leading edge of an airfoil. It is therefore not applied in this region, and, consistent with a practice successfully employed with airfoils, viscous effects are ignored in calculating flow at the vertex.

Concluding Remarks

In conclusion, it is appropriate to digest our results and to indicate the overall implications of this study. First, it is recalled that by virtue of Mach waves being largely absorbed in shock waves with which they interact, the whole disturbed flow field about an airfoil can be easily calculated with a generalized shock-expansion method. Further, it was demonstrated that this generalized method can be applied to the calculation of three-dimensional hypersonic flow fields, providing that disturbances associated with the divergence of stream lines in planes tangent to the surface of a body are of secondary importance compared to those associated with the curvature of stream lines in planes normal to the surface. Bodies of revolution were cited as an example of shapes producing flow fields satisfying this requirement. A comparison of theory with experiment substantiated this contention, showing that the generalized method predicted the surface pressures and bow shock waves of ogives when the hypersonic similarity parameter of the flow was greater than about 1. Finally, the two-dimensional concept of three-dimensional hypersonic flows was extended to steady boundary-layer flows, and a partial experimental check of the validity of this extension was obtained.

In the light of these results, we conclude that the generalized shock-expansion method should prove useful in treating three-dimensional hypersonic flow fields about practical aerodynamic configurations. Furthermore, it is proposed that methods of treating two-dimensional hypersonic boundary layers may, in like manner, prove useful in predicting three-dimensional hypersonic boundary layers.

References

[1] Epstein, Paul S., *On the Air Resistance of Projectiles*, Proceedings of the National Academy of Sciences, Vol. 17, pp. 532–547, 1931.

[2] Lighthill, M. J., *The Flow Behind a Stationary Shock*, Philosophical Magazine, Ser. 7, Vol. 40, pp. 214–220, February, 1949.

(*Continued on page 248*)

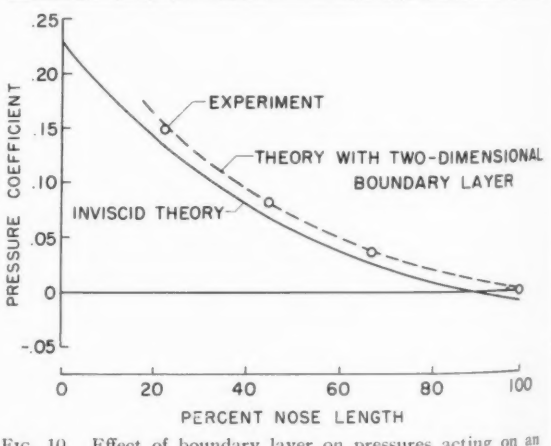

FIG. 10. Effect of boundary layer on pressures acting on an $l/d = 3$ ogive at $M_0 = 6.30$ and $\alpha = 0°$.

The Lift and Moment on a Ring Concentric to a Cylindrical Body in Supersonic Flow

F. EDWARD EHLERS*

Boeing Airplane Company and Oregon State College

SUMMARY

The supersonic flow at an angle of attack about a ring concentric to an infinite circular cylinder has been computed using linearized supersonic flow theory. Asymptotic formulas for the lift and moment on the body and on the ring have also been obtained. Several graphs of pertinent data for the cylindrical ring of zero thickness are given for ready reference.

NOTATION

A = aspect ratio
C = coefficient (such as Cp = pressure coefficient)
H = inverse Laplace transform of $\dfrac{I_0(p\beta R)K_1(p\beta) + I_1(p\beta)K_0(p\beta R)}{I_1(p\beta R)K_1(p\beta) - I_1(p\beta)K_1(p\beta R)}$
I_ν, K_ν = Bessel functions of imaginary argument (notation of Watson[1])
J_ν, Y_ν = Bessel functions of first kind (notation of Watson[1])
l = length of ring in units of cylinder radius
L = lift force
$L(l/\beta R)$ = lift function of Ward[1] for ring exterior
M = Mach Number of free stream
$M(l/\beta R)$ = moment function for ring exterior
m = moment on ring or body
p = Laplace transform variable (also pressure)
r = radial distance from axis in units of cylinder radius
R = mean radius of ring
$R(x)$ = radius of ring at station x
U = velocity of free stream
$V(x/\beta R)$ = pressure function for ring exterior
$W(x/\beta R)$ = inverse Laplace transform of $\dfrac{K_1(p\beta R) - K_0(p\beta R)}{K_1(p\beta R)}$
x = axial coordinate
z = $x/[\beta(R-1)]$
α = angle of attack
β^2 = $M^2 - 1$
δ_n = $\{(d/d\lambda)\,[J'_1(\lambda\beta R)Y_1'(\lambda\beta) - J_1'(\lambda\beta)Y_1'(\lambda\beta R)]\}_{\lambda=\mu_n}$
θ = azimuth angle in plane x = constant
ϕ = velocity potential
φ = perturbation velocity potential
φ_0 = perturbation velocity potential for symmetrical flow
φ_1 = perturbation velocity potential for cross flow
λ = p/i
λ_n = nth root of $J_1(\lambda\beta R)Y_1(\lambda\beta) - J_1(\lambda\beta)Y_1(\lambda\beta R) = 0$
μ_n = nth root of $J_1'(\lambda\beta R)Y_1'(\lambda\beta) - J_1'(\lambda\beta)Y_1'(\lambda\beta R) = 0$
τ = $l/[\beta(R-1)]$
$\chi(r)$ = $I_1(p\beta r)K_1'(p\beta) - I_1'(p\beta)K_1(p\beta r)$
ψ_n = $\{(d/d\lambda)\,[J_1(\lambda\beta R)Y_1(\lambda\beta) - J_1(\lambda\beta)Y_1(\lambda\beta R)]\}_{\lambda=\lambda_n}$

Received March 29, 1954. Revised and received October 20, 1954.

* Aerodynamicist, Boeing Airplane Company, on leave from the Mathematics Department, Oregon State College.

Subscripts and Superscripts

$_0$ = moment about $x = 0$, $r = 0$ (on m)
$_e$ = exterior or outer part of ring
$_i$ = ring interior
$_w$ = ring surface
$_b$ = body

INTRODUCTION

THIS COMPUTATION IS MADE in order to obtain an estimate of the lift and moment for a ring airfoil around an axially symmetric body. To simplify the computation, the body is chosen as an infinite circular cylinder of radius unity in a supersonic stream at an angle of attack, α. Concentric to the cylinder is a ring of length l (see Fig. 1). The inner and outer radii of this ring are assumed to vary only slightly from the constant value R. With small angle of attack, then, the assumptions of the linearized theory are satisfied, and the perturbation velocity potential φ is a solution of the differential equation

$$\varphi_{rr} + [(1/r)\varphi_r] - \beta^2\varphi_{xx} + (\varphi_{\theta\theta}/r^2) = 0$$

where $\beta = \sqrt{M^2 - 1}$ and r, θ, x are the usual cylindrical coordinates. To simplify the solution, the complete velocity potential ϕ is assumed to have the form

$$\phi = U\{x + \alpha[r + (1/r)]\cos\theta + \varphi_0(x, r) + \alpha\cos\theta\,\varphi_1(x, r)\}$$

The first two terms in the braces can be recognized as

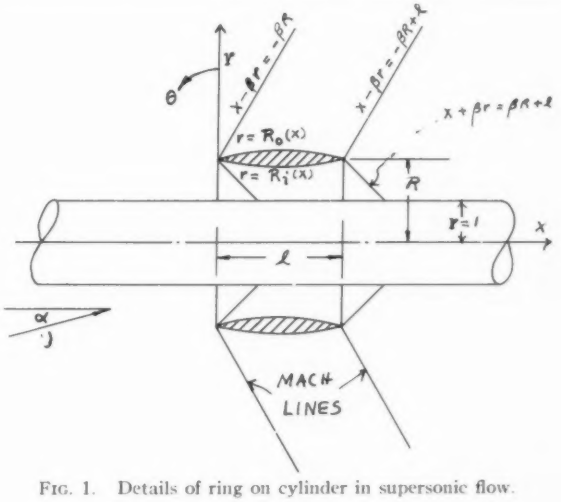

FIG. 1. Details of ring on cylinder in supersonic flow.

the velocity potential for the flow of velocity U over an infinite circular cylinder at a small angle of attack α. The potentials φ_0 and φ_1 are the perturbation potentials induced by the concentric ring, and they vanish identically for $x < 0$—i.e., ahead of the concentric ring. The method of solution is to apply the Laplace transform to the boundary conditions and the differential equations for φ_0 and φ_1. This reduces the problem to the solution of ordinary differential equations for the transforms of φ_0 and φ_1 with linear boundary conditions.

Occurring downstream of the ring is a vortex sheet. Under the assumption that this vortex sheet consists of a cylinder of radius R, the conditions of continuity of pressure and continuity of flow direction across the sheet leads to the result that the cross flow potential, φ_1, be identically zero for the region downstream of the Mach lines emanating from the trailing edge of the ring. Thus the pressure distribution that affects the lift and moment on the body is influenced by the ring only in the region $x = \beta(R-1)$ to $x = l + \beta(R-1)$.

General Theory and the Derivation of Results

(I) *Derivation of the Potentials φ_0 and φ_1*

Let the velocity potential for the supersonic flow be given by

$$\left.\begin{aligned}\phi &= U\{x + \varphi(x, r, \theta)\} \\ &= U\{x + \alpha\cos\theta[r + (1/r)] + \varphi_0(x, r) + \\ &\qquad \alpha\cos\theta\,\varphi_1(x, r)\}\end{aligned}\right\} \tag{1.1}$$

Since $\varphi(x, r\theta)$ must satisfy the equation in the introduction, it follows from the form of φ given in the second of Eqs. (1.1) that the potentials φ_0 and φ_1 must satisfy, respectively,

$$\varphi_{0rr} + (1/r)\varphi_{0r} - \beta^2\varphi_{0xx} = 0 \tag{1.2}$$

$$\varphi_{1rr} + (1/r)\varphi_{1r} - \beta^2\varphi_{1xx} - (\varphi_1/r^2) = 0 \tag{1.3}$$

Now if we multiply the above equations by pe^{-px} and integrate each derivative with respect to x from 0 to infinity and integrate the φ_{0xx} and φ_{1xx} terms by parts twice, we obtain

$$\bar{\varphi}_{0rr} + (1/r)\bar{\varphi}_{0r} - p^2\beta^2\bar{\varphi}_0 = 0 \tag{1.4}$$

$$\bar{\varphi}_{1rr} + (1/r)\bar{\varphi}_{1r} - [p^2\beta^2 + (1/r^2)]\bar{\varphi}_1 = 0 \tag{1.5}$$

where $\bar{\varphi} = p\int_0^\infty e^{-px}\varphi(x)dx$. The fundamental solutions of these equations are the Bessel functions of imaginary argument—$I_0(p\beta r)$, $K_0(p\beta r)$ and $I_1(p\beta r)$, $K_1(p\beta r)$ in the notation of Watson.[1]

(II) *Boundary Conditions*

On the boundary of the cylinder the flow direction must be tangential to the surface—i.e., at $r = 1$

$$\frac{(\partial\phi/\partial r)}{(\partial\phi/\partial x)} \simeq \frac{\partial\varphi}{\partial r} = \alpha\cos\theta\{[1 - (1/r^2)] + \varphi_{1r}\}_{r=1} + [\varphi_{0r}]_{r=1} = 0$$

Hence,

$$\varphi_{1r} = \varphi_{0r} = 0$$

and in terms of the transforms

$$\bar{\varphi}_{1r} = \bar{\varphi}_{0r} = 0 \tag{2.1}$$

at $r = 1$.

To develop the boundary conditions on the ring we assume that it is almost cylindrical so that the boundary conditions can be satisfied at $r = R$, a constant. If the distribution of radius for the ring is $R(x)$, then the condition of tangential flow direction on the surface of the ring is

$$\alpha\cos\theta[1 - (1/R^2) + \varphi_{1r}] + \varphi_{0r} = R'(x)$$

From this we see that at $r = R$ we must have

$$\bar{\varphi}_{0r} = \bar{R}'(p) \tag{2.2}$$

$$\bar{\varphi}_{1r} = -[1 - (1/R^2)] \tag{2.3}$$

Where $R'(p)$ denotes the Laplace transform of $R'(x)$.

(III) *The Symmetrical Solution*

Since the flow is supersonic, the flow between the ring and the cylinder is independent of the solution on the outside of the ring and therefore may be computed separately. The general solution of Eq. (1.4) is

$$\bar{\varphi}_0 = I_0(p\beta r)f(p) + K_0(p\beta r)g(p) \tag{3.1}$$

where I_0 and K_0 are the Bessel functions of imaginary argument in the notation of Watson[1] and $f(p)$ and $g(p)$ are analytic functions of p to be determined by the boundary conditions. Applying Eq. (2.2) and Eq. (2.1) to Eq. (3.1) yields

$$I_1(p\beta)f(p) - K_1(p\beta)g(p) = 0$$

$$I_1(p\beta R)f(p) - K_1(p\beta R)g(p) = \bar{R}'(p)/p\beta$$

Hence,

$$f(p) = \frac{K_1(p\beta)\bar{R}'(p)}{p\beta[I_1(p\beta R)K_1(p\beta) - I_1(p\beta)K_1(p\beta R)]}$$

$$g(p) = \frac{I_1(p\beta)\bar{R}'(p)}{p\beta[I_1(p\beta R)K_1(p\beta) - I_1(p\beta)K_1(p\beta R)]}$$

Substituting $f(p)$ and $g(p)$ into Eq. (3.1) gives us φ_0.

$$\varphi_0 = \frac{1}{2\pi i}\times \int_{\alpha-i\infty}^{\alpha+i\infty} \frac{e^{px}[I_0(p\beta r)K_1(p\beta) + I_1(p\beta)K_0(p\beta r)]}{p^2\beta[I_1(p\beta R)K_1(p\beta) - I_1(p\beta)K_1(p\beta R)]}\,\bar{R}'(p)dp$$

To find the pressure on the interior of the wing we need $\partial\varphi_0/\partial x$ at $r = R$. Using the Faltung integral this becomes

$$\frac{\partial\varphi_0}{\partial x} = \frac{1}{\beta}\int_0^x H'(x-t)R'(t)\,dt \tag{3.2}$$

where

$$H = \frac{1}{2\pi i}\int_{\beta_{r_1}} \frac{e^{px}[I_0(p\beta R)K_1(p\beta) + I_1(p\beta)K_0(p\beta R)]\,dp}{p\,[I_1(p\beta R)K_1(p\beta) - I_1(p\beta)K_1(p\beta R)]}$$

The integrand is analytic except for poles on the imaginary axis. Letting $p = i\lambda$ yields

$$H = \frac{1}{2\pi i} \times \int_{i\alpha+\infty}^{i\alpha-\infty} \frac{e^{i\lambda x}[J_0(\lambda\beta R)\,Y_1(\lambda\beta) - J_1(\lambda\beta)\,Y_0(\lambda\beta R)]d\lambda}{i\lambda\,[J_1(\lambda\beta R)\,Y_1(\lambda\beta) - J_1(\lambda\beta)\,Y_1(\lambda\beta R)]}$$

The function H can be expressed as the sum of the residues of the poles at the zeros of the denominator. Let λ_n be the nth root of

$$J_1(\lambda\beta R)\,Y_1(\lambda\beta) - J_1(\lambda\beta)\,Y_1(\lambda\beta R) = 0 \qquad (3.3)$$

Then the residue is

$$\frac{e^{\pm i\lambda_n x}[J_1(\lambda_n\beta R)\,Y_1(\lambda_n\beta) - J_1(\lambda_n\beta)\,Y_0(\lambda_n\beta R)]}{\pm i\lambda_n\{(d/d\lambda)[J_1(\lambda\beta R)\,Y_1(\lambda\beta) - J_1(\lambda\beta)\,Y_1(\lambda\beta R)]\}_{\lambda=\lambda_n}}$$

and at $\lambda = 0$

$$\frac{1}{2\pi i}\oint \frac{e^{px}\{(1/p\beta)\,[1 + 0(p^2\log p)]\}dp}{p[(R/2) - (1/2R)]} = \frac{2Rx}{\beta(R^2-1)}$$

Hence

$$H = \frac{2x}{\beta[R - (1/R)]} + 2\sum_{n=1}^{\infty} \frac{\sin\lambda_n x\,[J_0(\lambda_n\beta R)\,Y_1(\lambda_n\beta) - J_1(\lambda_n\beta)\,Y_0(\lambda_n\beta R)]}{\lambda_n\psi_n}$$

where

$$\psi_n = \{(d/d\lambda)\,[J_1(\lambda\beta R)\,Y_1(\lambda\beta) - J_1(\lambda\beta)\,Y_1(\lambda\beta R)]\}_{\lambda=\lambda_n} \qquad (3.4)$$

Substituting for H in Eq. (3.2) yields for the pressure

$$C_p = -2(\partial\varphi_0/\partial x) = 2R[R_t(0) - R_t(x)]/[\beta(R^2-1)] - 4\sum_{n=1}^{\infty} \frac{[J_0(\lambda_n\beta R)\,Y_1(\lambda_n\beta) - J_1(\lambda_n\beta)\,Y_0(\lambda_n\beta R)]}{\psi_n} \times \int_0^x \cos\lambda_n\,(x-t)R_t'(t)dt$$

where λ_n is the solution of Eq. (3.3) and ψ_n is defined in Eq. (3.4).

Now for the λ_n sufficiently large, the Bessel functions may be replaced by the first term of their asymptotic expansions—namely,

$$J_\nu(z) = (\pi/2z)^{1/2}\cos[z - (\nu\pi/2) - (\pi/4)]$$

$$Y_\nu(z) = (\pi/2z)^{1/2}\sin[z - (\nu\pi/2) - (\pi/4)]$$

Then the λ_n are solutions of

$$\cos[\lambda\beta R - (3\pi/4)]\sin[\lambda\beta - (3\pi/4)] - \cos[\lambda\beta - (3\pi/4)]\sin[\lambda\beta R - (3\pi/4)] = 0$$

or

$$\sin\lambda\beta(R-1) = 0$$

and, hence,

$$\lambda_n = \pm n\pi/[\beta(R-1)]$$

The residues then become

$$\frac{[\beta(R-1)]\,e^{\pm in\pi x/[\beta(R-1)]}\cos n\pi}{\pm in\pi[(d/d\lambda)\sin\lambda\beta(R-1)]_{\lambda=n\pi/[\beta(R-1)]}} = \frac{(-1)^n\,(e^{\pm in\pi(z+1)} + e^{\pm in\pi(z-1)})}{\pm 2in\pi}$$

where $z = x/[\beta(R-1)]$ The function reduces to a Fourier series—namely,

$$H = \frac{2Rz}{R+1} + \frac{1}{\pi}\sum_{n=1}^{\infty}\frac{\sin n\pi(z+1) + \sin n\pi(z-1)}{n}(-1)^n$$

This series may be summed to represent a simple algebraic function. From Carslaw,[2] page 242. we have

$$\theta = -2\sum_{n=1}^{\infty}\frac{(-1)^n}{n}\sin n\theta \qquad (3.5)$$

for $-\pi \le \theta \le \pi$. By the periodicity of Fourier series

$$\theta - 2\pi = -2\sum_{n=1}^{\infty}\frac{(-1)^n}{n}\sin n\theta \qquad (3.6)$$

for $\pi \le \theta \le 3\pi$. The function H finally simplifies to

$$H = [(R-1)/(R+1)]z + 1 = x/[\beta(R+1)] + 1$$

for $0 < x < 2\beta(R-1)$. Then

$$c_p = -\frac{2}{\beta}\int_0^x \frac{R_t'(t)dt}{\beta(R+1)} = \frac{2}{\beta^2(R-1)}\,[R(0) - R_t(x)] \qquad (3.7)$$

for the inside surface of the ring.

The exterior solution has been obtained by Ward[3] and is given here for the sake of completeness. Since only outgoing waves must prevail at infinity, the transform of the velocity potential, φ_0, will contain only $K_0(p\beta r)$. The solution of Eq. (1.4) which satisfies the boundary condition, Eq. (2.2), is

$$\bar{\varphi}_0 = \{-[K_0(p\beta r)]/[p\beta K_1(p\beta R)]\}\bar{R_0}'(p)$$

Hence,

$$\varphi_0 = -\frac{1}{2\pi i}\int_{\alpha-i\infty}^{\alpha+i\infty}\frac{e^{px}K_0(p\beta r)\bar{R_0}'(p)dp}{p^2\beta K_1(p\beta R)} \qquad (3.8)$$

and on the outer surface of the wing

$$c_p = -2\frac{\partial\varphi_0}{\partial x} = \frac{2}{2\pi i}\int_{\alpha-i\infty}^{\alpha+i\infty}\frac{e^{px}K_0(p\beta R)\bar{R_0}'(p)dp}{p\beta K_1(p\beta R)} \qquad (3.9)$$

$$= \frac{2}{\beta}\left\{\frac{1}{2\pi i}\int_{\alpha-i\infty}^{\alpha+i\infty}\frac{e^{px}}{p}\left[1 - \frac{K_1(p\beta R) - K_0(p\beta R)}{K_1(p\beta R)}\right]\times \bar{R_0}'(p)dp\right\}$$

$$= \frac{2}{\beta}\left\{R_0'(x) - \int_0^x W\left(\frac{x-t}{\beta R}\right)R_0'(t)dt\right\} \qquad (3.10)$$

The quantity $W(x/\beta R)$ is the inverse transform of $[K_1(p\beta R) - K_0(p\beta R)]/[K_1(p\beta R)]$ and is tabulated in reference 3.

(IV) The Cross-Flow Solution

The procedure for obtaining the potential, φ_1, is similar to that for φ_0. The general solution for the interior flow which satisfied Eq. (1.5) is given by

$$\tilde{\varphi}_1 = I_1(p\beta r)\, f_1(p) + K_1(p\beta r) g_1(p)$$

where $f_1(p)$ and $g_1(p)$ are analytic functions. The boundary conditions of Eqs. (2.1) and (2.3) yield

$$I_1'(p\beta) f_1(p) + K_1'(p\beta) g_1(p) = 0$$

$$I_1'(p\beta R) f_1(p) + K_1'(p\beta R) g_1(p) = -[1 - (1/R^2)]/p\beta$$

Solving for $f_1(p)$ and $g_1(p)$ leads to the following result for φ_1

$$\varphi_1 = -\frac{1}{2\pi i}\left(1 - \frac{1}{R^2}\right)\int_{\alpha - i\infty}^{\alpha + i\infty} \frac{e^{px}[I_1(p\beta r)K_1'(p\beta) - I_1'(p\beta_1)K_1(p\beta r)]dp}{p^2\beta\,[I_1'(p\beta R)K_1'(p\beta) - I_1'(p\beta)K_1'(p\beta R)]} \tag{4.1}$$

The procedure for evaluating and simplifying φ_1 is essentially the same as for φ_0 Writing $p = i\lambda$, then for $r = R$

$$\begin{aligned} c_p &= -2(\partial\varphi_1/\partial x)\alpha\cos\theta \\ &= \frac{2(R^2 - 1)}{\beta R^2}\,\alpha\cos\theta\left\{\frac{1}{2\pi i}\int_{i\alpha + \infty}^{i\alpha - \infty} \frac{ie^{i\lambda x}[J_1(\lambda\beta R)Y_1'(\lambda\beta) - J_1'(\lambda\beta)Y_1(\lambda\beta R)]d\lambda}{\lambda[J_1'(\lambda\beta R)Y_1'(\lambda\beta) - J_1'(\lambda\beta)Y_1'(\lambda\beta R)]}\right\} \end{aligned} \tag{4.2}$$

Let μ_n be the nth solution of

$$J_1'(\lambda\beta R)Y_1'(\lambda\beta) - J_1'(\lambda\beta)Y_1'(\lambda\beta R) = 0 \tag{4.3}$$

Then the residue is

$$\{ie^{\pm i\mu_n x}\,[J_1(\mu_n\beta R)Y_1'(\mu_n\beta) - J_1'(\mu_n\beta)Y_1(\mu_n\beta r)]\}/(\pm\mu_n\delta_n)$$

when

$$\delta_n = \{(d/d\lambda)\,[J_1'(\lambda\beta R)Y_1'(\lambda\beta) - J_1'(\lambda\beta)Y_1'(\lambda\beta R)]\}_{\lambda = \mu_n} \tag{4.4}$$

Then the resulting coefficient of pressure due to φ_1 on the inside surface of the ring becomes

$$c_p = \alpha\cos\theta\,\frac{2(R^2 - 1)}{\beta R^2}\sum_{n=1}^{\infty}\frac{\sin\mu_n x\,[J_1(\mu_n\beta R)Y_1'(\mu_n\beta) - J_1'(\mu_n\beta)Y_1(\mu_n\beta R)]}{\mu_n\delta_n}$$

For the sake of clarity, the complete coefficient of pressure for φ_0 and φ_1 on the inside surface of the ring is given here—namely,

$$\begin{aligned} c_p = \frac{2R[R_0 - R(x)]}{\beta(R^2 - 1)} - 4\sum_{n=1}^{\infty}\frac{[J_0(\lambda_n\beta R)Y_1(\lambda_n\beta) - J_1(\lambda_n\beta)Y_0(\lambda_n\beta R)]}{\psi_n}\int_0^x \sin\lambda_n(x - t)R_i'(t)dt + \\ \alpha\cos\theta\,\frac{2(R^2 - 1)}{\beta R^2}\sum_{n=1}^{\infty}\frac{\sin\mu_n x\,[J_1(\mu_n\beta R)Y_1'(\mu_n\beta) - J_1'(\mu_n\beta)Y_1(\mu_n\beta R)]}{\mu_n\delta_n} \end{aligned} \tag{4.5}$$

where ψ_n and δ_n are defined in Eqs. (3.4) and (4.4) and λ_n and μ_n are solutions of Eqs. (3.3) and (4.3).

If all the μ_n are large, then the Bessel functions may be replaced by the first term of their asymptotic expansions. Consequently Eq. (4.2) becomes

$$C_p = \frac{2(R^2 - 1)}{\beta R^2}\,\alpha\cos\theta\left\{\frac{1}{2\pi i}\int_{i\alpha + \infty}^{i\alpha - \infty}\frac{e^{i\lambda[x + \beta(R-1)]} + e^{+i\lambda[x - \beta(R-1)]}}{2i\lambda\sin\lambda[\beta(R - 1)]}\,d\lambda\right\}$$

The poles occur at

$$\sin\lambda\beta(R - 1) = 0$$

or

$$\lambda\beta(R - 1) = \pm n\pi$$

and

$$\mu_n = \pm n\pi/[\beta(R - 1)]$$

Evaluating the residues and simplifying yields

$$\begin{aligned} c_p &= \frac{2(R^2 - 1)}{\pi\beta R^2}\,\alpha\cos\theta\left\{\sum_{n=1}^{\infty}\frac{\sin n\pi(z + 1) + \sin n\pi(z - 1)}{n}(-1)^n\right\} \\ &= -\{[2(R^2 - 1)]/(\beta R^2)\}\,(z - 1)\alpha\cos\theta \end{aligned}$$

Finally, the approximation to the complete coefficient of pressure on the inside surface of the ring becomes

$$c_p = \frac{2[R(0) - R_i(x)]}{\beta^2(R+1)} - \frac{2\alpha\cos\theta(R+1)}{\beta^2R^2} \times [x - \beta(R-1)] \quad (4.6)$$

when $0 < x < 2\beta(R-1)$. For $R \to \infty$, the coefficient of pressure becomes

$$c_p = +(2\alpha\cos\theta)/\beta$$

Thus we obtain the result for the lower side of a two-dimensional flat plate at an angle of attack $\alpha\cos\theta$ (see reference 4, page 42).

The cross-flow potential for the exterior flow over an almost cylindrical tube has been found by Ward.[3] However, the theory requires some modification for our special problem. The potential φ_1 must represent out-going waves for $r > R$. Hence $\bar{\varphi}_1$ must have the form

$$\bar{\varphi}_1 = K_1(p\beta r)h(p)$$

where $h(p)$ is an analytic function of p. The boundary conditions yield

$$\partial\bar{\varphi}_1/\partial r = -[1 - (1/R^2)] = p\beta K_1'(p\beta R)h(p)$$

and, after solving for $h(p)$, we get

$$\bar{\varphi}_1 = -\{[1 - (1/R^2)]K_1(p\beta r)\}/[p\beta K_1'(p\beta R)] \quad (4.7)$$

Then the pressure coefficient on the upper side of the ring is

$$C_p = -2\frac{\partial\varphi_1}{\partial x}\alpha\cos\theta = \frac{2\alpha(R^2-1)}{\beta R^2}\left[\frac{1}{2\pi i}\int_{\alpha-i\infty}^{\alpha+i\infty}\frac{e^{px}K_1(p\beta R)dp}{pK_1(p\beta R)}\right]$$

$$= -\frac{2\alpha\cos\theta\,(R^2-1)}{\beta R^2}\,V\left(\frac{x}{\beta R}\right) \quad (4.8)$$

The function $V(z)$ is evaluated and tabulated in reference 3 and in Table 1 of this report. When $R \to \infty$, $v[x/(\beta R)] \to 1$ and

$$C_p = -(2\alpha/\beta)\cos\theta$$

This is the coefficient of pressure for the upper side of an infinite flat plate at an angle of attack $\alpha\cos\theta$.

(V) *The Influence of the Ring on the Pressure Distribution on the Body*

The ring directly affects the pressure on the body in the region $\beta(R-1) \le x \le l + \beta(R-1)$. For larger values of x, the pressure distribution is influenced also by the vortex sheet that extends from the trailing edge of the ring. When the ring is cylindrical, then $\varphi_0 \equiv 0$ and we need consider only the potential φ_1. We assume that the vortex sheet is nearly cylindrical, and, therefore, we are able to satisfy the boundary conditions on the sheet at $r = R$. We assume that the potentials in Eqs. (4.1) and (4.7) hold for the region downstream of the trailing edge. Additional potentials are added

TABLE 1

s	V(s)	L(s)	L(s)/s	M(s)	M(s)/s²
0	1.0000	.00000	1.000	.00000	.50000
0.2	.89827	.18983	.9492	.01796	.44912
0.4	.79576	.35926	.8982	.06913	.43205
0.6	.69580	.50829	.8472	.14265	.39625
0.8	.60006	.63780	.7973	.23365	.36508
1.0	.51064	.74872	.7487	.33253	.33253
1.2	.42829	.84253	.7021	.43608	.30283
1.4	.35356	.92055	.6575	.53662	.27379
1.6	.28661	.98447	.6153	.63292	.24723
1.8	.22738	1.03570	.5754	.71919	.22197
2.0	.17559	1.07592	.5380	.79604	.19901
2.2	.13089	1.10641	.5029	.85933	.17755
2.4	.09275	1.12872	.4703	.91108	.15817
2.6	.06067	1.14392	.4400	.94840	.14030
2.8	.03405	1.15335	.4119	.97434	.12428
3.0	.01232	1.15786	.3860	.98680	.10964
3.2	-.00507	1.15857	.3621	.99163	.09684

to satisfy the boundary conditions of the continuity of pressure and flow direction across the vortex sheet. Since the potentials already determined in Eqs. (4.1) and (4.7) satisfy the condition that the flow be tangential to the ring of radius R, then the condition that the flow direction be continuous at $r = R$ reduces to

$$\varphi_r^{(0)} = \varphi_r^{(i)} \quad (5.1)$$

at $r = R$, where $\varphi^{(0)}$ and $\varphi^{(i)}$ are the additional potentials that vanish when $x < l$ for the regions outside and inside of the vortex sheet, respectively. The condition of the continuity of pressure then requires that

$$\varphi_{1x}^{(0)} + \varphi_x^{(0)} = \varphi_{1x}^{(i)} \quad (5.2)$$

at $r = R$, where $\varphi_1^{(0)}$ and $\varphi_1^{(i)}$ are the potentials given in Eqs. (4.7) and (4.1) for the regions outside the ring and inside the ring, respectively, for $x < l$. Applying the Laplace transform to Eq. (5.2) yields

$$\bar{\varphi}_1^{(0)} + \bar{\varphi}^{(0)} = \bar{\varphi}_1^{(i)} + \bar{\varphi}^{(i)} \quad (5.3)$$

at $r = R$. For additional potentials we choose

$$\bar{\varphi}^{(0)} = K_1(p\beta R)f_2(p)e^{-pl} \quad (5.4)$$

$$\bar{\varphi}^{i} = [I_1(p\beta r)K_1'(p\beta) - I_1'(p\beta)K_1(p\beta r)]g_2(p)e^{-pl}$$

or

$$\bar{\varphi}^{i} = \chi(r)g_2(p)e^{-pl} \quad (5.5)$$

The interior solution $\bar{\varphi}^{(i)}$ is seen to satisfy the boundary condition on the body—namely $\partial\bar{\varphi}^{(i)}/\partial r = 0$ at $r = 1$; so we need to consider only the boundary conditions on the vortex sheet. Eqs. (5.1) and (5.2) yield

$$p\beta K_1'(p\beta R)f_2(p) - \chi'(R)g_2(p) = 0$$

$$K_1(p\beta R)f_2(p) - \chi(R)g_2(p) = -[\bar{\varphi}_1^{(0)} + \bar{\varphi}_1^{(i)}]e^{pl}$$

Solving for $f_2(p)$ and $g_2(p)$, we obtain

$$e^{-pl}f_2(p) = \frac{-[\bar{\varphi}_1^{(0)} - \bar{\varphi}_1^{i}]\chi'(R)}{K_1(p\beta R)\chi'(R) - p\beta K_1'(p\beta R)\chi(R)}$$

$$= \frac{-[\bar{\varphi}_1^{(0)} - \bar{\varphi}_i^{(i)}]}{(\{[K_1(p\beta R)]/[p\beta K_1'(p\beta R)]\} - [\chi(R)/\chi'(R)])p\beta K_1'(p\beta R)}$$

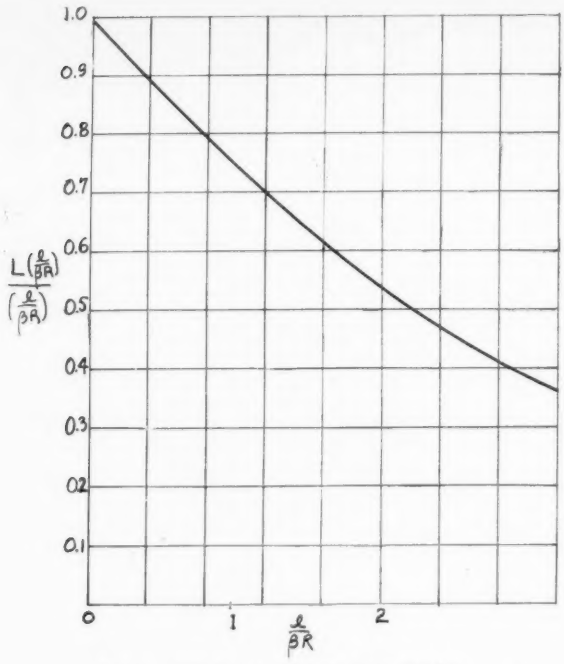

FIG. 2. Lift function for the ring exterior.

Since

$$\varphi_1^{(0)} = -\left(1 - \frac{1}{R^2}\right)\frac{K_1(p\beta R)}{p\beta K_1'(p\beta R)}$$

and

$$\varphi_1^{(l)} = -\{[1 - (1/R^2)]\chi(R)\}/\chi'(R)$$

we have

$$e^{-pl}f_2(p) = [1 - (1/R^2)]/[p\beta K_1(p\beta R)]$$

Similarly

$$e^{-pl}g_2(p) = \frac{[1 - (1/R^2)]}{p\beta[I_1'(p\beta R)K_1'(p\beta) - I'(p\beta)K_1(p\beta R)]}$$

Substitution into Eqs. (5.4) and (5.5) reveal that the additional potentials are the negative of the potentials given in Eqs. (4.1) and (4.7). Therefore, downstream of the characteristics $x - \beta(r - R) = l$ and $x + \beta(r - R) = l$ shown in Fig. 1, the cross-flow potential is identically zero. Therefore, the wing influences those pressures affecting the lift and moment on the body only in the region

$$\beta(R - 1) \leq x \leq l + \beta(R - 1)$$

To compute the pressure coefficient on the body, it is necessary to differentiate Eq. (4.1) with respect to x and set $r = 1$. Hence

$$C_p = -2(\partial\varphi_1/\partial x)\alpha\cos\theta$$

$$C_p = \frac{2\alpha\cos\theta(R^2 - 1)}{2\pi i R^2} \times \int_{\alpha - i\infty}^{\alpha + i\infty} \frac{e^{px}[I_1(p\beta)K_1'(p\beta) - I_1'(p\beta)K_1(p\beta)]dp}{p\beta[I_1'(p\beta R)K_1'(p\beta) - I_1'(p\beta)K_1'(p\beta R)]}$$

$$C_p = -\frac{2\alpha\cos\theta(R^2 - 1)}{2\pi i\beta^2 R^2} \times \int_{\alpha - i\infty}^{\alpha + i\infty} \frac{e^{px}dp}{p^2[I_1'(p\beta R)K_1'(p\beta) - I_1'(p\beta)K_1'(p\beta R)]}$$

Substituting the first term of the asymptotic expansions for I_1' and K_1' yields for the integrand

$$\sqrt{r}[(e^{p[x-\beta(R-1)]}/p) \pm i\,(e^{p[x-\beta(R+1)]}/p)]$$

Thus for $x < \beta(R - 1)$, $C_p = 0$, since the contour $\alpha - i\infty$ to $\alpha + i\infty$ can be replaced by the contour consisting of a semicircle in the right half plane; then the integral vanishes as the radius of this semicircle goes to infinity. For $x > \beta(R - 1)$, we take the closed contour in the left half plane consisting of a line parallel to the imaginary p-axis and a semicircle of increasing radius. We then evaluate the residues at the poles on the imaginary p-axis. Letting $p = i\lambda$ yields

$$C_p = \frac{4\alpha\cos\theta(R^2 - 1)}{\pi\beta^2 R^2}\frac{1}{2\pi i} \times \int_{i\alpha + \infty}^{i\alpha - \infty} \frac{ie^{i\lambda x}\,d\lambda}{\lambda^2[J_1'(\lambda\beta R)Y_1'(\lambda\beta) - J_1'(\lambda\beta)Y_1'(\lambda\beta R)]}$$

By steps similar to the computation of c_p for inside the ring, we finally obtain

$$C_p = \frac{8\alpha\cos\theta(R^2 - 1)}{\pi\beta^2 R^{3/2}} \sum_{n=1}^{\infty} \frac{\sin\mu_n x}{\mu_n^2\delta_n} \tag{5.6}$$

where μ_n is the nth root of Eq. (4.3) and δ_n is given in Eq. (4.4). Replacing μ_n and δ_n by their asymptotic values yields

$$C_p = \frac{4\alpha\cos\theta(R^2 - 1)}{\pi\beta R^{3/2}} \sum_{n=1}^{\infty} \frac{\sin n\pi z}{n}(-1)^n$$

where $z = x/[\beta(R - 1)]$. Finally

$$c_p = -[2\alpha\cos\theta\,(R + 1)/(\beta^2 R^{3/2})]\,[x - 2\beta(R - 1)],\quad \beta(R - 1) < x < 3\beta(R - 1) \tag{5.7}$$

(VI) *Approximate Formulas of Lift and Moment for the Cylindrical Ring of Zero Thickness*

With the above analysis, it is now possible to compute the lift and moment on the ring and on the body. The lift L on the wing is given by

$$\frac{L}{(1/2)\gamma p_\infty M^2} = \pm\int_0^{2\pi}\int_0^x C_p R(x)\cos\theta\,d\theta dx \tag{6.1}$$

where the positive sign is taken for the inside surface of the ring and the negative sign for the outside surface. Using Eq. (4.6) and the fact that $R(x)$ is the constant value R, we obtain for the contribution to the lift of the ring interior surface

$$\frac{L}{(1/2)\gamma p_\infty M^2} = -\frac{2\pi(R + 1)\alpha}{\beta^2 R}\int_0^l [x - \beta(R - 1)]dx$$

Let $l/\beta(R - 1) = \tau$ and $x/[\beta(R - 1)] = t$. Then

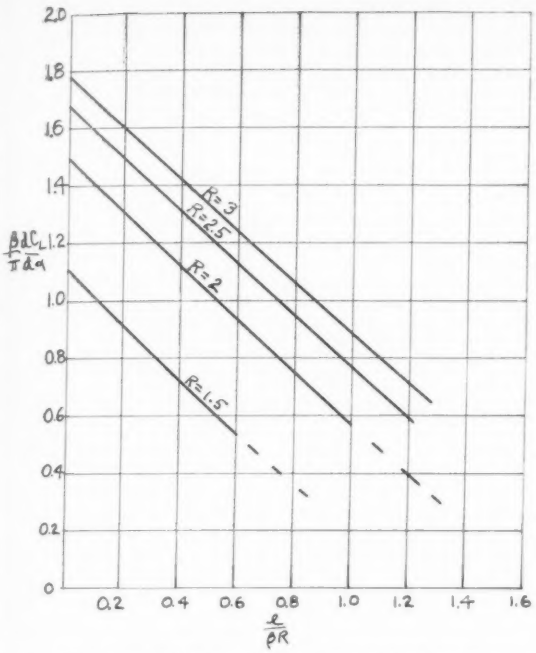

FIG. 3. The slope of lift coefficient for cylindrical ring alone. Asymptotic formula.

$$\frac{L}{(1/2)\gamma p_\infty M^2} = -\frac{2\pi(R+1)(R-1)^2}{R}\int_0^\tau (t-1)dt = -\pi(R+1)(R-1)^2\alpha\tau(\tau-2)/R$$

for $0 < \tau < 2$. The contribution to the coefficient of lift is found by dividing the above equation by $2Rl$, the projected area of the ring. Thus

$$C_{LW_i} = \pi\alpha(R^2-1)(2-\tau)/(2\beta R^2),\ 0<\tau<2 \quad (6.2)$$

For the exterior of the ring we obtain, using Eq. (4.8),

$$C_{LW_e} = \frac{L}{(\gamma/2)\,p_\infty M^2}\frac{1}{(2Rl)} = \frac{2\pi\alpha(R^2-1)}{2\beta R^2 l}\int_0^l V\left(\frac{x}{\beta R}\right)dx$$

$$= \frac{\pi\alpha(R^2-1)}{l}\int_0^{l/(\beta R)} V(z)dz$$

$$C_{LW_e} = \frac{\pi\alpha(R^2-1)}{\beta R}\frac{L\,[l/(\beta R)]}{[l/(\beta R)]} \quad (6.3)$$

The function $L[l/(\beta R)]$ is tabulated in Table 1. The values for $L(z)$ were found by applying Simpson's rule to the values of $V(z)$ in column 2 of Table 1. (See Fig. 2.)

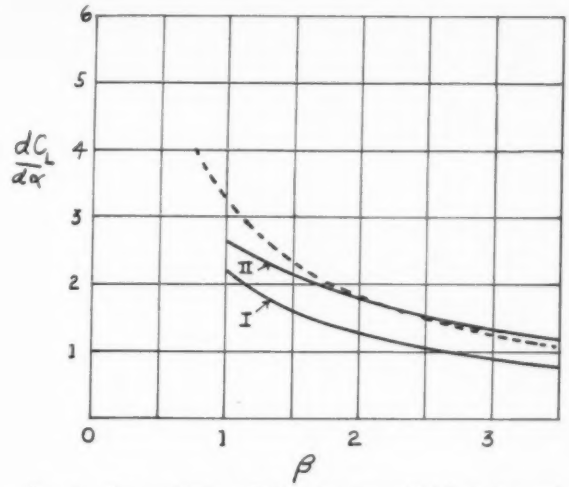

FIG. 4. Slope of lift coefficient for the cylindrical ring and cylinder combination computed from asymptotic formula. Ring radius = 2, ring length = 1.5, cylinder radius = 1. Curves I and II represent the lift for the ring and cylinder combined and for the ring alone, respectively. Dotted line gives $dC_L/d\alpha$ for rectangular flat plate of same aspect ratio as projected area of ring $A = 2R/l = 8/3$.

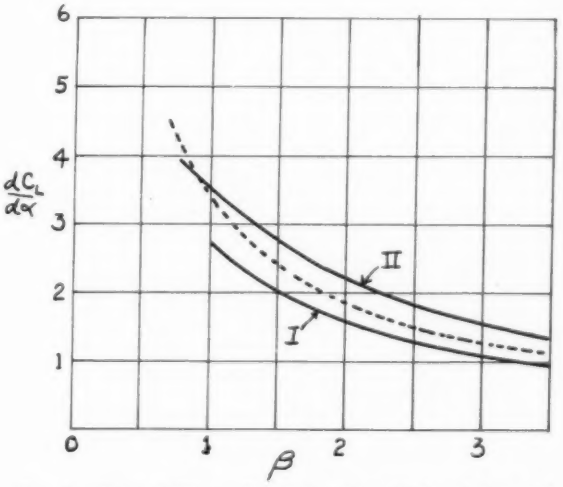

FIG. 5. Slope of lift coefficient for the cylindrical ring and cylinder combination computed from asymptotic formula. Ring radius = 2.5, ring length = 1.5, cylinder radius = 1. Curves I and II represent the lift for the ring and cylinder combined and for the ring alone, respectively. Dotted line gives $dC_L/d\alpha$ for rectangular flat plate of same aspect ratio as projected area of ring $A = 2R/l = 10/3$.

For the coefficient of lift on the body, we obtain

$$C_{LB} = \frac{L}{(\gamma/2)p_\infty M^2}\frac{1}{2Rl} = -\frac{1}{2Rl}\times\int_0^{2\pi}\int_{\beta(R-1)}^{l+\beta(R-1)} c_p\cos\theta\,dxd\vartheta$$

$$= \frac{2\pi\alpha(R+1)}{\beta^2 R^{3/2} l}\int_{\beta(R-1)}^{l+\beta(R-1)}[x-2\beta(R-1)]dx$$

$$C_{LB} = \left\{[\pi(R^0-1)]/(2\beta R^{3/2})\right\}(\tau-2),\quad 0<\tau<2 \quad (6.4)$$

The total lift coefficient for the ring alone is found by

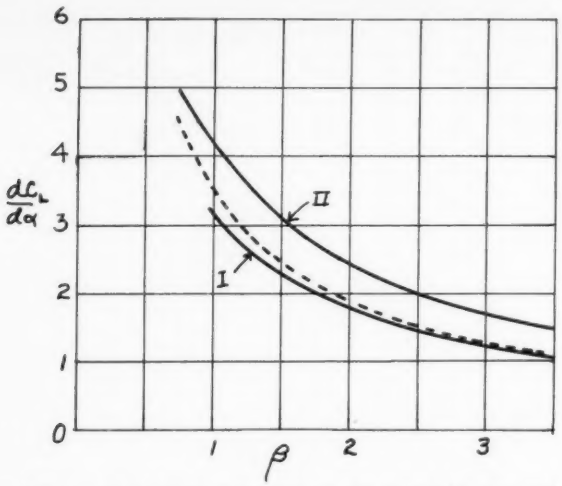

FIG. 6. Slope of lift coefficient for the cylindrical ring and cylinder combination computed from asymptotic formula. Ring radius = 3, ring length = 1.5, cylinder radius = 1. Curves I and II represent the lift for the ring and cylinder combined and for the ring alone, respectively. Dotted line gives $dC_L/d\alpha$ for rectangular flat plate of same aspect ratio as projected area of ring $A = 4$.

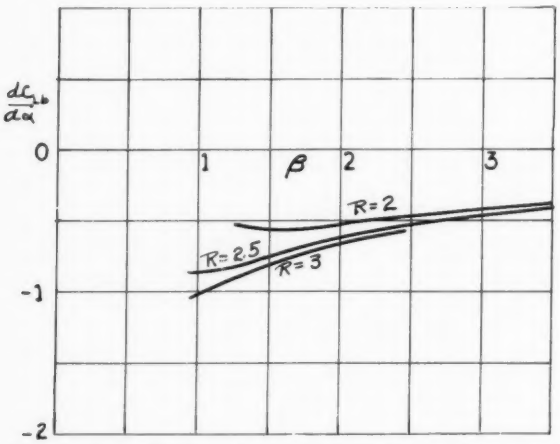

FIG. 7. Slope of lift coefficient on the cylinder from pressure induced by the ring. Computed from asymptotic formula.

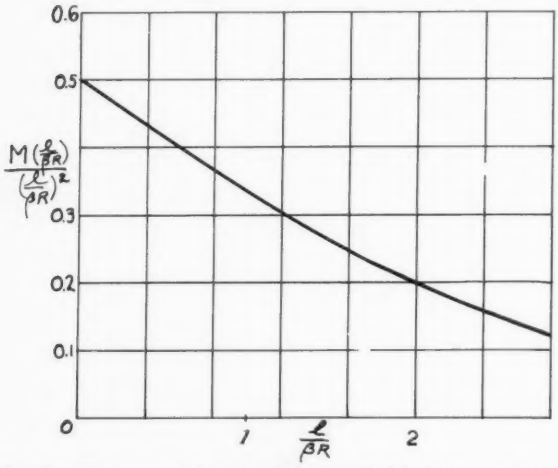

FIG. 8. The moment function for the cylindrical ring exterior.

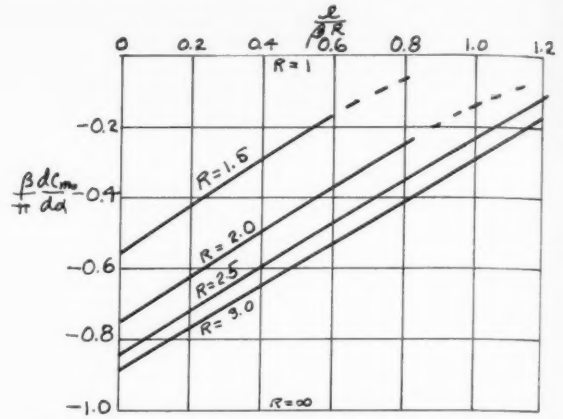

FIG. 9. Slope of moment coefficient for the cylindrical ring computed from asymptotic formula. Moment about the leading edge point on the axis; $x = 0$, $r = 0$.

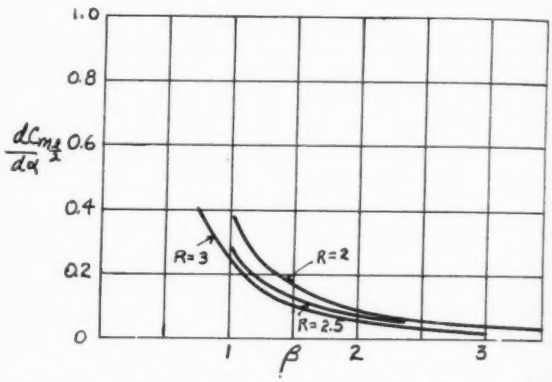

FIG. 10. Slope of moment coefficient for the cylindrical ring of length 1.5. Moment about the ring center $x = l/2$, $r = 0$. Computed from asymptotic formula.

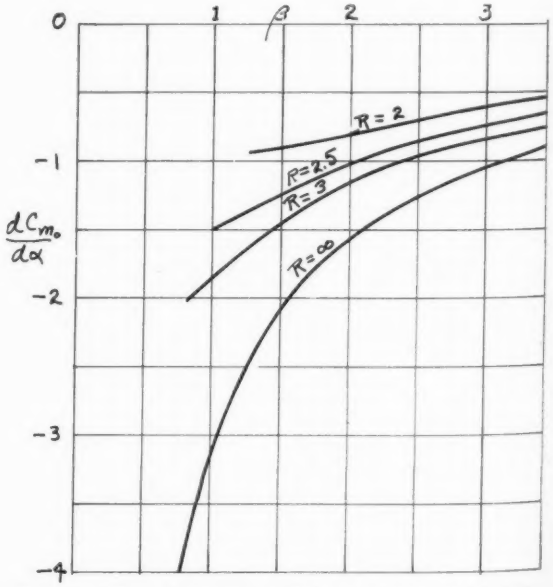

FIG. 11. Slope of moment coefficient for the cylindrical ring of length 1.5. Moment about the origin $x = 0$, $r = 0$. Computed from asymptotic formula.

combining Eqs. (6.2) and (6.3) The quantity (β/π) $(dC_L/d\alpha)$ can be expressed as a function of R and the variable $z = l/\beta R$—namely,

$$\frac{\beta}{\pi}\frac{dC_L}{d\alpha} = \left(1 - \frac{1}{R^2}\right)\left[\frac{L(z)}{z} + 1 - \frac{zR}{2(R-1)}\right]$$

This expression is plotted in Fig. 3. For the range of values considered, the curves (β/π) $(dC_L/d\alpha)$ for constant R are nearly straight lines. The maximum for (β/π) $(dC_L/d\alpha)$ is found for R infinite. Since $\lim_{z \to 0} L(z)/z = 1$, we have

$$\beta(dC_L/d\alpha) = 2\pi$$

This is $\pi/2$ times the value obtained for a flat plate of infinite aspect ratio. It also agrees with the results of Mirels[5] for the solution of a ring alone.

For a constant ring length $l = 1.5$, the coefficient of lift when $R = 2$, 2.5, and 3 is compared in Figs. 4, 5, and 6 with the lift coefficient for a rectangular flat plate having the same geometry as the projected area of the ring $2Rl$. From reference 4 the quantity $dC_L/d\alpha$ for a flat rectangular plate is

$$dC_L/d\alpha = (4/\beta)\left\{1 - [1/(2\beta A)]\right\}$$

where $A = 2R/l$ is the aspect ratio. The wing alone appears to be better than the rectangular plate for high values of β and R and is worse than the rectangular wing for β less than about 1 where the approximations we have made are not valid. The difference, however, is not large. The lift of the combination ring and cylinder is not as high as that for rectangular wing. The quantity $dC_L/d\alpha$ for the cylinder only is plotted in Fig. 7 for $R = 2$, 2.5, and 3. For $R \to \infty$ the coefficient of lift vanishes. The moment acting about the point on the axis at $l/2$, the midpoint of the ring, is

$$\frac{m}{(\gamma/2)pM^2} = \pm \int_0^{2\pi}\int_0^{l} C_p \cos\theta \left(x - \frac{l}{2}\right) R(x)dxd\theta$$

where the positive sign is used on the outside of the ring and the negative sign on the inside. The moment may be written as follows

$$\frac{m}{(\gamma/2)pM^2} = \pm \int_0^{2\pi}\int_0^{l} C_p \cos\theta x R(x)dxd\theta \mp \frac{l}{2}\int_0^{2\pi}\int_0^{l} C_p \cos\theta\, R(x)dxd\theta \quad (6.5)$$

Noting the difference in sign for the lift, we see that Eq. (6.5) can be written

$$\frac{m}{(\gamma/2)pM^2} = \frac{m_0}{(\gamma/2)pM^2} + \frac{l}{2}\frac{L}{(\gamma/2)pM^2}$$

where m_0 denotes the moment about the point $x = 0$ on the axis. The coefficient of moment then becomes

$$c_{m,\,l/2} = c_{m_0} + (1/2)C_L$$

Thus, by evaluating the moment about the point $x = 0$ we can also obtain without difficulty the moment about the midpoint $x = l/2$. A similar analysis about the quarter chord point yields

$$C_{m,\,l/4} = C_{m_0} + (1/4)C_L$$

The approximate moment about the leading edge contributed by the pressures on the interior surface of the cylindrical ring is, from Eqs. (6.5) and (4.6),

$$\frac{m_0}{(\gamma/2)pM^2} = \frac{2\pi\alpha(R+1)}{\beta^2 R}\int_0^{l} x[x - \beta(R-1)]dx = \{[\pi\alpha(R+1)\beta(R-1)^3]/3R\}\tau^2(2\tau - 3)$$

The contribution to the coefficient of moment for the interior surface of the ring is

$$c_{m_0 w_i} = \left\{[\pi\alpha(R^2-1)]/6\beta R^2\right\}(2\tau - 3),\ 0 < \tau < 2 \quad (6.6)$$

For the outside surface of the cylindrical ring

$$\frac{m_0}{(\gamma/2)pM^2} = -\frac{2\pi\alpha(R^2-1)}{\beta R}\int_0^{l} xV\left(\frac{x}{\beta R}\right)dx = -2\pi\alpha\beta R(R^2-1)\int_0^{l/\beta R} zV(z)dz$$

The contribution of the pressure on the outside surface of the ring to the coefficient of moment about the leading edge is

$$C_{m_0 w_0} = -\frac{\pi\alpha(R^2-1)}{\beta R^2}\left[M\left(\frac{l}{\beta R}\right)\right]\Big/\left(\frac{l}{\beta R}\right)^2$$

where

$$M\left(\frac{l}{\beta R}\right) = \int_0^{l/\beta R} zV(z)dz \quad (6.7)$$

and is found in Table 1. This was computed by using Simpson's rule and the values of $V(z)$ given in Table 1 and in reference 3. (See also Fig. 8.)

The pressures on the body are influenced by the ring in the region $\beta(R-1) < x < l + \beta(R-1)$. The coefficient of moment about the leading edge of the cylindrical ring on the axis is, using Eq. (5.7)

$$C_{m_0 b} = \frac{m_0}{(\gamma/2)pM^2(2Rl^2)} = -\frac{\pi\alpha(R+1)}{\beta^2 R^{5/2} l^2} \times \int_0^{l+\beta(R-1)} x[x - 2\beta(R-1)]dx = -\frac{\pi\alpha(R^2-1)}{3\beta R^{5/2}}\left(\tau - \frac{3}{\tau}\right),\quad 0 < \tau < 2 \quad (6.8)$$

By combining Eqs. (6.7) and (6.6), we obtain for the derivative of the coefficient of moment with respect to α about the leading edge of the ring alone

$$\frac{\beta}{\pi}\frac{dC_{m_0}}{d\alpha} = -\frac{(R^2-1)}{R^2}\left[\frac{M(z)}{z^2} + \frac{1}{2} - \frac{Rz}{3(R-1)}\right] \quad (6.9)$$

This is plotted against z for $R = 1.5$, 2, 2.5, and 3 in Fig. 9. For the range of values considered, the quantity $-\beta(dC_{m_0}/d\alpha)$ can be represented nearly by straight lines. In Fig. 10, the slope of the coefficient of moment

about the center chord point is plotted for $R = 2$, 2.5, and 3 and for $l = 1.5$. The coefficient of moment is seen to decrease with increasing R and vanishes for $R \to \infty$. Since $\lim_{z \to 0} M(z)/z^2 = 1/2$, Eq. (6.9) becomes

$$dC_{m_0}/d\alpha = -\pi/\beta$$

This is $\pi/2$ times the value for the moment about the leading edge of a two-dimensional flat plate. This is plotted against β in Fig. 11 and compared with the corresponding values when $R = 2$, 2.5, and 3 for $l = 1.5$.

References

[1] Watson, G. N., *A Treatise on the Theory of Bessel Functions*, 2nd Ed., Cambridge University Press, London, 1948.

[2] Carslaw, H. S., *Introduction to the Theory of Fourier Series and Integrals*, 3rd Ed., Dover Publications, Inc., 1930.

[3] Ward, G. N., *Flow Past a Quasi-Cylindrical Tube*, Quarterly Journal of Mechanics and Applied Mathematics, Vol. I, Part 2, pp. 225–245, June, 1948.

[4] Ferri, A., *Elements of Aerodynamics of Supersonic Flows*, The Macmillan Company, New York, 1949.

[5] Mirels, H., *Theoretical Wave Drag and Lift of Thin Supersonic Ring Airfoils*, NACA TN 1678, 1948.

[6] Haack, W., *Charakteristikenverfahren zur Naehrungsweisen Berechnung der Unsymmetrischen Ueberschallstroemung um Ringfoermige Koerper*, Zeitschrift für Angewandte Mathematik und Physik, Vol. II, No. 5, pp. 357–375, 1951.

The Generalized Shock-Expansion Method and Its Application to Bodies Traveling at High Supersonic Air Speeds

(*Continued from page 238*)

[3] Pai, S. I., *On the Flow Behind an Attached Curved Shock*, Journal of the Aeronautical Sciences, Vol 19, No. 11, pp 734–742, November, 1952.

[4] Eggers, A. J., Jr., and Syvertson, Clarence A., *Inviscid Flow About Airfoils at High Supersonic Speeds*, NACA TN 2646, 1952.

[5] Crocco, Luigi, *Singolarita della Corrente Gassosa Iperacustica Nell'Intorno di una Prora a Diedro*, L'Aerotecnica, Vol. 17, No. 6, pp. 519–534, June, 1937.

[6] Munk, M. M., and Prim, R. C., *Surface-Pressure Gradient and Shock-Front Curvature at the Edge of a Plane Ogive with Attached Shock Front*, Journal of the Aeronautical Sciences, Vol. 15, No. 11, pp. 691–695, November, 1948.

[7] Chu, Boa-Teh, *On Weak Interaction of Strong Shock and Mach Waves Generated Downstream of the Shock*, Journal of the Aeronautical Sciences, vol. 19, No. 7, pp. 433–446, July, 1952.

[8] Eggers, A. J., Jr., and Savin, Raymond C., *Approximate Methods for Calculating the Flow About Nonlifting Bodies of Revolution at High Supersonic Airspeeds*, NACA TN 2579, 1951.

[9] Eggers, A. J., Jr., *On the Calculation of Flow About Objects Traveling at High Supersonic Speeds*, NACA TN 2811, 1952.

[10] Graustein, William C., *Differential Geometry*, MacMillan Company, pp. 149–156, January, 1935, reprinted April, 1947.

[11] Eggers, A. J., Jr., and Nothwang, George J., *The Ames 10-by 14-Inch Supersonic Wind Tunnel*, NACA TN 3095, 1954.

[12] Mass. Inst. Tech., Dept. Elec. Engr., Center of Analysis. *Tables of Supersonic Flow Around Cones*, by the staff of the Computing Section, Center of Analysis, under the direction of Zdenek Kopal, Tech. Rep. No. 1, Cambridge, 1947.

[13] Rossow, Vernon J., *Applicability of the Hypersonic Similarity Rule to Pressure Distributions Which Include the Effects of Rotation for Bodies of Revolution at Zero Angle of Attack*, NACA TN 2399, 1951.

[14] Mass. Inst. Tech., Dept. Elec. Engr., Center of Analysis. *Tables of Supersonic Flow Around Cones of Large Yaw*, by the staff of the Computing Section, Center of Analysis, under the direction of Zdenek Kopal, Tech. Rep. No. 5, Cambridge, 1949.

[15] Allen, H. Julian, and Perkins, Edward W., *A Study of Effects of Viscosity on Flow over Slender Inclined Bodies of Revolution*, NACA Rep. 1048, 1951.

[16] Mangler, W., *Compressible Boundary Layers on Bodies of Revolution*, M. A. P. Volkenrode Ref. VG 83, Rept. and Trans. No. 47, March, 1946.

[17] Bertram, Mitchel H., *An Approximate Method for Determining the Displacement Effects and Viscous Drag of Laminar Boundary Layers in Two-Dimensional Hypersonic Flow*, NACA TN 2773, 1952.

The Application of Finite Difference Methods to Boundary-Layer Type Flows*

W. T. ROULEAU† AND J. F. OSTERLE†
Carnegie Institute of Technology

ABSTRACT

Finite difference techniques are applied to the problem of slightly viscous, incompressible, constant pressure flow confined by boundaries (solid or porous) on which the "no-slip" condition prevails. The "stepwise" representation and method of solution developed by Friedrich and Forstall, which is unstable at boundaries on which there is no slip, is extended to include this case. An always stable "implicit" form of the difference equations is developed, and for it methods of solution by relaxation and iteration techniques are presented. Both the stepwise and implicit procedures are suitable for programing on digital computers. Several original solutions are obtained by these methods, including the important problems of the boundary layer over a flat plate with an arbitrary distribution of suction and the slot-jet issuing adjacent to a plate into a moving stream.

LIST OF SYMBOLS

a = characteristic dimension
j = subscript denoting jth column of mesh points
k = subscript denoting kth row of mesh points
l = length of plate
M = number of points in column
N = number of points in column
Q = residue at a mesh point
u = velocity in x-direction
u_m = maximum u-velocity at beginning of computation region
u_{jm} = maximum velocity in jet
u_0 = uniform stream velocity
U = dimensionless velocity in X-direction
v = velocity in y-direction
$v_0(x)$ = velocity at surface of porous plate
V = dimensionless velocity in Y-direction
x = downstream coordinate
x_0 = distance from leading edge to beginning of porous region
X = dimensionless downstream coordinate
y = transverse coordinate
Y = dimensionless transverse coordinate
δ^* = displacement thickness of boundary layer
ϵ = coefficient of eddy kinematic viscosity
ν = kinematic viscosity

INTRODUCTION

IN MANY PROBLEMS IN FLUID DYNAMICS described by Prandtl's simplification of the Navier-Stokes equations and the continuity equation, the boundary conditions are such that exact solutions have not been obtained. One such problem is that of longitudinal flow over a porous flat plate when there is an arbitrary distribution of normal velocity at the plate surface and when an initial boundary layer is present at the beginning of the porous region (see Fig. 1). This problem is of practical importance because porous surfaces through which suction is applied have been recognized as being useful in keeping boundary layers laminar and thus reducing drag.[1] Schlichting[2] was able to develop an exact solution for porous plate flow, but only with the restrictive conditions of constant normal velocity at the plate surface and porosity beginning at the leading edge of the plate. Another problem that has defied exact treatment is the mixing of a two-dimensional jet and a parallel uniform stream when the jet discharges parallel and adjacent to a flat plate (see Fig. 2). This problem is of immediate importance in the design of gas turbine combustors in which the liner is cooled by means of air injection between the combustion gases and the liner from circumferential slots.

This paper is concerned with the development and solution of finite difference representations of the two-dimensional form of the Prandtl and continuity equations. A difference representation similar to that developed by Friedrich and Forstall[3] for axially symmetrical flow and having similar stability criteria is developed, and for it the "stepwise" method of solution

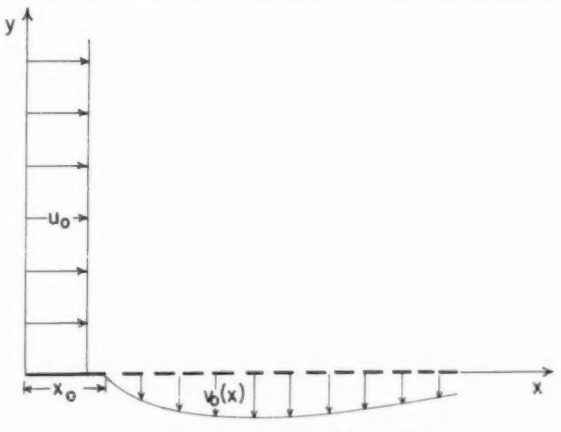

FIG. 1. Porous plate with suction.

Received June 21, 1954.
* This research was partially supported by the United States Air Force, through the Office of Scientific Research of the Air Research and Development Command, and by the National Science Foundation; it was done in part by Wilfred T. Rouleau in partial fulfillment of the requirements of the degree of Doctor of Philosophy at the Carnegie Institute of Technology.
† Assistant Professor, Department of Mechanical Engineering.

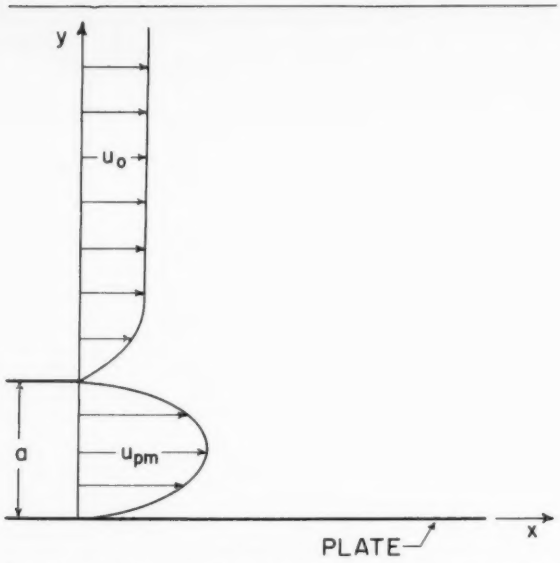

FIG. 2. Two-dimensional jet discharging adjacent and parallel to flat plate into parallel uniform stream.

used by them, extended to include the case where the longitudinal velocity is zero at a boundary, is presented. An "implicit" difference representation is developed which is always stable, and for it solutions by relaxation and iteration methods are described.

FUNDAMENTAL EQUATIONS

The flows to be considered here are described by the Prandtl simplification of the Navier-Stokes equations

$$[u(\partial u/\partial x)] + [v(\partial u/\partial y)] = \nu(\partial^2 u/\partial y^2) \qquad (1)$$

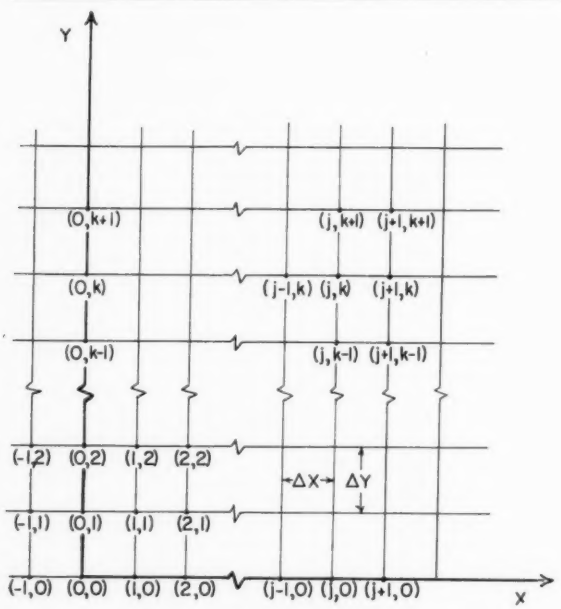

FIG. 3. Designation of mesh points.

and the continuity equation

$$(\partial u/\partial x) + (\partial v/\partial y) = 0 \qquad (2)$$

where the x-axis is taken in the direction of the main flow, u is the velocity in the x-direction, v is the velocity in the y-direction, and ν is the kinematic viscosity.

Strictly speaking, Eq. (1) applies only to nonturbulent flows. However, the same equation with mean velocities being used and the kinematic viscosity, ν, replaced by the coefficient of eddy kinematic viscosity, ϵ, has often been applied to the turbulent cases of the flows here considered,[4–6] yielding fairly good results. Thus the methods developed in this paper may be applied to such treatments of turbulent flows provided that ϵ is known as a function of position.

Since the Prandtl equation does not describe the flow in the immediate vicinity of a velocity discontinuity, in this paper such discontinuities (as at jet outlets) are not employed as idealizations of real problems but rather the actual existing boundary layers are taken into account.

Eqs. (1) and (2) may, for convenience, be put into dimensionless form by use of the variables

$$\left.\begin{aligned} Y &= y/a \\ X &= \nu x/a^2 u_m \\ U &= u/u_m \\ V &= av/\nu \end{aligned}\right\} \qquad (3)$$

where a is some characteristic dimension (for example, the width of a nozzle or a measure of the initial boundary-layer thickness) and u_m is the maximum u-velocity at the beginning of the region (say $x = 0$) where the difference forms of Eqs. (1) and (2) are to be applied. Upon substitution of the variables, Eqs. (3), Eqs. (1) and (2) become

$$[U(\partial U/\partial X)] + [V(\partial U/\partial Y)] = \partial^2 U/\partial Y^2 \qquad (4)$$

$$(\partial U/\partial X) + (\partial V/\partial Y) = 0 \qquad (5)$$

FINITE DIFFERENCE REPRESENTATION OF EQUATIONS

For the development of the stepwise and implicit difference representations, a rectangular mesh is superposed on the flow field having fixed axes X and Y, and the partial derivatives in the Prandtl and continuity equations are approximated by difference quotients. The subscript pair (j, k) is used to denote the mesh point in the jth column (Y-direction) and the kth row (X-direction). (See Fig. 3.)

Stepwise Form

The approximations for the stepwise form are

$$\left.\begin{aligned} \partial U/\partial X &= (U_{j+1,k} - U_{j,k})/\Delta X \\ \partial U/\partial Y &= (U_{j,k+1} - U_{j,k-1})/2\Delta Y \\ \partial^2 U/\partial Y^2 &= (U_{j,k+1} - 2U_{j,k} + U_{j,k-1})/(\Delta Y)^2 \\ \partial V/\partial Y &= (V_{j+1,k+1} - V_{j+1,k})/(\Delta Y) \end{aligned}\right\} \qquad (6)$$

Substitution of these approximations in Eqs. (4) and (5) gives the stepwise equations

$$U_{j,k}\frac{U_{j+1,k}-U_{j,k}}{\Delta X}+V_{j,k}\frac{U_{j,k+1}-U_{j,k-1}}{2\Delta Y}=\frac{U_{j,k+1}-2U_{j,k}+U_{j,k-1}}{(\Delta Y)^2} \quad (7)$$

$$[(U_{j+1,k}-U_{j,k})/\Delta X]+[(V_{j+1,k+1}-V_{j+1,k})/\Delta Y]=0 \quad (8)$$

If, for some j, $U_{j,k}$ and $V_{j,k}$ are considered known for all k, Eq. (7) can be solved for $U_{j+1,k}$ for all k, and with these values Eq. (8) yields $V_{j+1,k+1}$ in terms of $V_{j+1,k}$, so that if $V_{j+1,\,k}$ is known for some k, say $k=0$ (perhaps from a boundary condition), $V_{j+1,k+1}$ can be determined in "stepwise" fashion for successive k's, starting with the known value $V_{j+1,0}$. A knowledge of $U_{j,k}$ and $V_{j,k}$ thus leads to a knowledge of $U_{j+1,k}$ and $V_{j+1,k}$. This stepwise procedure is carried out in the calculation of the velocities in successive columns downstream.

Implicit Form

In the implicit form the U difference quotients in the Y-direction are taken in the $(j+1)$th column as distinguished from the jth column in the stepwise form. These approximations are

$$\left.\begin{aligned}\partial U/\partial Y &= (U_{j+1,k+1}-U_{j+1,k-1})/2\Delta Y\\ \partial^2 U/\partial Y^2 &= (U_{j+1,k+1}-2U_{j+1,k}+U_{j+1,k-1})/(\Delta Y)^2\end{aligned}\right\} \quad (9)$$

which, together with the appropriate difference quotients of Eqs. (6), give the implicit equations

$$U_{j,k}\frac{U_{j+1,k}-U_{j,k}}{\Delta X}+V_{j,k}\frac{U_{j+1,k+1}-U_{j+1,k-1}}{2\Delta Y}=\frac{U_{j+1,k+1}-2U_{j+1,k}+U_{j+1,k-1}}{(\Delta Y)^2} \quad (10)$$

$$[(U_{j+1,k}-U_{j,k})/\Delta X]+[(V_{j+1,k+1}-V_{j+1,k})/\Delta Y]=0 \quad (8)$$

In Eq. (10) there are three unknowns—$U_{j+1,k}$, $U_{j+1,k+1}$, and $U_{j+1,k-1}$. If there is a boundary at $Y=0$ ($k=0$) where $U_{j+1,0}=0$, a sufficient number of points N is taken in the column j so that the uppermost point $(j+1, N+1)$ of Eq. (10) lies in essentially undisturbed fluid. Thus $U_{j+1,N+1}$ is known, and in the N simultaneous equations of the form (10), there are only N unknowns $U_{j+1,k}$ that may be solved for by either a relaxation or iteration procedure. If there is not a wall at $Y=0$, then, of course, equations of the form (10) must be set up for the region below the X-axis with the lowermost point being in essentially undisturbed fluid as well as the uppermost point. When the known velocities at these two extreme points are substituted in the equations, there is obtained a set of M simultaneous equations in M unknowns.

In the iterative type solution the selection of N is more or less of a trial process; N should be large enough so that $U_{j+1,\,N-N*}$ is arbitrarily close to the free-stream velocity, the value of N^* depending on the accuracy desired. Alternatively, once the computations have been carried out for the $U_{j+1,\,k}$'s ($k=0, 1, \ldots N+1$), the value of N could be increased, the computations again performed, the two sets of $U_{j+1,\,k}$'s compared, and the values accepted if they agree as closely as desired. In a relaxation solution, N is determined directly because the number of points may be increased at will during the relaxation until the velocity of the undisturbed stream is attained (or approached as closely as desired) at the last point.

In the solution of the simultaneous equations of the form (10) by relaxation, the residue, $Q_{j+1,\,k}$, at each point in the column $j+1$ is given by

$$Q_{j+1,\,k}=U_{j,k}\frac{U_{j+1,k}-U_{j,k}}{\Delta X}+V_{j,k}\frac{U_{j+1,k+1}-U_{j+1,k-1}}{2\Delta Y}+\frac{2U_{j+1,\,k}-U_{j+1,\,k+1}-U_{j+1,\,k-1}}{(\Delta Y)^2} \quad (11)$$

The effect of a change in velocity $\Delta U_{j+1,\,k}$ on the residues at $(j+1, k)$ and the neighboring points $(j+1, k+1)$ and $(j+1, k-1)$ is given by

$$\left.\begin{aligned}\Delta Q_{j+1,\,k} &= \{(U_{j,k}/\Delta X)+[2/(\Delta Y)^2]\}\Delta U_{j+1,\,k}\\ \Delta Q_{j+1,\,k+1} &= -\{(V_{j,\,k+1}/2\Delta Y)+[1/(\Delta Y)^2]\}\Delta U_{j+1,\,k}\\ \Delta Q_{j+1,\,k-1} &= \{(V_{j,\,k-1}/2\Delta Y)-[1/(\Delta Y)^2]\}\Delta U_{j+1,\,k}\end{aligned}\right\} \quad (12)$$

As is usual with a relaxation procedure, values for the $U_{j+1,\,k}$'s are estimated and residues are computed. Corrections are then made in these values to reduce the residues to as near zero as desired. $V_{j+1,\,k+1}$ may then be computed from Eq. (8). The process is repeated for successive columns downstream.

In the solution of the simultaneous equations of form (10) by iteration, $U_{j+1,\,k}$ may be solved for in each equation to give

$$U_{j+1,\,k}=\frac{1}{\{[2/(\Delta Y)^2]+(U_{j,\,k}/\Delta X)\}}\times\left[\left(\frac{1}{(\Delta Y)^2}+\frac{V_{j,\,k}}{2\Delta Y}\right)U_{j+1,\,k-1}+\left(\frac{1}{(\Delta Y)^2}-\frac{V_{j,\,k}}{2\Delta Y}\right)U_{j+1,\,k+1}+\frac{U_{j,\,k}{}^2}{\Delta X}\right] \quad (13)$$

where the $U_{j,\,k}$'s and $V_{j,\,k}$'s are known. Estimated values are first assigned to the $U_{j+1,\,k}$'s and substituted in the set of simultaneous equations of the form of (13) to obtain more nearly correct values. These values are next substituted to obtain a better approximation

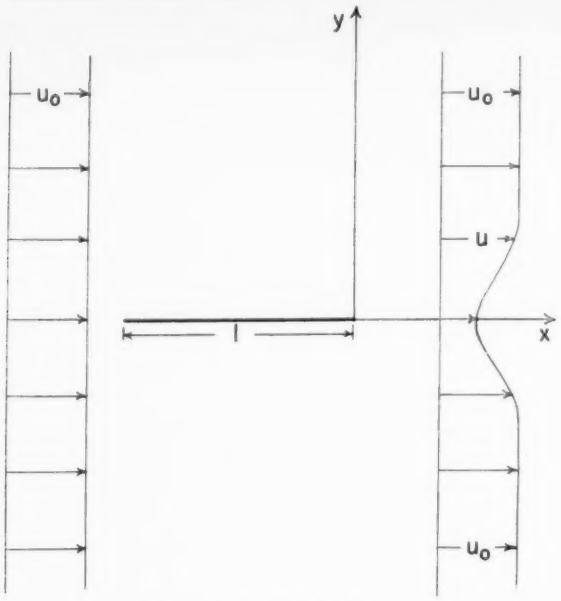

FIG. 4. Wake behind flat plate.

for the $U_{j+1,\,k}$'s; this process is continued until there is is no further significant change in the $U_{j+1,\,k}$'s. Coefficients are then computed for the points $(j + 1, k)$ once the $V_{j+1,\,k}$'s have been computed from Eq. (8), and the $U_{j+2,\,k}$'s and the $V_{j+2,\,k}$'s computed. This procedure is followed for successive columns downstream.

An advantage of the iteration process is that it may be quickly carried out with a digital computer.

STABILITY

In a stable difference representation "round-off" errors occurring in the calculations either remain constant or decrease; if instability occurs, the round-off errors grow and eventually cause oscillations in the calculations. The technique of stability analysis referred to here is due to J. von Neumann, as explained by O'Brien, Hyman, and Kaplan.[7]

Stability of Stepwise Equations

It is found that for Eq. (7) to be stable the following inequalities must be satisfied.

$$\left.\begin{aligned} \Delta X/[U_{j,\,k}(\Delta Y)^2] &\leq 1/2 \\ |V_{j,\,k}|\Delta Y &\leq 2 \end{aligned}\right\} \qquad (14)$$

It can be shown that Eq. (8) is stable at least at all points where Eq. (7) is stable.

At points on a boundary, say $k = 0$, along which $U_{j,\,0} = 0$, Eq. (7) is obviously unstable regardless of the mesh geometry. But Eq. (8) is stable at such a boundary since $U_{j,\,0}$ and $U_{j+1,\,0}$ are both zero there and thus contain no round-off error; consequently, the error in $V_{j+1,\,1}$ is the same as in $V_{j+1,\,0}$. Thus the stepwise equations can be used to calculate flows characterized by the presence of a boundary on which the no-slip condition prevails provided that the stability criteria (14) are observed at all mesh points in the region except those on the boundary.

Stability of the Implicit Form

The stability analysis shows that Eq. (10), and hence Eq. (8), is always stable, regardless of mesh size or velocities. Thus Eq. (10) is useful when it is desired to determine velocities near to a boundary where $U_{j,\,k} = 0$ and still have the computations progress rapidly downstream. Also, the implicit equations can be applied to a jet discharging into a stationary medium, for which inequalities (14) show the stepwise equations to be unstable.

INHERENT ERROR

The inherent error in the difference Eqs. (7), (8), and (10), which arises from the replacement of derivatives by difference quotients, may be determined by the methods of reference 8 and is found to decrease as the mesh size decreases, as would be expected.

EXAMPLE

As a check on the accuracy of the numerical methods developed in this paper, they are applied to the problem of the determination of the velocity distribution in the laminar wake behind a flat plate immersed in a uniform stream parallel to the direction of flow (as in Fig. 4), since for this problem an analytical solution[9] (due to Goldstein) exists.

For the numerical calculations a boundary condition on V is necessary; from symmetry it is evident that at $Y = 0$, $V = 0$. Thus, one row of mesh points is taken on the X-axis. At the trailing edge of the plate, where the difference equations are first applied, $U = 0$, and, consequently, the stepwise equations cannot be used because they would be unstable. This stability difficulty is circumvented by use of the always stable

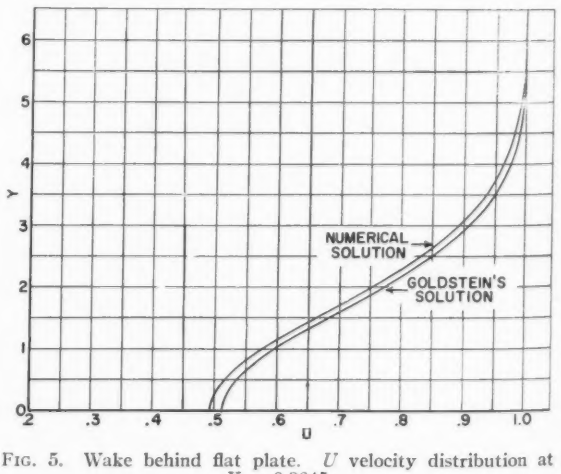

FIG. 5. Wake behind flat plate. U velocity distribution at $X = 0.3645$.

TABLE 1

Velocity Distribution in Flow over Porous Plate with Suction

x† = 0.005 ft.		x = 0.1925 ft.			x = 1.519 ft.			x = 8.269 ft.		
k ($y = k/25$)	u(Blasius), ft. per sec.	k ($y = k/12.5$)	u(numerical), ft. per sec.	u(Schlichting), ft. per sec.	k ($y = k/3.125$)	u(numerical), ft. per sec.	u(Schlichting), ft. per sec.	k ($y = k/3.125$)	u(numerical), ft. per sec.	u(Schlichting), ft. per sec.
0	0	0	0	0	0	0	0	0	0	0
1	0.572	1	0.308	0.314	1	0.625	0.591	1	0.573	0.552
2	0.921	2	0.552	0.545	2	0.876	0.840	2	0.819	0.799
3	0.996	3	0.733	0.705	3	0.966	0.939	3	0.924	0.910
4	1.000	4	0.855	0.814	4	0.993	0.977	4	0.969	0.960
5	1.000	5	0.930	0.884	5	0.999	0.992	5	0.987	0.982
		6	0.970	0.928	6	1.000	0.997	6	0.995	0.992
		7	0.989	0.956	7	1.000	0.999	7	0.998	0.996
		8	0.996	0.974	8	1.000	1.000	8	0.999	0.998
		9	0.999	0.984				9	1.000	0.999
		10	1.000	0.990				10	1.000	1.000
		11	1.000	0.994				11	1.000	1.000
		12	1.000	0.997				12	1.000	1.000
		13	1.000	0.998						
		δ^* (numerical) = 0.1713 ft.			δ^* (numerical) = 0.3088 ft.			δ^* (numerical) = 0.3731 ft.		
		δ^* (Schlichting) = 0.1908 ft.			δ^* (Schlichting) = 0.3490 ft.			δ^* (Schlichting) = 0.3985 ft.		

† x is measured from the leading edge of the plate.

implicit equations, solved by relaxation, to compute the velocities in the first, second, and third column of points; then a transition is made to the stepwise equations, which are more easily solved by hand.

The arbitrarily chosen parameters are: $u_0 = 1$ ft. per sec., $\nu = 1$ ft.^{2} per sec., $l = 1$ ft., and $a = 1$ ft. For the relaxation solution the mesh has the dimensions $\Delta Y = 0.4$, $\Delta X = 0.05$; for the stepwise solution $\Delta Y = 0.4$, $\Delta X = 0.025$ (except for the last interval, where $\Delta X = 0.0145$).

The results of the numerical analysis are compared with the analytical solution in Fig. 5 at the dimensionless distance $X = 0.3645$. The inherent error analysis indicates that with a smaller mesh the agreement would have been better.

PROBLEMS

(A) *Boundary Layer over a Porous Plate*

The velocity distribution over a porous flat plate in longitudinal flow with an arbitrary distribution of normal velocity, $v_0(x)$, at the plate surface when the porosity begins at some distance, say x_0, from the leading edge (see Fig. 1) may be calculated by the numerical procedures developed, the stepwise procedure being used for this particular case.

For the numerical calculations it is arbitrarily assumed that $v_0(x)$ is constant and the flow is laminar; under these assumptions the problem is solved numerically in dimensional form for the velocities and displacement thicknesses (δ^*), and the results are compared with Schlichting's[2] exact values in Table 1.

Arbitrarily assume that $x_0 = 0.005$ ft., $u_0 = 1.000$ ft. per sec., $v_0 = -0.250$ ft. per sec., and $\nu = 0.1$ ft.^{2} per sec., where x_0 is small enough to approximate Schlichting's geometry, yet large enough so that the Blasius boundary-layer solution[10, 11]—used to obtain the initial values in the difference equations—is valid. The value of v_0, although physically too large, provides for convenience in the computations; the mathematics remain valid and the results can still be compared with Schlichting's. At the beginning the mesh has the dimensions $\Delta x = 1/400$ ft., $\Delta y = 1/25$ ft.; as the boundary layer thickens downstream the mesh must be made larger to comply with the stability criteria. The final mesh has the dimensions $\Delta x = 1/4$ ft., $\Delta y = 1/3.125$ ft.

(B) *Two-Dimensional Jet Discharging Adjacent and Parallel to Flat Plate into Parallel Uniform Stream*

The stepwise or implicit equations may be applied to find the velocity distribution resulting from a two-dimensional jet discharging parallel and adjacent to a flat plate from a slot into a uniform stream. (See Fig. 2.)

In this problem, which is solved here by the stepwise equations, the velocity distribution at $x = 1/50$ ft. is calculated for illustration. It is assumed that the fluid has a parabolic velocity distribution at the exit of the

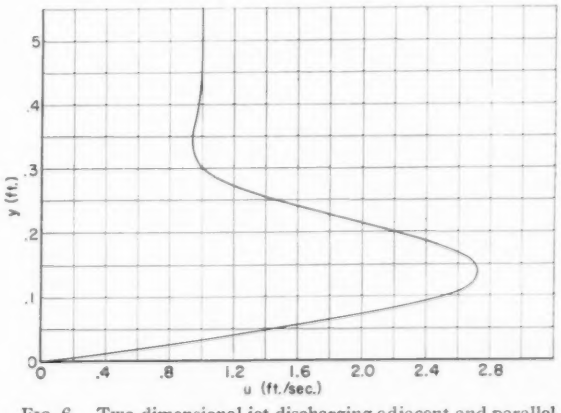

FIG. 6. Two-dimensional jet discharging adjacent and parallel to flat plate into parallel uniform stream. u velocity profile at $x = 1/50$ ft.

slot of width $a = 0.250$ ft. and that the uniform main stream of the same fluid has an initial laminar boundary layer at the beginning of the mixing region corresponding to that which exists at a distance of 0.01 ft. from the leading edge of a flat plate. Also it is assumed that: u_0, uniform (or secondary) stream velocity, = 1.0 ft. per sec.; u_{pm}, maximum jet (or primary) stream velocity, = 3.0 ft. per sec.; and $\nu = 0.1$ ft.^{2} per sec.

The numerically calculated u-velocity profile at $x = 1/50$ ft. is shown in Fig. 6.

Conclusions

It has been shown that the "stepwise" and "implicit" difference forms of the Prandtl and continuity equations developed herein are suitable for the determination of the velocity field in fluid flows described by those equations. The stepwise form allows immediate computation of velocities at successive points but is limited in applicability by stability criteria. The implicit equations have no stability restrictions whatever; by hand they may best be solved by relaxation, but if a digital computer is available they may be rapidly solved by iteration.

Two original solutions have been obtained by means of the finite difference forms:

(1) The velocity distribution in longitudinal flow over a porous flat plate with an initial boundary layer and an arbitrary distribution of normal velocity at the plate surface (worked for a constant suction velocity, although any other distribution of transverse velocity could have been handled just as easily).

(2) The velocity distribution in the flow field of a two-dimensional jet discharging adjacent and parallel to a flat plate into a uniform stream.

References

[1] Schlichting, H., *Lecture Series "Boundary Layer Theory," Part I–Laminar Flows*, NACA TM 1217, p. 110, April, 1949.

[2] Schlichting, H., *Die Grenzschicht an der eben Platte mit Absaugung und Ausblasen*, Luftfahrt-Forschung, Vol. 19, p. 293, 1942.

[3] Friedrich, C. M., and Forstall, W., Jr., *A Numerical Method for Computing the Diffusion Rate of Coaxial Jets*, Proceedings of the Third Midwestern Conference on Fluid Mechanics, Minneapolis, Minn., p. 635, 1953.

[4] Pai, S. I., *Two-Dimensional Jet Mixing of a Compressible Fluid*, Journal of the Aeronautical Sciences, Vol. 16, No. 7, p. 463, July, 1949.

[5] Goldstein, S., *Modern Developments in Fluid Dynamics*, p. 206, Clarendon Press, Oxford, England, 1938.

[6] Forstall, W., Jr., and Shapiro, A. H., *Momentum and Mass Transfer in Coaxial Jets*, Journal of Applied Mechanics, Transactions of the ASME, Vol. 72, p. 399, 1950.

[7] O'Brien, G. G., Hyman, M. A., and Kaplan, S., *A Study of the Numerical Solution of Partial Differential Equations*, Journal of Mathematics and Physics, Vol. 29, p. 223, 1950.

[8] Scarborough, J. B., *Numerical Mathematical Analysis*, Second Ed., Johns Hopkins Press, Baltimore, 1950.

[9] Goldstein, S., *Concerning Some Solutions of the Boundary Layer Equations in Hydrodynamics*, Proceedings of the Cambridge Philosophical Society, Vol. 26, p. 1, 1930.

[10] Blasius, H., *Grenzschichten in Flüssigkeiten mit kleiner Reibung*, Zeitschrift für Mathematik und Physik, Vol. 56, p. 1, 1908.

[11] Schlichting, H., *Lecture Series "Boundary Layer Theory." Part I–Laminar Flows*, NACA TM 1217, p. 51, April, 1949.

[12] Friedrich, C. M., *A Numerical Difference Equation Method for Determining Velocity Distribution in Coaxial Jets*, Doctoral Dissertation, Carnegie Institute of Technology, 1952.

[13] Thom, A., *Flow Past Circular Cylinders at Low Speeds*, Proceedings of the Royal Society of London, Series A, Vol. 141, p. 651, 1933.

A Provisional Analysis of Turbulent Boundary Layers with Injection*

JOSEPH H. CLARKE,† HANS R. MENKES,‡ AND PAUL A. LIBBY**

Polytechnic Institute of Brooklyn

Summary

Prandtl's analysis of the incompressible turbulent boundary layer over a flat plate is extended in this report to include the effect of uniform, transverse fluid injection. The nondimensional parameters characterizing such a flow are deduced by dimensional reasoning. A velocity profile is generated by considering the flow over a plane wall; this distribution reduces to the universal log law when the mass transfer is zero. The expression also serves to relate the local skin friction to the boundary-layer thickness. When these relationships are used in conjunction with the von Kármán integral, the problem becomes mathematically specified. Since only a limited amount of experimental data is available, it is necessary to assign to certain parameters that arise in the velocity profile the constant values they have for no mass transfer. When more measurements are completed, it may be possible to adjust these parameters as or if required.

The results give the variation of average skin-friction coefficient with the injection ratio and the Reynolds Number based on the streamwise coordinate. The agreement between these results and the experimental data available is found to be satisfactory. The significant reductions in skin friction, and therefore in heat transfer, to be realized with small rates of injection are indicated.

Symbols

A = arbitrary function of V_0/U_τ
B = arbitrary function of V_0/U_τ
C = arbitrary function of V_0/U_τ
C_F = average skin-friction coefficient
D = drag per unit span
F = integral defined by Eq. (20)
g = arbitrary function of V_0/U_τ
l = mixing length
P = time mean of static pressure
R_x = Reynolds Number based on x
R_ϑ = Reynolds Number based on ϑ
U = time mean of x component of velocity
u' = fluctuation of x component of velocity
U_τ = friction velocity defined by Eq. (8)
V = time mean of y component of velocity
v' = fluctuation of y component of velocity
δ = boundary-layer thickness
η = nondimensional thickness defined by Eq. (13)
ϑ = momentum thickness
μ = dynamic viscosity
ν = kinematic viscosity
ρ = mass density
τ = Reynolds shear stress defined by Eq. (4)
Φ = integral defined by Eq. (23)
φ = nondimensional velocity defined by Eq. (12)
ψ = integral defined by Eq. (28)
$(\ \bar{}\ )$ = time mean at a spatial point
$(\ )_1$ = evaluated at the outer edge of the layer
$(\ )_0$ = evaluated at the surface

Received May 12, 1954. Revised and received, September 17, 1954.

* This research was conducted under the auspices of Project SQUID, jointly sponsored by the Office of Naval Research, Department of the Navy, Office of Scientific Research, Department of the Air Force, and Office of Ordnance Research, Department of the Army.

† Formerly, Research Associate, Department of Aeronautical Engineering and Applied Mechanics, now, Assistant Professor of Aeronautical Engineering.

‡ Formerly, Research Fellow, Department of Aeronautical Engineering and Applied Mechanics, now, Research Fellow, Department of Aeronautical Engineering, University of Michigan.

** Associate Professor of Aeronautical Engineering.

Introduction

There is considerable interest in the application of the sweat-cooling technique to the solution of some of the critical heat-transfer problems associated with the flow of high energy gas streams within propulsion devices and around high-speed missiles and aircraft.[1–4] This technique involves the injection of a gaseous or liquid coolant through a permeable wall and leads to the establishment of a thick, heat-insulating layer between the high energy outer flow and the surface.

Studies of skin friction and heat transfer for the case of a laminar boundary layer with injection have been carried out in detail and may be considered in good order. Most of the analyses consider gaseous coolants—namely, the same gas as that constituting the main stream. Turbulent boundary layers are, however, more likely to prevail in the applications for which the sweat-cooling method is contemplated. First, the gas streams in propulsion devices usually involve high levels of vorticity and turbulence. Second, permeable walls are inherently rough. Third, the influence of continuous injection is destabilizing with respect to a laminar boundary layer—especially since the injection may actually involve a large number of discrete jets. These factors tend to cause early transition to turbulent flow.

Thus, an estimate of the influence of injection on turbulent boundary layers should find technical application. Because the physical mechanism of turbulent flow still awaits precise, tractable formulation, a sound scientific analysis of this phenomenon is not possible. However, the earlier semiempirical analyses of turbulent boundary layers on impermeable walls have led to results of engineering utility.[5, 6] It would seem reasonable to attempt to calculate the effect of injection on turbulent boundary layers by extending these methods. It is recognized that detailed and reliable measure-

ments are required to establish the validity of any such extension. Since considerable difficulty in making the measurements is involved, such data might not be available for some time. Moreover, the results presented here indicate the high degree of accuracy which will be required for meaningful experiments.

In this paper, the classic analysis by Prandtl of the impermeable, incompressible turbulent boundary layer on a flat plate at zero incidence is extended to include the effect of uniform fluid injection in such a manner that the results reduce to those of the impermeable analysis at each step if the mass transfer is set equal to zero. The result of the analysis is the variation of average skin-friction coefficient with injection ratio and Reynolds Number based on the streamwise coordinate. These curves are compared to available data,[7] and reasonable agreement is found.

The skin-friction variation can be used to estimate the variation of Nusselt Number with Reynolds Number and injection ratio if the Reynolds analogy is used. Because of the existence of this analogy, attention has been restricted to skin friction in the present development.

The Velocity Profile Obtained from Flow over a Plane Wall

For the two-dimensional mean flow of an incompressible, turbulent fluid in boundary layers of small pressure gradient, the Reynolds equations are reduced, following Prandtl, to the form

$$U\frac{\partial U}{\partial x} + V\frac{\partial U}{\partial y} = -\frac{1}{\rho}\frac{\partial P}{\partial x} + \frac{\partial}{\partial y}\left(\nu\frac{\partial U}{\partial y} + \frac{\tau}{\rho}\right) \quad (1)$$

$$\partial P/\partial y = 0 \quad (2)$$

These are supplemented by the continuity equation

$$(\partial U/\partial x) + (\partial V/\partial y) = 0 \quad (3)$$

In Eq. (1)

$$\tau = -\rho\overline{u'v'} \quad (4)$$

According to the momentum transfer theory, Eq. (4) may be written

$$\tau = \rho l^2(\partial U/\partial y)^2 \quad (5)$$

where l is the mixing length of Prandtl.

Dimensional reasoning attendant upon empiricism indicates that the velocity in the turbulent boundary layer under transverse injection is of the form[8]

$$U = U_\tau f[(U_\tau y/\nu), (V_0/U_\tau)] \quad (6)$$

and that the mixing length for higher Reynolds Numbers is of the form[8]

$$l = yg(V_0/U\tau) \quad (7)$$

In Eqs. (6) and (7) U_τ, the so-called friction velocity, is related to the wall shear stress by

$$U_\tau^2 = \nu(\partial U/\partial y)_0 \quad (8)$$

Since, in the neighborhood of a permeable wall

$$V(\partial U/\partial y) \gg U(\partial U/\partial x)$$

in Eq. (1), it is proposed to idealize the problem to that of the one-dimensional flow over a plane wall for the purpose of generating a boundary-layer velocity profile. It is remarked that the universal log law can be developed in the same way. The essential shear aspect is retained in such a model. Moreover, impermeable measurements indicate a certain insensitivity of the general profile shape in terms of the variables of Eq. (6) to the precise physical environment.

With the assumption of no variation with x, Eq. (3) yields, together with the boundary condition on V,

$$V = V_0 = \text{constant} \quad (9)$$

while Eq. (1) reduces to

$$V_0(dU/dy) = d/dy(\tau/\rho) \quad (10)$$

after neglecting the purely viscous shear contribution. Combining Eqs. (5), (7), and (10), one obtains

$$V_0(dU/dy) = g^2(d/dy)[y^2(dU/dy)^2] \quad (11)$$

After introduction of the nondimensional variables

$$\varphi \equiv U/U_\tau \quad (12)$$

$$\eta \equiv U_\tau y/\nu \quad (13)$$

in accord with Eq. (6), Eq. (11) may be integrated with respect to y to yield

$$\varphi = A + B\ln\eta + (1/4g^2)(V_0/U_\tau)\ln^2\eta \quad (14)$$

In view of Eq. (6), A and B, as well as g, are to be regarded as functions of V_0/U_τ in general. As is to be expected from its derivation, Eq. (14) reverts to the universal log law when the injection velocity vanishes.

Turbulent Boundary Layer over Flat Plate with Uniform Injection

The turbulent boundary layer over a flat plate under the action of uniform injection may be anayzed if Eq. (14) is assumed to represent the distribution of velocity through the thickness. The same expression, when evaluated at the outer edge of the boundary layer, serves to relate the friction velocity to the boundary-layer thickness. Because viscous stresses have been neglected, the profile cannot be expected to hold in the immediate vicinity of the wall. Indeed, impermeable data indicate that the log law fails when η is less than 30. However, Eq. (14) can be extended to serve as an interpolation formula in the immediate neighborhood of the wall if the arguments of the logarithms are increased by one. This change has little effect outside of this sublayer where $\eta \gg 1$. After rearrangement, Eq. (14) thus becomes

$$\varphi = B\ln(1 + C\eta) + (1/4g^2)(V_0/U_1)\varphi_1\ln^2(1 + \eta) \quad (15)$$

where C is, in general, another function of V_0/U_τ, and the subscript one signifies evaluation at the outer edge

TABLE 1
Abridged Table of Functions

	$V_0/U_1 = 0.005$			$V_0/U_1 = 0.010$		
η_1	$F \times 10^{-3}$	$\Phi \times 10^{-6}$	$\psi \times 10^{-3}$	$F \times 10^{-3}$	$\Phi \times 10^{-6}$	$\psi \times 10^{-3}$
45	0.7072	0.00906	0.04468	1.272	0.00798	0.0328
85	1.081	0.02246	0.08446	2.460	0.02071	0.0596
165	1.702	0.05708	0.15990	5.412	0.05672	0.1045
325	2.778	0.1436	0.2978	14.50	0.1616	0.1811
485	3.768	0.2473	0.4264	29.85	0.3102	0.2490
685	4.950	0.3953	0.5781	63.65	0.5602	0.3229
885	6.147	0.5603	0.7227	126.8	0.9034	0.3882
1,085	7.335	0.7400	0.8617	248.5	1.358	0.4469
1,285	8.539	0.9340	0.9960	479.0	1.962	0.5002
1,485	9.786	1.139	1.126	915.9	2.767	0.5486
1,685	11.01	1.356	1.253	1,995	3.871	0.5930
1,885	12.29	1.584	1.377	4,499	5.440	0.6342
2,085	13.59	1.823	1.498	11,440	7.778	0.6723
2,285	14.94	2.072	1.617	35,170	11.55	0.7077
2,980	∞	∞		∞	∞	
81,970						

of the boundary layer. It is observed that $(V_0/U_\tau) \equiv (V_0/U_1)\varphi_1$, where V_0/U_1 is termed the injection ratio. von Kármán's integral of Eq. (1) for zero pressure gradient

$$\frac{d}{dx}\int_0^\delta \frac{U}{U_1}\left(1 - \frac{U}{U_1}\right) dy - \frac{V_0}{U_1} = \frac{U_\tau^2}{U_1^2} \tag{16}$$

may be transformed by means of Eqs. (12) and (13) to the form

$$\frac{\nu}{U_1}\frac{d\eta_1}{dx}\frac{d}{d\eta_1}\left[\int_0^{\eta_1} \varphi\left(1 - \frac{\varphi}{\varphi_1}\right) d\eta\right] - \frac{V_0}{U_1} = \frac{1}{\varphi_1^2} \tag{17}$$

since Eq. (15) is of the functional form

$$\varphi = \varphi[\varphi_1, \eta, (V_0/U_1)] = \varphi[\eta_1, \eta, (V_0/U_1)] \tag{18}$$

and the integral is thereby dependent upon the variable η_1 alone. After differentiation under the integral sign and some rearrangement, Eq. (17) may be written

$$\frac{\nu}{U_1} F\left(\frac{V_0}{U_1}, \eta_1\right)\frac{d\eta_1}{dx} = 1 + \frac{V_0}{U_1}\varphi_1^2 \tag{19}$$

where

$$F\left(\frac{V_0}{U_1}, \eta_1\right) \equiv \int_0^{\eta_1}\left[\left(1 - 2\frac{\varphi}{\varphi_1}\right)\varphi_1^2\frac{\partial\varphi}{\partial\eta_1} + \varphi^2\frac{d\varphi_1}{d\eta_1}\right] d\eta \tag{20}$$

As is usual, the boundary layer is assumed turbulent from the leading edge of the plate. Since the effect of injection on the initial growth of the boundary layer is slight, the initial condition on Eq. (19) will be taken as

$$\eta_1(0) = 0 \tag{21}$$

just as in the impermeable case. Thus, Eqs. (19) and (21) give

$$U_1 x/\nu \equiv R_x = \Phi[(V_0/U_1), \eta_1] \tag{22}$$

where

$$\Phi\left(\frac{V_0}{U_1}, \eta_1\right) \equiv \int_0^{\eta_1} \frac{F[(V_0/U_1), \eta_1]\, d\eta_1}{[1 + (V_0/U_1)\varphi_1^2]} \tag{23}$$

The two-dimensional drag is defined by

$$D = \int_0^x \rho U_\tau^2 \frac{dx}{d\eta_1}\, d\eta_1 \tag{24}$$

Using Eqs. (12) and (19), one obtains

$$D = \mu U_1 \int_0^{\eta_1} \frac{F[(V_0/U_1), \eta_1]\, d\eta_1}{\varphi_1^2[1 + (V_0/U_1)\varphi_1^2]} \tag{25}$$

With the definition

$$C_F \equiv 2D/(\rho U_1^2 x) \tag{26}$$

and Eq. (22), Eq. (25) may be written

$$C_F = \{2\psi[(V_0/U_1), \eta_1]\}/\{\Phi[(V_0/U_1), \eta_1]\} \tag{27}$$

where

$$\psi\left(\frac{V_0}{U_1}, \eta_1\right) \equiv \int_0^{\eta_1} \frac{F[(V_0/U_1), \eta_1]\, d\eta_1}{\varphi_1^2[1 + (V_0/U_1)\varphi_1^2]} \tag{28}$$

Eqs. (27) and (22) give the average skin-friction coefficient as a function of the Reynolds Number in terms of the parameter η_1. Thus, the problem formulates to the evaluation of the three integrals given by Eqs. (20), (23), and (28), where $\varphi[\eta_1, \eta, (V_0/U_1)]$ and $\varphi_1[\eta_1, (V_0/U_1)]$ follow from Eq. (15). This development is parallel to that of the impermeable plate drag law of Prandtl.

Quadrature awaits specification of the unknown functions B, C, and g, whose arguments are the product $(V_0/U_1)\varphi_1$. These three parameters will now be taken as constants conforming with impermeable measurements made in conjunction with the universal log law.[6] Thus, let

$$\left.\begin{aligned} B &= 2.493 = 1/g \\ C &= 8.93 \\ g &= 0.401 \end{aligned}\right\} \tag{29}$$

It will be shown below that the limited experimental data available at the present time do not suggest greater refinement.

Substituting Eq. (15) into Eq. (20) and integrating, one obtains for B, C, and g constant

$$F[(V_0/U_1), \eta_1] = (B^2/C)(d\varphi_1/d\eta_1)[(1 + C\eta_1) \times \ln^2 (1 + C\eta_1) - 2(1 + C\eta_1) \ln (1 + C\eta_1) + 2C\eta_1] + (V_0/U_1)(\varphi_1^2/4g^2)(d\varphi_1/d\eta_1) [(1 + \eta_1) \ln^2 (1 + \eta_1) - 2(1 + \eta_1) \ln (1 + \eta_1) + 2\eta_1] - (V_0/U_1)^2 \times (\varphi_1/4g^2)^2(d\varphi_1/d\eta_1) [(1 + \eta_1) \ln^4 (1 + \eta_1) - 4(1 + \eta_1) \ln^3 (1 + \eta_1) + 12(1 + \eta_1) \times \ln^2 (1 + \eta_1) - 24(1 + \eta_1) \ln (1 + \eta_1) + 24\eta_1] \quad (30)$$

where $d\varphi_1/d\eta_1$ follows directly from Eq. (15).

The integrals of Eqs. (23) and (28) may now be evaluated numerically for selected values of the injection ratio by means of Simpson's rule if Eqs. (29) are used. In Table 1, an abridged tabulation of the functions F, Φ, and ψ versus η_1 is given for injection ratios of 0.005 and 0.010. It is found from Eq. (22) that R_x increases monatonically with η_1 to become infinite at a value of η_1 which is finite for nonvanishing injection ratios. From Eq. (15) this value of η_1 is found to correspond to infinite φ_1, or zero local skin friction, a result physically compatible with the corresponding infinite Reynolds Number. The finiteness of this limit value of η_1 is illustrative of the asymptotic behavior of the product δU_x. The limit values of η_1 for injection ratios of 0.005 and 0.010 are given in Table 1.

The average skin-friction coefficient is computed from Eq. (27). The variation of Reynolds Number based on momentum thickness with Reynolds Number based on the streamwise coordinate follows immediately from Eq. (16) in its integrated form.

$$C_F = 2[(R_\vartheta/R_x) - (V_0/U_1)] \quad (31)$$

Figs. 1 and 2 present the variation of R_ϑ with R_x and of C_F with R_x, respectively, for injection ratios of 0, 0.005, and 0.010. It is seen from Fig. 2 that the indicated reduction of skin friction, and hence of heat transfer, under the action of injection is large.

In addition, velocity profiles in the physical plane have been computed and shown in Fig. 3 for the above injection ratios, a nominal free-stream velocity of 26 ft. per sec. and a nominal Reynolds Number based on streamwise coordinate of 600,000.

Comparison with Experiment

Shown in Figs. 1 and 2 are data for the corresponding injection ratios collected by Mickley, et al.[7] The data of Fig. 1 follow directly from the measurement of the momentum thickness at various streamwise stations under particular stream and injection conditions. The average skin-friction coefficient for each Reynolds Number is then computed from Eq. (31). All data shown were collected at a nominal velocity of 26 ft. per sec.

Because of environmental anomalies at the leading edge, there exists in these data, as in most turbulent boundary-layer raw data, an uncertainty in the location of the effective origin of the streamwise coordinate for each run. The data may be adjusted for this effect in the usual manner by shifting all the points indicating the variation of R_ϑ with R_x for a given injection ratio to the right by some constant amount which results in the best agreement with the theory. The effect of this shift is shown in Fig. 1. It is seen that the shifts are small, amounting to increments in Reynolds Number of zero for no injection, to 25,000 for an injection ratio of 0.005, and to 10,000 for an injection ratio of 0.010. The variation of skin-friction coefficient with Reynolds Number may be recomputed from Eq. (31) and is shown in Fig. 2. The adjustment in C_F due to a small length correction is appreciable and brings the data in reasonable agreement with the present analysis. In particular, the reduction in skin friction achieved by an injection ratio of one-half per cent is well given.

By comparing the orders of magnitude of the average skin-friction coefficient and the injection ratio from Fig. 2, it can be observed from Eq. (31) that the skin friction for injection ratios of order 0.01 is given by the small difference of two measured quantities. Consequently, the precision of the measured values in Fig. 2 in this range is significantly reduced; indeed, the value at the highest Reynolds Number may be virtually meaningless. The numerical counterpart in the theory lies in the behavior of the functions F, Φ, and ψ in the neighborhood of the limit value of η_1.

For purposes of comparison, theoretical velocity profiles are compared in Fig. 3 with corresponding measurements (uncorrected for length) collected at the same station under different injection ratios. The nominal velocity is 26 ft. per sec. and the nominal Reynolds Number is 600,000; the precise conditions are noted on the figure. It is seen that the thickening effect is well-predicted by the theory but that the general shape is not. However, the discrepancy in shape between theory and experiment is qualitatively independent of injection ratio. The theoretical profile for no injection is the universal log law, which has been amply verified near the wall at higher Reynolds Numbers. Hence it might be inferred that the observed discrepancy is in reasonable measure an effect of the low test Reynolds Numbers. In common with all boundary-layer integral methods, the precision of the distribution of velocity is characteristically inferior to the predicted average effects.

Thus the simple assumptions made in Eq. (29) for the function B, C, and g appear to result in reasonable agreement with the limited drag data available. More accurate and complete measurements are required to fully establish the validity of the relationships derived and, further, to determine if or how the assumptions made for the aforementioned functions are to be modi-

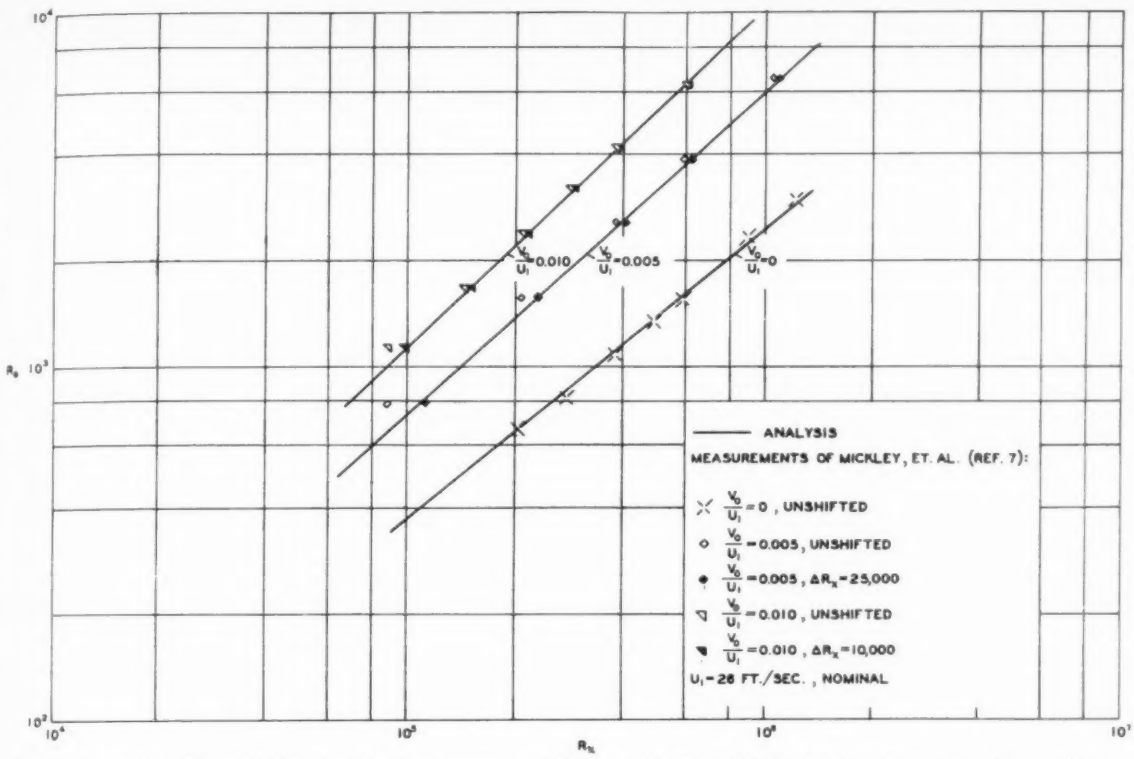

FIG. 1. Variation of Reynolds Number based on momentum thickness with Reynolds Number based on streamwise coordinate

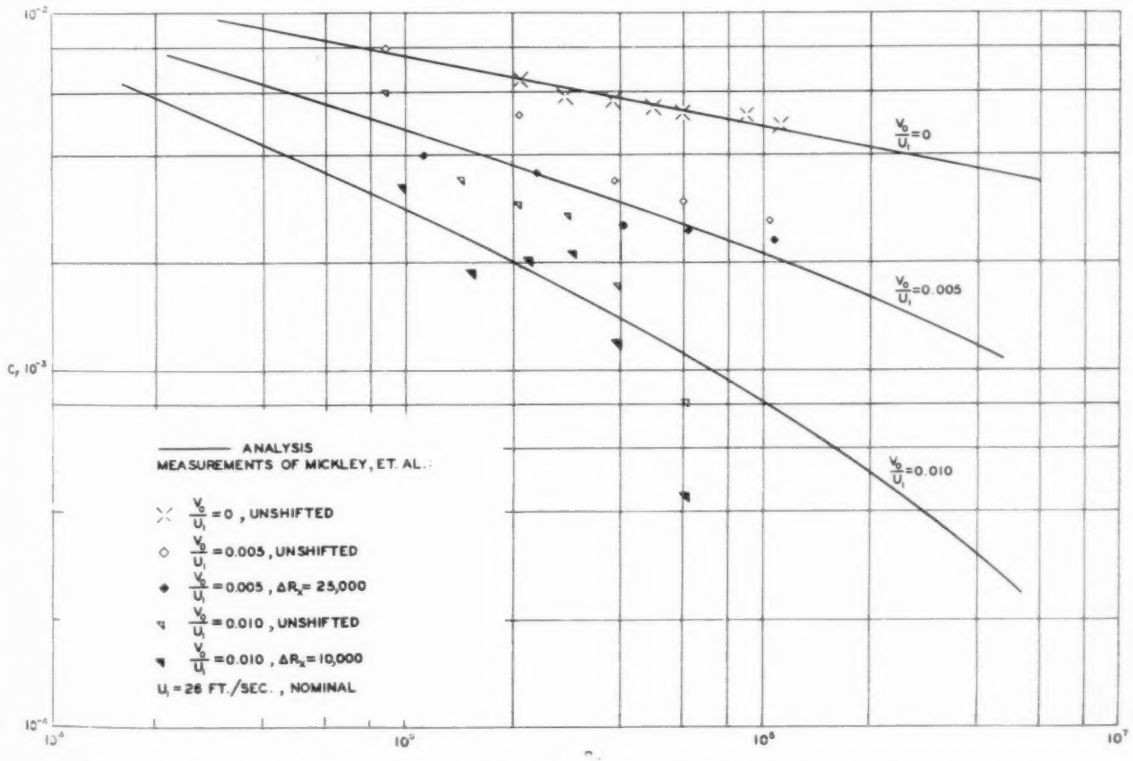

FIG. 2. Variation of average skin-friction coefficient with Reynolds Number based on streamwise coordinate.

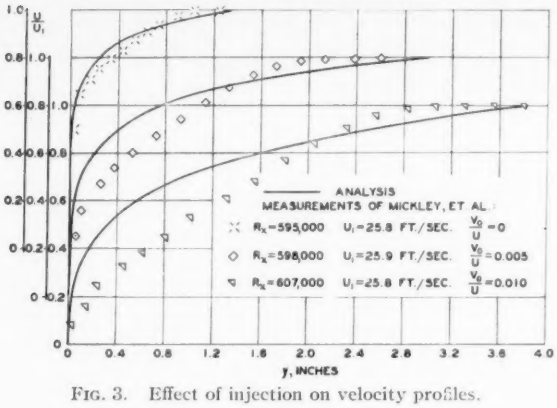

FIG. 3. Effect of injection on velocity profiles.

fied. In this sense, the analysis is considered provisional.*

CONCLUDING REMARKS

The Prandtl analysis of the incompressible turbulent boundary layer has been extended to include the effect of mass transfer.

The variation of average skin-friction coefficient with Reynolds Number for various injection ratios predicted by this extension is in satisfactory agreement with the measurements of reference 7. The Reynolds Number range covered in this comparison is about 10^5 to 10^6. The calculated results involve no empirical constants determined from permeable wall measurements. Therefore, until a comparison with more accurate and extensive measurements is possible, the present results must be regarded as provisional. The Reynolds analogy, confirmed by the Mickley measurements of permeable velocity and temperature profiles, can be used to deduce the effect of injection on Nusselt Number variation from the theoretical skin-friction coefficient relations.

The velocity profile and the parametric relations for average skin-friction coefficient in terms of Reynolds Number automatically revert to those of Prandtl when the injection ratio is set equal to zero. The minor adjustment made in the final interpolation formula of Schlichting[6] does not, however, follow.

The relations developed presumably apply also to the case of suction, but no comparison with measurements has been made.

* After this analysis was first submitted for publication, a paper by W. H. Dorrance and F. J. Dore entitled *The Effect of Mass Transfer on the Compressible Turbulent Boundary-Layer Skin Friction and Heat Transfer* appeared in the Journal of Aeronautical Sciences, Vol. 21, No. 6, pp. 404–410, June 1954. The velocity profile expressed here by Eq. (14) is derived in that report in a similar way excepting that a wall boundary condition which yields a relation between the parameters A and B is imposed. The remainder of the two analyses are, however, quite dissimilar. It is of interest to compare the results of each analysis with each other and with the measurements of reference 7. The present writers have compared the variation at low speeds of local skin-friction coefficient with Reynolds Number in the range of the measurements for an injection ratio of 0.005. The agreement of local skin friction predicted by the present method with both the shifted and unshifted data of reference 7 was found good—the local skin-friction results being relatively insensitive to the present length correction. The values of the coefficients predicted by Dorrance and Dore at this injection ratio are about one-half the above values at corresponding Reynolds Numbers. The agreement cited by Dorrance and Dore of their results with reference 7 is asserted on the basis of a different mode of representation of these results, wherein the measured coefficients are normalized to the corresponding measured impermeable coefficients. The discrepancy between their results and the present results may be due to the interchange of average and local coefficients at one stage of their analysis, an assumption which would appear to restrict subsequent results to small injection ratios.

REFERENCES

[1] Duwez, P., and Wheeler, H. L., Jr., *Experimental Study of Cooling by Injection of a Fluid Through a Porous Material*, Journal of the Aeronautical Sciences, Vol. 15, No. 9, p. 509, September, 1948.

[2] Eckert, E. R. G., *Laminar Heat Transfer and Temperature Profiles in Laminar Boundary Layers on a Sweat-Cooled Wall*, A.A.F. Technical Report 5646, Air Materiel Command, November, 1947.

[3] Yuan, S. W., *Heat Transfer in Laminar Compressible Boundary Layer on a Porous Flat Plate with Fluid Injection*, Journal of the Aeronautical Sciences, Vol. 16, No. 12, p. 741, December, 1949.

[4] Morduchow, M., *On Heat Transfer over a Sweat-Cooled Surface in Laminar Compressible Flow with a Pressure Gradient*, Journal of the Aeronautical Sciences, Vol. 19, No. 10, p. 705, October, 1952.

[5] Goldstein, S., *Modern Developments in Fluid Dynamics;* Oxford University Press, New York, 1938.

[6] Schlichting, H., Lecture Series *Boundary Layer Theory, Part II, Turbulent Flows*, NACA TM 1218, April, 1949.

[7] Mickley, H. S., Ross, R. C., Squyers, A. L., and Stewart, W. E., *Heat, Mass and Momentum Transfer for Flow over a Flat Plate with Blowing or Suction*, NACA TN 3208, July, 1954.

[8] Goldstein, S., *ibid.*, Vol. 2, pp. 331–336.

On Supersonic Flow Past a Finite Wedge at the Crocco Mach Number

KŌ TAMADA* AND YOSHIO SHIBAOKA†

Kyoto University and Osaka City University, Japan

SUMMARY

In the present paper the supersonic flow past a finite wedge at the Crocco Mach Number is investigated by the hodograph method. An explicit expression for the stream function is obtained, assuming that the nose angle of the wedge is so small that the transonic approximation is applicable. Then, the drag coefficient C_D of the wedge is calculated, the result being

$$C_D = 2.679\,(\gamma+1)^{-1/3}\alpha^{5/3}$$

$$(\gamma+1)^{3/2}/\alpha^{2/3}(M-1)^{-4} = 1.6483$$

where γ, α, and M are, respectively, the adiabatic exponent, the seminose angle of the wedge, and the Mach Number of the undisturbed flow. The velocity distribution along the side of the wedge is also calculated.

(1) INTRODUCTION

THE CONTINUOUS TRANSITION from attached to detached shocks in supersonic flow past a finite wedge was first discussed by Guderley.[1] In a previous paper,[2] Tamada gave an approximate analysis of the process of transition. There the whole analysis was carried out in the physical plane, and an expression for the flow field near the nose A (Fig. 1) was obtained on the basis of a linearized field equation. Also, using the expression so obtained, the drag coefficient of the wedge was calculated. It is somewhat questionable whether the linearized expression is valid over the entire wedge. It is probable that the flow near the shoulder B (Fig. 1) may require a different representation.

Now, the flow past a wedge, in general, can be treated conveniently in the hodograph plane, since the boundaries consist of straight lines only. Especially, when the Mach Number of the oncoming flow takes a particular value (the Crocco Mach Number), the flow is regular at the nose A and the analysis can be considerably simplified. Therefore, in the present paper, the flow in the Crocco state will be analyzed by the hodograph method, making the assumption that the seminose angle of the wedge is so small that the transonic approximation is admissible.

(2) FORMULATION OF THE PROBLEM

In the following, the "critical speed" (which is invariant in passing through the shock wave) is taken as the unit of velocity. Let M be the Mach Number of the uniform flow, and let q and θ be the magnitude of the velocity vector and its angle of inclination to the direction of the uniform flow, respectively. If one writes

$$\left.\begin{aligned} q &= 1 + [2m/(\gamma+1)]\xi \\ \theta &= (4\sqrt{2}/3)\,[m^{3/2}/(\gamma+1)]\eta \\ m &= M-1 \quad \text{or} \quad (M^2-1)/2 \end{aligned}\right\} \tag{1}$$

where γ is the adiabatic exponent, one may assume that m is small and ξ and η are finite in the transonic field under consideration. Then the fundamental field equation for the stream function ψ reduces to the Tricomi equation

$$\psi_{\xi\xi} - (9/4)\xi\psi_{\eta\eta} = 0 \tag{2}$$

Further, it can be shown that the equation for the shock polar becomes

$$\eta = \pm(3/2\sqrt{2})\,(1-\xi)\,(1+\xi)^{1/2} \tag{3}$$

and the condition on the shock wave is represented by the equation

$$\left.\begin{aligned} &\psi_\xi - S(\xi)\psi_\eta = 0 \\ &S(\xi) = (3/2\sqrt{2})\,(1+\xi)^{1/2}\,[(1+7\xi)/(3+5\xi)] \end{aligned}\right\} \tag{4}$$

along the shock polar [Eq. (3)].

Now, let (ξ_A, η_A) be the coordinates of the nose A of the wedge in the (ξ, η)-plane (Fig. 2), and let $\psi = 0$ along the wall AB ($\eta = \text{const.} = \eta_A$). Then, Eqs. (3), (4), and (1) show that the condition (4) is compatible (without singularity at A) with the condition $\psi = 0$ along AB when and only when

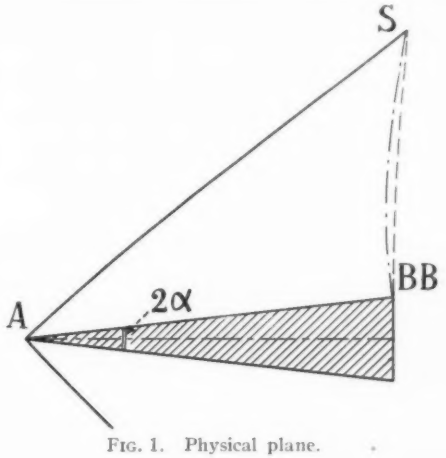

FIG. 1. Physical plane.

Received April 27, 1954.

* Assistant Professor in the Physical Institute.

† Assistant Professor in the Institute of Polytechnics.

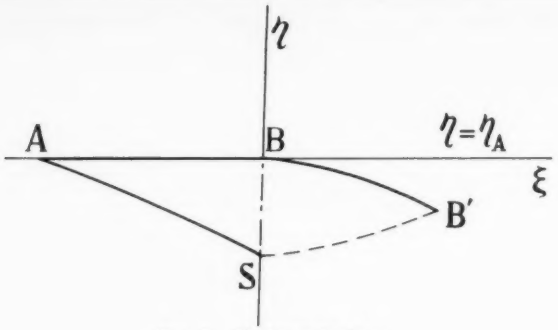

FIG. 2. Hodograph plane.

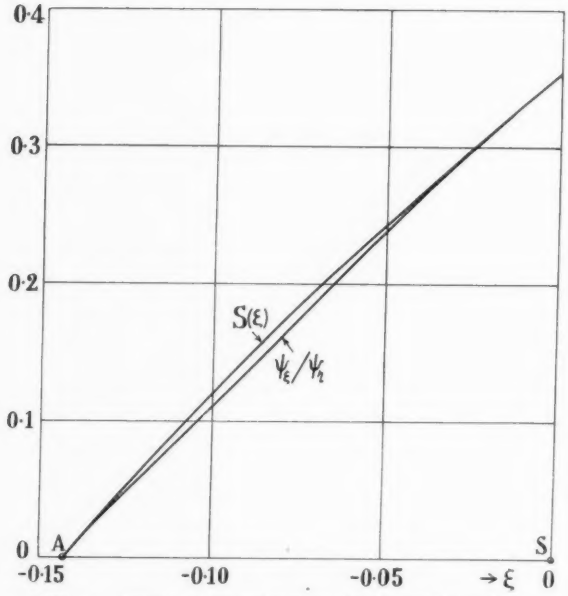

FIG. 3. Degree of approximation for the condition (4).

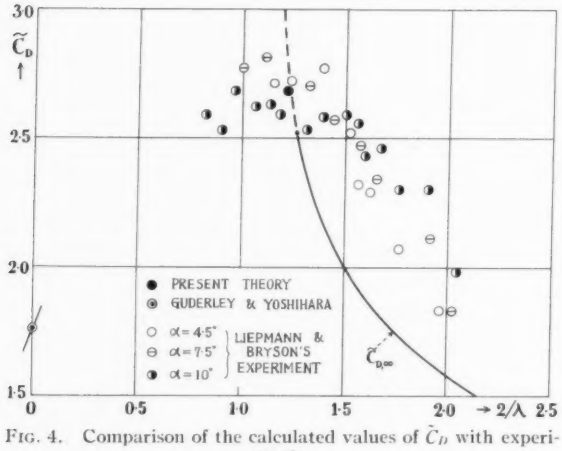

FIG. 4. Comparison of the calculated values of $\tilde{C}_D$ with experiments.

$$\left.\begin{aligned} \xi_A &= -(1/7) \qquad \eta_A = (12/7)\sqrt{3/7} \\ \lambda &= (\gamma+1)^{2/3}\alpha^{2/3}m^{-1} = (8/7)3^{1/3} \cong 1.6483 \end{aligned}\right\} \quad (5)$$

where α is the seminose angle and λ is the transonic parameter. This is the Crocco state and will be exclusively discussed below. Further, $\psi = 0$ along the characteristic BB′ ($\eta_A - \eta = \xi^{3/2}$) in the ($\xi$, η)-plane, since there occurs a Prandtl-Meyer expansion at the shoulder B of the wedge. Thus, the problem reduces to finding the solution $\psi(\xi, \eta)$ of Eq. (4) which vanishes along ABB′ and satisfies the condition [Eq. (3)] on the shock polar AS in the (ξ, η)-plane.

(3) The Stream Function

First, it is noticed that Eq. (2) has a general solution of the form

$$\psi = \frac{\Gamma(2/3)}{\Gamma(1/2)\Gamma(1/6)}\int_{-1}^{1}(1-t^2)^{-5/6}F(\xi^{3/2}t+\vartheta)\,dt + \frac{\Gamma(4/3)}{\Gamma(1/2)\Gamma(5/6)}\,\xi\int_{-1}^{1}(1-t^2)^{-1/6}G(\xi^{3/2}t+\vartheta)\,dt \quad (6)$$

where

$$\vartheta = \eta_A - \eta \quad (7)$$

It may be observed here that

$$F(\vartheta) = \psi(0, \vartheta)$$

$$G(\vartheta) = \psi_\xi(0, \vartheta)$$

From the boundary condition that $\psi = 0$ along the characteristic BB′($\xi = \vartheta^{2/3}$), there arises an integral equation of Abel's type which connects the arbitrary functions $F(\vartheta)$ and $G(\vartheta)$. The solution of this equation is written as

$$F(\vartheta) = -\frac{1}{3}\,\frac{\Gamma(1/6)}{\Gamma(1/2)\Gamma(2/3)}\,\vartheta^{2/3}\int_0^1(1-\tau)^{-1/2}\times G(\vartheta\tau)\,d\tau \quad (8)$$

(For details of the deduction, reference may be made to Tricomi's well-known memoir.[3])

Further, the condition $\psi = 0$ along AB ($\vartheta = 0$, $\xi < 0$) requires the following homogeneous integral equation to hold.

$$-\frac{\Gamma(5/6)}{\Gamma(1/2)\Gamma(1/3)}\int_{-1}^{1}(1-t^2)^{-5/6}(i|\xi|^{3/2}t)^{2/3}\times dt\int_0^1(1-\tau)^{-1/3}G(i|\xi|^{3/2}t\tau)\,d\tau + \xi\int_{-1}^{1}(1-t^2)^{-1/6}G(i|\xi|^{3/2}t)\,dt = 0 \quad (9)$$

It can be shown that this equation possesses characteristic solutions of the form

$$G(\vartheta) = \vartheta^{(2/3)+2n}, \qquad (n = 0, 1, 2, \ldots) \quad (10)$$

From Eqs. (10), (8), and (6) one obtains a system of characteristic solutions $\psi_n(\xi, \vartheta)$ of Eq. (2).

$$\psi_n = -\frac{1}{3}\frac{\Gamma(1/6)\Gamma[(5/3)+2n]}{\Gamma(1/2)\Gamma[(7/3)+2n]}\vartheta^{(4/3)+2n}\times F\left(-\frac{1}{6}-n,-\frac{2}{3}-n;\frac{2}{3};\frac{\xi^3}{\vartheta^2}\right)+\xi\vartheta^{(2/3)+2n}F\left(\frac{1}{6}-n,-\frac{1}{3}-n;\frac{4}{3};\frac{\xi^3}{\vartheta^2}\right)$$

$$=(-1)^{n+1}\frac{2}{\sqrt{3}}\frac{\Gamma(1/3)\Gamma[(4/3)+n]}{\Gamma(1/2)\Gamma[(7/6)+n]}\times|\xi|^{(1/2)+3n}\vartheta F\left(-\frac{1}{6}-n,\frac{1}{6}-n;\frac{3}{2};\frac{\vartheta^2}{\xi^2}\right) \quad (11)$$

Thus, a general form of ψ that vanishes along ABB′ can be written as

$$\psi = \sum_{n=0}^{\infty} A_n\psi_n \quad (12)$$

where A_n's are arbitrary constants.

Finally, the shock condition [Eq. (4)] along AS determines the constants A_n's. The writers have actually used the first four terms in series (12) so that the value ψ_ξ/ψ_η and its slope agrees with the curve $S(\xi)$ at two of the points A ($\xi = -1/7$) and $S(\xi = 0)$. The results are

$$\left.\begin{aligned} A_0 &= 1\\ A_1 &= -0.18776\vartheta_s^{-2}\\ A_2 &= 0.15801\ \vartheta_s^{-4}\\ A_3 &= 0.02985\vartheta_s^{-6}\\ \vartheta_s &= \eta_A - \eta_s = \frac{12}{7}\sqrt{\frac{3}{7}}-\frac{3}{2\sqrt{2}} \cong 0.061603 \end{aligned}\right\} \quad (13)$$

After determining these constants, the degree of approximation for the condition [Eq. (4)] is examined. The result is shown in Fig. 3.

(4) Drag Coefficient

The pressure coefficient C_p is defined, as usual, in the form

$$C_p = (2/\gamma M^2)\,[(p/p_u) - 1] \quad (14)$$

where p_u and p are, respectively, the pressures in the uniform flow and the flow behind the shock wave. In the transonic approximation, C_p is related to the reduced velocity ξ as

$$C_p = [4/(\gamma+1)]m(1-\xi) \quad (15)$$

Hence, the drag coefficient C_D of the wedge is given by

$$C_D = \alpha\int_0^l C_p\,ds\Big/\int_0^l ds = \frac{4}{\gamma+1}\,\alpha m\times\int_0^l(1-\xi)\,ds\Big/\int_0^l ds \quad (16)$$

where l is the length of the side AB and s is the distance along AB from the nose A in the physical plane.

Now, since $q = d\phi/ds$, ϕ being the velocity potential, and $\phi_\xi = -(3/\sqrt{2})m^{1/3}\xi\psi_\vartheta$ in the transonic approximation, it follows that along AB ($\vartheta = 0$)

$$ds = -(3/\sqrt{2})m^{1/3}\xi\psi_\vartheta\,d\xi \quad (17)$$

Also, from Eqs. (12) and (11)

$$\left.\begin{aligned} \psi_\vartheta &= \sum_{n=0}^{\infty} A_n a_n|\xi|^{(1/3)+3n}\\ a_n &= (-1)^{n+1}\frac{2}{\sqrt{3}}\frac{\Gamma(1/3)\Gamma[(4/3)+n]}{\Gamma(1/2)\Gamma[(7/6)+n]} \end{aligned}\right\} \quad (18)$$

along AB. Inserting Eqs. (17) and (18) into Eq. (16), a formula for the drag coefficient can be obtained in the form

$$\bar{C}_D = (\gamma+1)^{1/3}\alpha^{-5/3}C_D = \frac{7}{2}3^{-1/3}\left\{1+\frac{1}{7}\left(\sum_{n=0}^{\infty}7^{-3n}\frac{a_nA_n}{7+6n}\right)\times\left(\sum_{n=0}^{\infty}7^{-3n}\frac{a_nA_n}{5+6n}\right)^{-1}\right\} \quad (19)$$

In the four-term approximation mentioned above, the value of $\bar{C}_D$ is calculated to be

$$\bar{C}_D \cong 2.679 \quad (20)$$

It may be added here for comparison that in the transonic approximation the drag coefficient $\bar{C}_{D,\infty}$ of an infinite wedge (not of a finite wedge) is given [from Eqs. (1), (3), and (16)] as a function of the transonic parameter λ by the relations

$$\bar{C}_{D,\infty} = 2^{4/3}(1-\xi)^{1/3}(1+\xi)^{-1/3}$$
$$\lambda = 2^{2/3}(1-\xi)^{2/3}(1+\xi)^{1/3}$$

or

$$\lambda = 8\bar{C}_{D,\infty}^{\ 3}/(16+\bar{C}_{D,\infty}^{\ 3})$$

and especially $\bar{C}_{D,\infty} = 2.773$ for $\lambda = 1.6483$ ($\xi = -1/7$) corresponding to the Crocco state considered above.

(Continued on page 269)

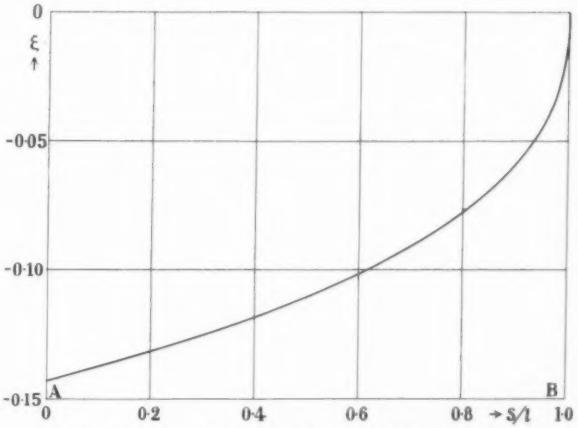

Fig. 5. Velocity distribution along the side of the wedge.

Effect of Large Deflections and Initial Imperfections on the Buckling of Cylindrical Shells Subject to Hydrostatic Pressure

WILLIAM A. NASH*
University of Florida

ABSTRACT

Numerous treatments of the elastic buckling of thin cylinders under various loadings and with various boundary conditions exist in the literature. In general, those analyses which involve classical small deflection shell theory predict higher buckling loads than actually found during test. In an effort to explain the discrepancy between these theoretical values and experiment, Donnell in 1934 introduced the concept of large deflections together with the consideration of initial deviations from perfect shape. This approach has been employed by Donnell and Wan to investigate the phenomena of buckling of cylinders subject to axial compression and by Loo to study torsional buckling. Both of these studies yielded results that are in substantial agreement with experiment. In this paper the buckling of a cylinder subjected to hydrostatic pressure is analyzed from the standpoint of large deflections together with initial imperfections because of the marked discrepancy between small deformation theory and test for this type of loading. The relations derived are in line with test results.

INTRODUCTION

NUMEROUS PAPERS CONCERNING the buckling strength of cylindrical shells subject to various loadings have appeared in the literature. In general, the treatments may be separated into two broad categories: (1) so-called classical analyses, based on the small deflection shell theory presented by Love[1] and the assumptions of linear elasticity and perfect initial shape; and (2) large deflection analyses, in some of which initial imperfections are specifically treated. The classical analyses, in general, predict much higher buckling loads than those found during test. For the case of buckling under axial compression, for example, experiments give only an average of from two-tenths of the classical value for extremely thin cylinders to five- or six-tenths for rather thick ones. For the case of torsional buckling, the average experimental result is about 75 per cent of the classical small deflection value. Several attempts[2, 3] were made to explain such discrepancies but the most promising one was the rather general theory presented by Donnell[4] in 1934 in which considerations of both nonlinear terms due to large deflections and the concept of initial deviations from perfect shape were introduced.

In 1939 von Kármán and Tsien[5] presented a new conception of the buckling process for thin sheets. Their analysis of a spherical shell subject to uniform normal pressure, which extended Marguerre's treatment of the "durchschlag" of a curved bar loaded by a concentrated force,[6] indicated the existence of configurations not far from the spherical form which involve a lower level of potential energy. They advanced the hypothesis that the shell would "jump" over into one of these configurations. For the sphere, they calculated such a "lower" buckling load, which is equal to the minimum load necessary to keep the shell in a buckled state with finite deformations and which is independent of the initial imperfections of the shell. In 1941 these same authors applied nonlinear large deflection theory and the concept of a "durchschlag" phenomenon to the study of the postbuckling behavior of a thin cylinder under axial compression.[7] Equilibrium positions with a buckled shape involving a lower load than given by classical theory were found, again without any specific consideration of initial imperfections. The initial maximum resistance of the cylinder was still found to be that indicated by classical theory, but no complete explanation was offered for this fact. Extensions of this work have been presented by Leggett and Jones,[8] Michielsen,[9] Kempner,[10] and Yoshimura.[11] Several other investigators have also considered the discrepancies between theory and experiment.[12–17]

In 1950 Donnell and Wan[18] considered the problem of axial compression of a cylinder and utilized the fundamental finite deflection equations for shells developed by Donnell in 1934 together with a consideration of the initial imperfections of the specimen. The solution obtained was in reasonable agreement with experimental evidence. In 1952 Loo[19] extended this analysis to the case of torsional buckling of thin cylindrical shells (again using finite-deflection theory together with a consideration of initial imperfections) and found for this loading that the specimen was less sensitive to initial imperfections than in the case of axial compression. The fact that his results are in substantial agreement with experiment lends further support to the validity of this approach. Each of these treatments is in excellent agreement with classical buckling theory for the special case of small deflections of perfect specimens.

The problem of the elastic buckling of cylindrical shells subject to hydrostatic pressure has been considered by several authors[20–24] for a variety of boundary

Received March 29, 1954.

* Associate Professor, Department of Engineering Mechanics, University of Florida, Gainesville, Fla.

conditions. To date, only the classical small deformation type of analysis has been employed in analyzing this phenomenon. Again, as in the cases of axial compression and torsion, there is a considerable disparity between the results obtained by classical theory and experimentally obtained buckling loads.[25, 26]

In view of the success attained by Donnell and Wan, and later by Loo, in explaining the discrepancies between classical buckling theories and experiment, the same fundamental approach—i.e., the use of finite-deflection equations together with a consideration of the initial imperfections of the shell—is employed in this paper to study the phenomenon of buckling of cylindrical shells subject to hydrostatic pressure. The following general assumptions are made:

(1) The material follows Hooke's law.

(2) The displacements are small compared to the length or diameter of the cylinder but may be of the order of magnitude of the thickness.

(3) There are no normal stresses in the radial direction.

(4) Lines originally normal to the median surface of the shell remain so after loading.

(5) The thickness of the shell at any point is small compared to either of the principal radii of curvature at that point.

Analysis

Fundamental Equations

Let us consider a cylinder of mean radius R, length L, and thickness h. Let x, s, and z denote orthogonal coordinates in the axial, tangential, and radial directions, respectively. Further, let u, v, and w (positive inward) be the components of displacement (in the x, s, and z directions, respectively) of any point in the middle surface of the shell. In the thin cylinder the stress field may be considered to be composed of membrane and bending action and each system will be treated independently. For a homogeneous, isotropic medium, the strain-displacement relations, in general, are given by

$$\left.\begin{aligned}
\epsilon_x &= \frac{\partial u}{\partial x} + \frac{1}{2}\left[\left(\frac{\partial u}{\partial x}\right)^2 + \left(\frac{\partial v}{\partial x}\right)^2 + \left(\frac{\partial w}{\partial x}\right)^2\right] \\
\epsilon_s &= \frac{\partial v}{\partial s} + \frac{1}{2}\left[\left(\frac{\partial u}{\partial s}\right)^2 + \left(\frac{\partial v}{\partial s}\right)^2 + \left(\frac{\partial w}{\partial s}\right)^2\right] \\
\epsilon_{xs} &= \left(\frac{\partial u}{\partial s} + \frac{\partial v}{\partial x}\right) + \left(\frac{\partial u}{\partial x}\frac{\partial u}{\partial s} + \frac{\partial v}{\partial x}\frac{\partial v}{\partial s} + \frac{\partial w}{\partial x}\frac{\partial w}{\partial s}\right)
\end{aligned}\right\} \tag{1}$$

The higher order terms in u and v in Eq. (1) may reasonably be neglected in computing the membrane stresses and strains in a thin cylinder, since these displacements are small compared to w. Eqs. (1) then become, after adding the term $-w/R$ to account for the curvature,[4]

$$\left.\begin{aligned}
\epsilon_x &= \frac{\partial u}{\partial x} + \frac{K}{2}\left(\frac{\partial w}{\partial x}\right)^2 \\
\epsilon_s &= \frac{\partial v}{\partial s} + \frac{K}{2}\left(\frac{\partial w}{\partial s}\right)^2 - \frac{w}{R} \\
\epsilon_{xs} &= \left(\frac{\partial u}{\partial s} + \frac{\partial v}{\partial x}\right) + K\frac{\partial w}{\partial x}\frac{\partial w}{\partial s}
\end{aligned}\right\} \tag{2}$$

where $K = 1 + (2w_0/w) = 1 + (2a_0/a) = 1 + (V/a) =$ constant, w_0 representing the initial radial deviation from perfect shape, a_0h the amplitude of w_0, and ah the amplitude of w. The fact that K is taken to be constant implies that only the component of the initial deviation, which is of the same shape as the displacements, can be taken into account. This is the same as is often assumed in column theory and is equivalent to assumptions made by both Donnell and Wan and also Loo. This component of the deviation is by far the most important one. By assuming that the equations of equilibrium for an element in the plane of the cylinder wall are approximately the same as those in flat plate theory and by introduction of the Airy stress function, Donnell[4] obtained the following basic relation between the stress function F of the membrane stresses and the radial displacement w.

$$\left(\frac{\partial^2}{\partial x^2} + \frac{\partial^2}{\partial s^2}\right)^2 F = EK\left[\left(\frac{\partial^2 w}{\partial x \partial s}\right)^2 - \frac{\partial^2 w}{\partial x^2}\frac{\partial^2 w}{\partial s^2}\right] - \frac{E}{R}\frac{\partial^2 w}{\partial x^2} \tag{3}$$

where E is the modulus of elasticity. The second-order terms on the right side of Eq. (3) correspond to membrane stresses due to the finite displacements, while the last term corresponds to membrane stresses due to the curvature. If w is known or assumed, then F may be readily found from Eq. (3). The stress function will, of course, be the sum of a particular solution of Eq. (3) and the general solution of the corresponding homogeneous equation. The latter solution, to be consistent with the physical conditions of the problem, is merely

$$F = c_1x^2 + c_2s^2 \tag{4}$$

Knowing F, the membrane energy of the cylinder may be expressed in terms of the stress function as follows.[4]

$$E_m = \frac{h}{2E}\int_0^L\int_0^{2\pi R}\left\{\left(\frac{\partial^2 F}{\partial x^2} + \frac{\partial^2 F}{\partial s^2}\right)^2 + 2(1+\nu)\left[\left(\frac{\partial^2 F}{\partial x \partial s}\right)^2 - \frac{\partial^2 F}{\partial x^2}\frac{\partial^2 F}{\partial s^2}\right]\right\} dx\, ds \tag{5}$$

where ν denotes Poisson's ratio. The strain energy of bending is given by the expression[4]

$$E_b = \frac{Eh^3}{24(1-\nu^2)}\int_0^L\int_0^{2\pi R}\left\{\left(\frac{\partial^2 w}{\partial x^2} + \frac{\partial^2 w}{\partial s^2}\right)^2 + 2(1-\nu)\left[\left(\frac{\partial^2 w}{\partial x \partial s}\right)^2 - \frac{\partial^2 w}{\partial x^2}\frac{\partial^2 w}{\partial s^2}\right]\right\} dx\, ds \tag{6}$$

The total strain energy is consequently given as the sum of E_m and E_b.

Knowing the elastic strain energy stored in the shell, it is next necessary to calculate the work done by the external forces acting on the shell. This work done may be calculated as the hydrostatic pressure p multiplied by the decrease of volume of the cylinder. The change of volume is given, approximately, by the relation[24]

$$\Delta V = \epsilon L \pi R^2 + \int_0^L \int_0^{2\pi R} \left[w - \frac{K w^2}{2R} \right] dx\, ds \quad (7)$$

where ϵ denotes the mean unit axial compression of the cylinder. This mean compression is given by the nonperiodic terms occurring on the right side of the expression

$$\partial u/\partial x = (1/E)(\sigma_x - \nu\sigma_s) - (K/2)(\partial w/\partial x)^2 \quad (8)$$

which is readily obtained from the stress-displacement relationships.[7] It is assumed that the pressure acting on the shell at the start of buckling is practically the same as that at the end point of buckling.

Consequently, the total potential U_t is given by the sum of the strain energies and the potential of the external loads. U_t contains a term involving the mean axial and circumferential stresses from Eq. (4), but this term has no effect upon the problem because it represents work done during the ordinary elastic compression of the shell under load. It is to be noted that the total potential reduces to that obtained by Loo[19] for the special case of axial compressive forces only and with the wave lengths in the axial and circumferential directions assumed to be equal.

Displacement Pattern

Let us assume a deflection shape of the form

$$w = ah[\sin(ms/R)\sin\delta x + d(1 - \cos 2\delta x)] \quad (9)$$

where a, d, m, and n are arbitrary parameters and $\delta = n\pi/L$. The first term corresponds to a simple-support type of reaction at the ends of the shell and was the only term used by von Mises[20] in his small deflection analysis of the buckling of such a cylindrical shell. The second term, which represents an axially symmetric deformation, becomes important in the case of large displacements, where it reduces the circumferential stresses by balancing large deflection strains against strains due to change of radius. Even though this term does introduce some longitudinal bending, the total internal strain energy is considerably reduced. It was found by trial that addition of a constant term inside the bracket (corresponding to a uniform inward displacement) has a negligible effect on the final results. Also, for the particular displacement pattern assumed, it was found that the requirement that the circumferential displacement be a periodic function of the circumferential coordinate led to the same equations derived below. This condition must, of course, be enforced, and it is probable that other displacement patterns would reflect its influence more than does the one selected here. For this assumed configuration, the Airy function is found from Eq. (3) to be

$$F = c_1 x^2 + c_2 s^2 + c_3 \cos(2ms/R) + c_4 \cos 2\delta x + c_5 \sin(ms/R)\sin 3\delta x + c_6 \sin(ms/R)\sin\delta x \quad (10)$$

where

$$\left.\begin{aligned} c_3 &= [(EK\delta^2R^2)/(32m^2)]a^2h^2 \\ c_4 &= \{[(EKm^2)/(32\delta^2R^2)]a^2h^2\} - \{[(Ed)/(4\delta^2R)]\,ah\} \\ c_5 &= \frac{2EK\delta^2m^2d}{[9\delta^2 + (m^2/R^2)]^2R^2}\,a^2h^2 \\ c_6 &= -\frac{2EK\delta^2m^2d}{[\delta^2 + (m^2/R^2)]^2R^2}\,a^2h^2 + \frac{E\delta^2}{[\delta^2 + (m^2/R^2)]^2R}\,ah \end{aligned}\right\} \quad (11)$$

and c_1 and c_2 are proportional to the mean circumferential and axial stresses, respectively. Knowing w and F, the total potential U_t is readily determined.

Minimization of Potential

The variation of the total potential with respect to each of the arbitrary parameters must vanish for equilibrium. If the differentiations indicated by

$$\partial U_t/\partial a = 0 \qquad \partial U_t/\partial d = 0 \quad (12)$$

are carried out, they lead to the simultaneous equations

$$\frac{Eh^3a}{12(1-\nu^2)}\left[\frac{1}{2}\left(\delta^2 + \frac{m^2}{R^2}\right)^2 + 16\delta^4d^2\right] + \frac{Eh^3}{2}\left\{\frac{\delta^4h^2}{64}(4a^3 + 6Va^2 + 2V^2a) + \frac{2ad^2}{R^2} + \frac{m^4h^2}{64R^4}(4a^3 + 6Va^2 + 2V^2a) - \frac{m^2dh}{4R^3}(3a^2 + 2Va) + \frac{2\delta^4m^4d^2h^2}{[9\delta^2 + (m^2/R^2)]^2R^4}(4a^3 + 6Va^2 + 2V^2a) + \frac{2\delta^4m^4d^2h^2}{[\delta^2 + (m^2/R^2)]^2R^4}(4a^3 + 6Va^2 + 2V^2a) + \frac{a\delta^4}{[\delta^2 + (m^2/R^2)]^2R^2} - \frac{2\delta^4m^2dh}{[\delta^2 + (m^2/R^2)]^2R^3}(3a^2 + 2Va)\right\} - p\left[\frac{m^2h^2}{4R}(2a + V) - \frac{(2a + V)h^2}{2R}\left(\frac{1}{2} + 3d^2\right) + \frac{R\delta^2h^2}{8}(2a + V) + R\delta^2d^2h^2(2a + V)\right] = 0 \quad (13)$$

$$\frac{Eh^5a^2}{24(1-\nu^2)}(32\delta^4 d) + \frac{Eh^3}{2}\left\{\frac{2a^2d}{R^2} - \frac{m^2}{4R^3}\left(1+\frac{V}{a}\right)a^3h + \frac{4\delta^4m^4d}{[9\delta^2+(m^2/R^2)]^2R^4}\left(1+\frac{2V}{a}+\frac{V^2}{a^2}\right)a^4h^2 + \frac{4\delta^4m^4d}{[\delta^2+(m^2/R^2)]^2R^4}\left(1+\frac{2V}{a}+\frac{V^2}{a^2}\right)a^4h^2 - \frac{2\delta^4m^2}{[\delta^2+(m^2/R^2)]^2R^3}\left(1+\frac{V}{a}\right)a^3h\right\} - p\left[-\frac{3a^2h^2d}{R}\left(1+\frac{V}{a}\right)+2R\delta^2d\left(1+\frac{V}{a}\right)a^2h^2\right] = 0 \quad (14)$$

The potential U_t could be minimized with respect to the parameter m, but it was deemed easier to do this on a numerical basis, starting with the number of circumferential waves predicted by classical theory and varying this number until the minimum pressure was found for any configuration. For the case of hydrostatic pressure, $n = 1$.

For assigned values of a and V, Eqs. (13) and (14) may be solved for d and p for any shell geometry, various values of m being investigated until a minimum value of p is found for each pair a, V. It is of interest to note that if d is set equal to zero in Eq. (9), which reduces the assumed value of w to that treated by von Mises,[20] and if further V is taken to be zero, which corresponds to the case of an initially perfect cylinder, then minimization of the total potential U_t with respect to the single remaining parameter a yields for p the value

$$p_{cl} = \left\{\frac{Eh^3}{48(1-\nu^2)}\left(\delta^2+\frac{m^2}{R^2}\right) + \frac{Eh\delta^4}{4[\delta^2+(m^2/R^2)]^2R^2}\right\}\Big/\left(\frac{m^2}{4R}+\frac{R\delta^2}{8}-\frac{1}{4R}\right) \quad (15)$$

This is equivalent to the classical small deformation result von Mises obtained using differential equations of equilibrium of a shell element. It was later derived by Salerno and Levine[21] as a special case of their analysis of a cylinder reinforced by circumferential rings.

Proposal of Formula for Imperfection Factor

Initial imperfections in the shell may include: (1) initial deviations from the assumed perfect geometrical shape, (2) initial stresses, (3) deviations from uniform, isotropic elastic behavior, and (4) accidental lateral loadings. The first three are all properties of the specimen and some "equivalent geometric deviation" would have the same effect as all three together. This equivalent deviation may, of course, be characterized by the parameter K appearing in Eqs. (2).

Donnell and Wan[18] and later Loo[19] employed the concept of an "unevenness" factor U_0, which for a thin cylinder is assumed to be related to a_0/h (the amplitude of w_0) in the following manner.

$$a_0 = U_0\{[(L_xL_s)/(L_x+L_s)]\,(1/h)\}^{\delta_1} = V/2$$

where L_x and L_s are the half-wave lengths in the axial and circumferential directions, respectively. Let us adopt the value of $\delta_1 = 2$, which is consistent with recommendations[18] for strength of columns. On the basis of numerical calculations carried out with Eqs. (13) and (14) for several unreinforced cylinders tested by Windenburg and Trilling[25] (where buckling pressures are available in the literature), it is suggested that a value of $U_0 = 3\ (10)^{-4}$ will probably provide a reasonable guide for estimating the buckling strength of cylinders subject to hydrostatic pressure. This value of U_0 is somewhat higher than those previously recommended for axial compression and torsion loadings.[18, 19] The number of circumferential waves (and hence L_s) is predicted with sufficient accuracy by small-deflection theory.

Such a suggested value of U_0 is obviously approximate and awaits refinement from further experimental evidence. Also, it is undoubtedly possible to have a larger value of U_0 at one part of the cylinder than at other parts, since buckling usually occurs over only a part of the shell.[25, 26] In addition, deflection configurations other than that indicated by Eq. (9) should be investigated.

Numerical Example

Let us consider a cylindrical shell having the following characteristics.[25]

$L = 8$ in.
$R = 8$ in.
$h = 0.0901$ in.
$E = 29 \times 10^6$ lbs. per sq.in.
$\nu = 0.3$

(Data from this shell were not used in determining the afore-mentioned value of U_0.) For various assigned values of a and V, Eqs. (13) and (14) may be solved for d and p and these values plotted as in Fig. 1

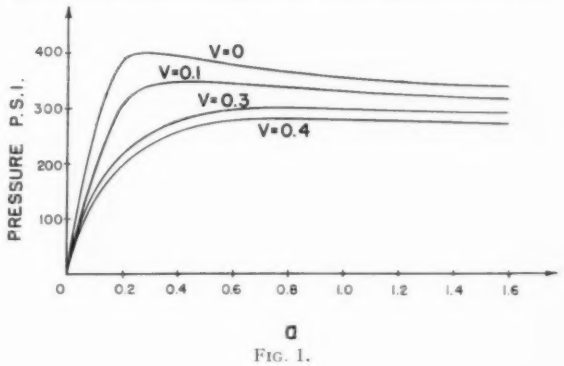

FIG. 1.

Throughout these computations it was found that a configuration corresponding to eight circumferential waves led to the minimum pressure. From these curves and with the previously suggested value of U_0, the peak pressure such a shell could carry is approximately 290 lbs. per sq.in. Experimentally, Windenburg and Trilling[25] found that the first lobe formed in it at 281 lbs. per sq.in. Such close agreement may not, of course, exist with other geometries. Classical small deformation theory, assuming simply supported ends, indicates a buckling pressure of 386 lbs. per sq.in. for this shell.

Concluding Remarks

The problem of buckling of a thin cylindrical shell subject to hydrostatic pressure has been considered from the standpoint of large deflections together with initial deviations from perfect shape. An approximate value of an "unevenness" factor, expressed as a function of the geometry of the shell, is suggested which is only slightly greater than existing recommendations for cylinders subject to axial compression or torsion.

Certainly deflection configurations other than that indicated by Eq. (9) should also be investigated. It is evident that this approach does not allow a rigorous consideration of boundary conditions at the ends of the shell, because those boundary conditions having to do with axial and circumferential displacements cannot be treated directly. Consequently, considerable experimental data should be gathered to determine the minimum length-diameter ratio for which this treatment could be expected to yield reasonable results. (For the case of axial compression the minimum value of this ratio is approximately 3/4.[27]) Also, since the "large deflection" theory used here is only a second approximation, its validity for deflections of the order of several times the thickness should be further investigated.

Thus it is evident that a considerable amount of experimental data should be collected and further refinements in theory considered to yield a completely satisfactory solution to the problem of hydrostatic buckling of a cylindrical shell. Nevertheless the present theory should give a reasonable quantitative estimate of the buckling strength of such a shell.

Acknowledgment

The author is indebted to both Dr. L. H. Donnell of the Illinois Institute of Technology and Dr. T. T Loo of the Rensselaer Polytechnic Institute for several inspiring conversations on the topic of buckling of shells.

References

[1] Love, A. E. H., *A Treatise on the Mathematical Theory of Elasticity*, Dover Publications, New York, N.Y., 1944.

[2] Flügge, W., *Die Stabilitat der Kreissylinderschale*, Ingenieur Archiv, Vol. 3, pp. 463–506, 1932.

[3] Cox, H. L., and Pribram, E., *The Elements of the Buckling of Curved Plates*, Journal of the Royal Aeronautical Society, Vol. 52, p. 551, 1948.

[4] Donnell, L. H., *A New Theory for the Buckling of Thin Cylinders Under Axial Compression and Bending*, Trans. ASME Vol. 56, pp. 795–806, 1934.

[5] von Kármán, Th., and Tsien, H. S., *The Buckling of Spherical Shells by External Pressure*, Journal of the Aeronautical Sciences, Vol. 7, No. 2, pp. 43–50, December, 1939.

[6] Marguerre, K., *Die Durchschlagskraft eines schwach gekrummten Balkens*, Sitzungsberichte der Berliner Mathematischen Gesellschaft, vol. 37, pp. 22–40, 1938.

[7] von Kármán, Th., and Tsien, H. S., *The Buckling of Thin Cylindrical Shells Under Axial Compression*, Journal of the Aeronautical Sciences, Vol. 8, No. 8, pp. 303–312, June, 1941.

[8] Leggett, D. M. A., and Jones, R. P. N., *The Behavior of a Cylindrical Shell Under Axial Compression When the Buckling Load Has Been Exceeded*, ARC, R & M No. 2190, August, 1942.

[9] Michielsen, H. F., *The Behavior of Thin Cylindrical Shells After Buckling Under Axial Compression*, Journal of the Aeronautical Sciences, Vol 15, No. 12, pp. 738–744, December, 1948.

[10] Kempner, J., *Analysis of the Post-Buckling Behavior of an Axially Compressed Cylindrical Shell*, Polytechnic Institute of Brooklyn, Report No. 212, 1953.

[11] Yoshimura, Y., *On the Mechanism of Buckling of a Circular Cylindrical Shell Under Axial Compression*, (in Japanese), Report of the Institute of Science and Technology, University of Tokyo, Vol. 5, pp. 179–198, 1951.

[12] Cicala, P., *The Effect of Initial Deformations on the Behavior of a Cylindrical Shell Under Axial Compression*, Quarterly of Applied Mathematics, Vol. 9, pp. 273–293, 1951.

[13] Cicala, P., *Il cilindro in parete sottile compresso assialmente. Nuovo orientamento dell'indagine sulla stabilita elastica*, L'Aerotecnica, Vol. 24, pp. 3–18, 1944.

[14] Sturm, R. G., *A Study of the Collapsing Pressure of Thin-Walled Cylinders*, University of Illinois Engineering Experiment Station Bulletin No. 329, 1941.

[15] Bodner, S. R., and Berks, W., *The Effect of Imperfections on the Stresses in a Circular Cylindrical Shell Under Hydrostatic Pressure*, Polytechnic Institute of Brooklyn Report No. 210, 1952.

[16] Wu, T. S., Goodman, L. E., and Newmark, N. M., *Effect on Small Initial Irregularities on the Stresses in Cylindrical Shells*, Civil Engineering Studies, Structural Research Series No. 50, University of Illinois, 1953.

[17] Kelley, J. B., *The Effect of Initial Imperfections on the Buckling of a Long Circular Cylinder*, Doctoral dissertation, New York University, 1949.

[18] Donnell, L. H., and Wan, C. C., *Effect of Imperfections on Buckling on Thin Cylinders and Columns Under Axial Compression*, Journal of Applied Mechanics, Vol. 17, No. 1, pp. 73–83, 1950.

[19] Loo, T. T., *Effects of Large Deflections and Imperfections on the Elastic Buckling of Cylinders Under Torsion and Axial Compression*, Doctoral dissertation, Illinois Institute of Technology, 1952.

[20] von Mises, R., *Der Kritische Aussendruck für allseits belastete zylindrische Rohre*, Fest. zum 70 Geburstag von Prof. Dr. A. Stodola, Zurich, pp. 418–430, 1929.

[21] Salerno, V. L., and Levine, B., *Buckling of Circular Cylindrical Shells with Evenly Spaced, Equal Strength Circular Ring Frames*, Parts I and II, Polytechnic Institute of Brooklyn Reports 167, 169, 1950.

[22] Salerno, V. L., Levine, B., and Pulos, J. G., *Charts for the Determination of the Upper and Lower Limit of Hydrostatic Buckling Pressures for Reinforced Circular Cylindrical Shells*, Polytechnic Institute of Brooklyn Report 177, 1950.

[23] Salerno, V L., and Levine, B., *The Determination of the Hydrostatic Buckling Pressures for Circular Cylindrical Shells Rein-*

(Concluded on next page)

forced with Rings, Polytechnic Institute of Brooklyn Report 182, 1951.

[24] Nash, W. A., *Buckling of Multiple-Bay Ring-Reinforced Cylindrical Shells Subject To Hydrostatic Pressure*, Journal of Applied Mechanics, Vol. 20, pp. 469–474, 1953.

[25] Windenburg, D. F., and Trilling C., *Collapse by Instability of Thin Cylindrical Shells Under External Pressure*, Trans. ASME, Vol. 56, 1934.

[26] Slankard, R. C., and Nash, W. A., *Tests of the Elastic Stability of a Ring-Stiffened Cylindrical Shell, Model BR-5* ($\lambda = 1.705$) *Subjected To Hydrostatic Pressure*, David Taylor Model Basin Report 822, 1953.

[27] von Kármán, Th., Dunn, L. G., and Tsien, H. S., *The Influence of Curvature on the Buckling Characteristics of Structures*, Journal of the Aeronautical Sciences, Vol. 7, No. 7, pp. 276–289, May, 1940.

On Supersonic Flow Past a Finite Wedge at the Crocco Mach Number

(*Continued from page 263*)

Also, it is obvious that $\bar{C}_D$ should coincide with $\bar{C}_{D,\infty}$ at $\lambda = 2^{2/3}$ ($\xi = 0$) when the field behind the shock becomes uniform and sonic, and, therefore, $\bar{C}_D = 2^{4/3} = 2.520$ at $\lambda = 2^{2/3} = 1.5874$. A comparison of the above results with experiments is made in Fig. 4.

In a previous paper,[2] the value of C_D for the Crocco state was calculated to be 0.276 for a wedge of $\alpha = 20°$, while the above formula $C_D = 2.679(\gamma + 1)^{-1/3}\alpha^{5/3}$ gives the value 0.346. Agreement of the two values is not so good. Possibly this is due partly to the inaccuracy of the velocity distribution in the previous calculation and partly to the extrapolation of the present (transonic) theory to the case of such a thick wedge.

(5) Velocity Distribution

Finally, integration of Eq. (17) gives

$$\frac{s}{l} = 1 - |7\xi|^{5/2} \sum_{n=0}^{\infty} \frac{a_n A_n}{5 + 6n} |\xi|^{3n} \times \left\{ \sum_{n=0}^{\infty} \frac{a_n A_n}{5 + 6n} 7^{-3n} \right\}^{-1} \qquad (21)$$

From this equation it is possible to calculate the velocity distribution along the side AB of the wedge, and the four-term approximation is shown in Fig. 5. It will be seen that the curve is smooth at the nose A (characteristic to the Crocco state) but has vertical tangent at the shoulder B. This rapid expansion, being common in a subsonic field adjacent to a Prandtl-Meyer expansion, was ignored in the previous paper mentioned above. In this respect the previous calculation is unsatisfactory.

In conclusion, the writers wish to express their thanks to Professor S. Tomotika for his continual interest and encouragement throughout this work. The writers' thanks are also due to Dr. G. Guderley for his valuable criticism of the previous work of one of the writers.

References

[1] Guderley, G., *Considerations on the Structure of Transonic Flow Patterns*, Wright Field Report F-TR-2168-ND, 1947.

[2] Tamada, K., *On the Detachment of Shock Wave from the Leading Edge of a Finite Wedge*, Jour. Phys. Soc. Japan, Vol. 8, pp. 242–247, March-April, 1953.

[3] Tricomi, F., *On Linear Differential Equations of the Second Order of Mixed Type*, Brown University Translation A9-T-26. Original source: Atti reale accad. nazl. Lincei, Ser. V, Mem. Classe sci. fis. mat. e nat., 14, 1923.

Readers' Forum

BRIEF REPORTS of investigations in the aeronautical sciences and discussions of papers published in the JOURNAL are presented in this special department. Publication is completed as soon as possible after receipt of the material. The Editorial Committee does not hold itself responsible for the opinions expressed by the correspondents.

The Second-Order Thin Airfoil Theory for Compressible Flow

Isao Imai
Department of Physics, Faculty of Science, University of Tokyo, Tokyo, Japan
October 20, 1954

IN A RECENT note in the Readers' Forum, Van Dyke[1] presented a remarkable rule that expresses the second-order subsonic pressure distribution over any thin two-dimensional airfoil directly in terms of the incompressible pressures. Thus if the incompressible pressure coefficient is expanded in powers of the thickness parameter t in the form

$$C_{p0} = tf(x) + t^2 g(x) + \ldots \tag{1}$$

then at any subsonic Mach Number M the pressure coefficient is given by

$$C_{pM} = K_1 tf(x) + K_2 t^2 g(x) + \ldots \tag{2}$$

where

$$K_1 = \frac{1}{\sqrt{1-M^2}} = \frac{1}{\mu}, \qquad K_2 = \frac{(\gamma+1)M^4 + 4\mu^2}{4\mu^4} \tag{2a}$$

The purpose of the present note is to present the general formulas that give the velocity and pressure distributions over any thin airfoil directly in terms of its shape.

About 10 years ago the present writer[2] obtained a general expression for the velocity distribution on the surface of any arbitrary airfoil, based on the so-called "thin-wing-expansion method." Thus if the airfoil is represented by

$$x = \cos\vartheta, \qquad y = g(\vartheta) \tag{3}$$

then its velocity distribution q is given by

$$\frac{q}{U} = \left[\sin\vartheta + \frac{1}{\mu}\{g^{*\prime}(\vartheta) - \alpha\cos\vartheta + \kappa_{10}\} + S'(\vartheta) + \frac{\lambda}{2}T(\vartheta) + \kappa_2\right]\{\sin^2\vartheta + [g'(\vartheta)]^2\}^{-1/2} \tag{4}$$

where U is the undisturbed flow velocity, α is the angle of attack, and

$$\mu = \sqrt{1-M^2}, \qquad \lambda = \frac{M^2}{\mu^2}\left(1 + \frac{\gamma+1}{4}\frac{M^2}{\mu^2}\right) \tag{5}$$

$$S(\theta) = \frac{\alpha^2}{2}\cos\theta - \alpha g(\theta) + \{g^{*\prime}(\theta) - \alpha\cos\theta + \kappa_{10}\} \times \frac{h(\theta)}{\sin\theta} - \left\{g'(\theta)\frac{h(\theta)}{\sin\theta} + \alpha h(\theta)\right\}^*$$

$$T(\theta) = -\mathrm{Re}\left\{\left(\frac{df_0}{d\theta} - \kappa_{10}\right)^2 \frac{d\theta}{d\sigma}\, e^{-i\omega}\right\} - \{P'(\theta) - Q^{*\prime}(\theta)\}$$

$$h(\theta) = g^*(\theta) - (1/2)\,[g^*(0) - g^*(\pi)]\cos\theta - g^{*\prime}(0)\sin\theta - (1/2)\,[g^*(0) + g^*(\pi)]$$

$$f_0(\theta) = -\{g^*(\theta) + ig(\theta) - i\alpha e^{-i\theta}\}$$

$$\frac{d\sigma}{d\theta}\, e^{i\omega} = -\sin\theta + \mu h'(\theta) + i\mu\{g'(\theta) + \alpha\sin\theta\}$$

$$P(\theta) + iQ(\theta) = \bar{f}_0\left(\frac{df_0}{d\theta} - \kappa_{10}\right)\frac{d\theta}{d\sigma} - e^{i\omega}$$

Here $\bar{f}_0$ is the complex conjugate of f_0, and g^* is the conjugate Fourier series associated with g, so that, if

$$g(\theta) = a_0 + \sum_{n=1}^{\infty}(a_n\cos n\theta + b_n\sin n\theta) \tag{6}$$

then

$$g^*(\theta) = \sum_{n=1}^{\infty}(a_n\sin n\theta - b_n\cos n\theta) = -\frac{1}{2\pi}\int_0^{2\pi}[g(\theta+\varphi) - g(\theta)]\cot\frac{\varphi}{2}\,d\varphi \tag{7}$$

Also, the circulation around the airfoil is given by

$$\Gamma = 2\pi(\mu^{-1}\kappa_{10} + \kappa_2)$$

By use of the above formulas, velocity distributions and lift and moment of the general Joukowski airfoils (including elliptic cylinders and circular arc airfoils as special cases) were discussed. Recently, Asaka[3] has extended the analysis to the third order and treated symmetrical biconvex circular arc airfoils at zero angle of attack.[4]

Inspired by the surprising elegance of Van Dyke's result, the writer re-examined the above-mentioned formula (4) and discovered that there exists a simple functional relation between the two functions $S(\theta)$ and $T(\theta)$. Thus, Eq. (4) can be put in a considerably simpler form,

$$\frac{q}{U} = \left\{\left(1 - \frac{\alpha^2}{2}\right)\sin\vartheta - \alpha g'(\vartheta) + \frac{1}{\mu}A + (1+\lambda)C + \frac{\lambda(A^2 - B^2)\sin\vartheta}{2\sin^2\vartheta + \mu^2 B^2}\right\}\{\sin^2\vartheta + [g'(\vartheta)]^2\}^{-1/2} \tag{8}$$

where

$$A = g^{*\prime}(\vartheta) - \alpha\cos\vartheta + \kappa_{10} \tag{9a}$$

$$B = g'(\vartheta) + \alpha\sin\vartheta \tag{9b}$$

$$C = P'(\vartheta) - Q^{*\prime}(\vartheta) + \kappa_{20} \tag{9c}$$

$$P + iQ = -i\frac{g(\vartheta)}{\sin\vartheta}(A + iB) \tag{9d}$$

and the circulation is given by

$$\Gamma = 2\pi\{\mu^{-1}\kappa_{10} + (1+\lambda)\kappa_{20}\} \tag{10}$$

On the assumption that $g(\vartheta) = 0(\epsilon)$, $\alpha = 0(\epsilon)$, we have $A = 0(\epsilon)$, $B = 0(\epsilon)$, $C = 0(\epsilon^2)$, so that Eq. (8) can be further simplified for $\vartheta \neq 0, \pi$ to give

$$q/U = 1 + q_1 + q_2 + \ldots \tag{11}$$

where

$$q_1 = (1/\mu)\,(A/\sin\vartheta) \tag{12a}$$

$$q_2 = \frac{\lambda}{2}\frac{A^2}{\sin^2\vartheta} - (1+\lambda)\left(\frac{1}{2}\frac{B^2}{\sin^2\vartheta} - \frac{C}{\sin\vartheta}\right) \tag{12b}$$

Hence the pressure coefficient is expressed as

$$C_p \equiv \frac{p - p_\infty}{(1/2)\rho_\infty U^2} = -2q_1 - \mu^2 q_1^2 - 2q_2 + 0(\epsilon^3)$$

$$= -\frac{2}{\mu}\frac{A}{\sin\vartheta} - (1+\lambda)\left(\frac{A^2 - B^2}{\sin^2\vartheta} + \frac{2C}{\sin\vartheta}\right) \tag{13}$$

For the incompressible case ($M = 0$), Eq. (13) reduces to

$$C_{p0} = -\frac{2A}{\sin\vartheta} - \left(\frac{A^2 - B^2}{\sin^2\vartheta} + \frac{2C}{\sin\vartheta}\right) \tag{14}$$

It is obvious that Eqs. (13) and (14) have similar constructions to those of Van Dyke's Eqs. (2) and (1). But our formula (13) has the merit that it enables the pressure distribution to be calculated directly from the function representing the airfoil,

$$g(\vartheta) = tg_1(\vartheta) + t^2 g_2(\vartheta) + \ldots \tag{15}$$

by means of Eqs. (9a)–(9d). Moreover, it must be pointed out that *Van Dyke's formula (2) is, in reality, applicable only to the case* $g_2(\vartheta) \equiv 0$ *(such as elliptic cylinders) but not to the general case of nonvanishing* $g_2(\vartheta)$ *(such as Kaplan's profiles).*

In the following the application of our formulas will be illustrated by taking two typical cases.

EXAMPLE (1)—ELLIPTIC CYLINDER AT ZERO ANGLE OF ATTACK

Here

$$g(\vartheta) = t\sin\vartheta \tag{16}$$

Hence

$$g^*(\vartheta) = -t\cos\vartheta$$

and from Eqs. (9a)–(9d), we have in succession

$$A = t\sin\vartheta, \qquad B = t\cos\vartheta$$

$$P + iQ = t^2 e^{-i\vartheta}, \qquad P - Q^* = 0$$

$$C = 0$$

Consequently, Eq. (13) becomes

$$C_p = -(2t/\mu) - (1+\lambda)t^2(1 - \cot^2\vartheta) \tag{17}$$

This is in agreement with Van Dyke's relations (1) and (2).

EXAMPLE (2)—KAPLAN'S PROFILE AT ZERO ANGLE OF ATTACK

Kaplan's profiles are parametrically given in the form[5]

$$x = \cos\theta - (t/4)\,(\cos\theta - \cos 3\theta) \tag{18}$$

$$y = (t/4)\,(3\sin\theta - \sin 3\theta) \tag{19}$$

which can be also expressed in the form (3) with

$$g(\vartheta) = \frac{t}{4}\,(3\sin\vartheta - \sin 3\vartheta) - \frac{3}{8}\,t^2\left(\sin\vartheta + \frac{1}{2}\sin 3\vartheta - \frac{1}{2}\sin 5\vartheta\right) + 0(t^3) \tag{20}$$

Inserting this into Eqs. (9a), (9b), (9d) gives

$$A = \frac{3}{4}\,t\,(\sin\vartheta - \sin 3\vartheta) - \frac{3}{8}\,t^2\left(\sin\vartheta + \frac{3}{2}\sin 3\vartheta - \frac{5}{2}\sin 5\vartheta\right) \tag{21a}$$

$$B = \frac{3}{4}\,t\,(\cos\vartheta - \cos 3\vartheta) - \frac{3}{8}\,t^2\left(\cos\vartheta + \frac{3}{2}\cos 3\vartheta - \frac{5}{2}\cos 5\vartheta\right) \tag{21b}$$

$$P + iQ = \frac{3}{4}\,t^2\sin^2\vartheta\,(e^{-i\vartheta} - e^{-3i\vartheta}) + 0(t^3)$$

$$= -\frac{3}{16}\,t^2\,e^{i\vartheta} + P(e^{-i\vartheta})$$

where $P(e^{-i\vartheta})$ is a polynomial in $e^{-i\vartheta}$, which contributes nothing to $P - Q^*$. Thus,

$$P - Q^* = -(3/8)t^2\cos\vartheta$$

and hence

$$C = (3/8)t^2\sin\vartheta \tag{21c}$$

Substitution of Eqs. (21a), (21b), (21c) into Eqs. (12a), (12b), and (13) gives

$$q_1 = -\frac{3}{2}\frac{t}{\mu}\cos 2\vartheta + \frac{3}{8}\frac{t^2}{\mu}(\cos 2\vartheta + 5\cos 4\vartheta) \tag{22a}$$

$$q_2 = \frac{9}{16}\lambda t^2(1 + \cos 4\vartheta) - \frac{3}{16}(1+\lambda)t^2(1 - 3\cos 4\vartheta) \tag{22b}$$

$$C_p = \frac{3t}{\mu}\cos 2\vartheta - \frac{3}{4}\frac{t^2}{\mu}(\cos 2\vartheta + 5\cos 4\vartheta) - \frac{3}{4}(1+\lambda)t^2(1 + 3\cos 4\vartheta) \tag{23}$$

which agree with Kaplan's results. For $M = 0$, (23) becomes

$$C_{p0} = 3t\cos 2\vartheta - (3/4)t^2(1 + \cos 2\vartheta + 8\cos 4\vartheta) \tag{24}$$

It will readily be seen that Eqs. (23) and (24) do not satisfy Van Dyke's relations (1) and (2). In this case the knowledge of the incompressible pressure distribution does not suffice to predict the compressible pressure distribution.

Finally, it may be interesting to remark that *the formula (8) is uniformly valid near the stagnation points* $\vartheta = 0, \pi$, so that it is essentially the extension to the compressible case of the second-order velocity formula which has been obtained by Lighthill[6] with the aid of his famous technique.

In conclusion, I wish to express my sincere thanks to Dr. Milton Van Dyke for sending me the manuscript of his paper before publication.

REFERENCES

[1] Van Dyke, M. D., *The Second-Order Compressibility Rule for Airfoils*, Journal of the Aeronautical Sciences, Vol. 21, No. 9, pp. 647–648, September, 1954.

[2] Imai, Isao, *Two-Dimensional Aerofoil Theory for Compressible Fluids* (in Japanese with English abstract), Rep. Aeron. Res. Inst. Tokyo Imp. Univ., No. 294, 1944.

[3] Asaka, Saburo, *On the Velocity Distribution over the Surface of a Symmetrical Aerofoil at High Speeds, I*, Natural Sci. Rep. Ochanomizu Univ., Vol. 4, No. 2, pp. 213–226, 1953.

[4] Asaka, Saburo, *On the Velocity Distribution over the Surface of a Symmetrical Aerofoil at High Speeds, II*, Natural Sci. Rep. Ochanomizu Univ., Vol. 5, No. 1, pp. 59–78, 1954.

[5] Kaplan, Carl, *The Flow of a Compressible Fluid Past a Curved Surface*, NACA Report No. 768, 1943.

[6] Lighthill, M. J., *A New Approach to Thin Aerofoil Theory*, Aero. Quart., Vol. 3, Part 3, pp. 193–210, November, 1951.

Wedge Pressure Coefficients in Transonic Flow by Hydraulic Analogy

Richard G. Fleddermann and Robert T. Stancil*

Associate Professor and Graduate Student, Respectively, Daniel Guggenheim School of Aeronautics, Georgia Institute of Technology

October 18, 1954

THERE HAS BEEN much discussion lately concerning the use of the hydraulic analogy for experimental research in the transonic field. This interest has been accelerated by the cheap-

* Now, Aerodynamics Department, Convair, Fort Worth, Tex.

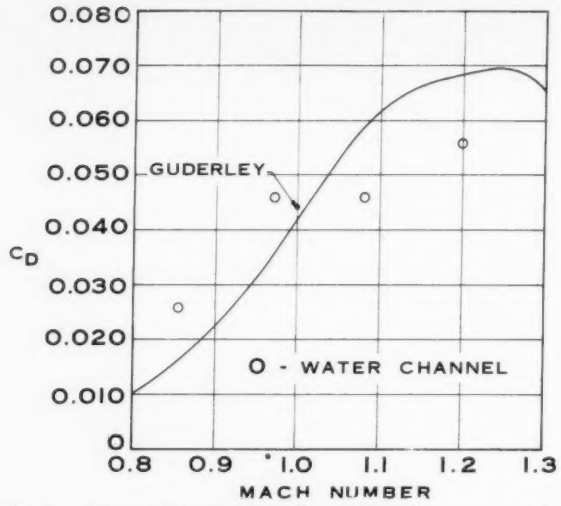

FIG. 1. Pressure drag coefficient for a 15° wedge at zero angle of attack.

ness of the water table apparatus to construct and its ease of operation. Moreover, the problem of wall shock wave reflection in transonic testing is easily eliminated by suitable traps at the edges of the water table.

In the Georgia Tech water table the model is towed through water of $\frac{1}{4}$-in. depth. The water height in the vicinity of the model was measured by means of surface contact probes. The probes were connected to an electrical system that produced a signal at the time of contact between probe and water. All probes were originally backed off and gradually lowered during a run until surface contact was made. The ratio of the water height, d, thus measured to the static height, d_s, yields the density and temperature on the body. The pressure coefficient is given by the usual formula

$$C_p = (1/M_s^2)\,[(d/d_s)^2 - 1] \qquad (1)$$

The pressure coefficients obtained by the hydraulic analogy are restricted to the flow of a perfect gas of specific heat ratio, γ = 2.0. The pressure data must be corrected to $\gamma = 1.4$ by the use of suitable correction factors as outlined in reference 1.

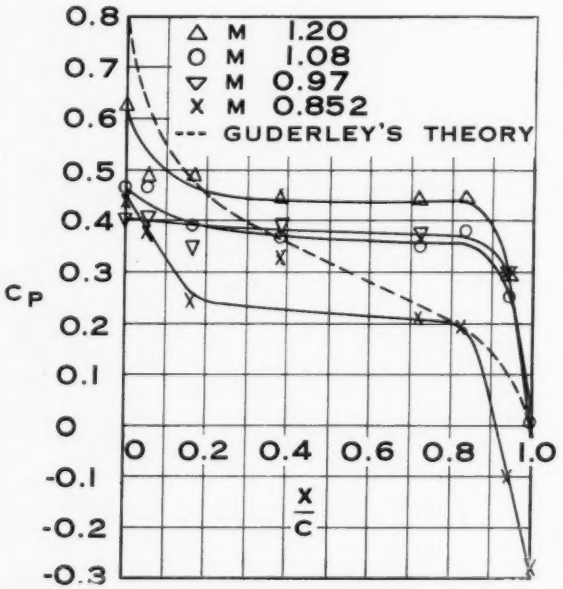

FIG. 2. Pressure distributions over a 15° wedge at zero angle of attack.

Crossley and Harleman[1] found transonic pressure distributions over 9° and 20° wedges using the hydraulic analogy. In most cases they found good agreement (with theory) over the approximate range $0.2 \leq x/c \leq 0.8$, where c is the chord length and x is the distance from the leading edge. Near the nose and the trailing edge of the wedge the agreement was poor. Laitone and Nielsen[2] utilized 10° and 40° wedges in a series of transonic flow experiments using the hydraulic analogy. They were concerned primarily with the pressure distribution from the nose of the wedge to the detached bow shock wave. The pressure distributions, as compared with the results of small perturbation theory, also exhibit poor agreement in the vicinity of the nose. If the analogy is to be used to obtain data in the transonic, it is imperative to find whether this poor agreement is caused by something inherent in the analogy itself.

Griffith[3] obtained accurate pressure and drag data for wedges of various included angles in transonic airflow. The drag coefficient curve of Fig. 1 was determined by Griffith to be the best fit to the various theoretical and experimental results for a 15° included angle wedge. The experimental points in Fig. 1 were found in the water channel for an 18-in., blunt-based, 15° wedge. There is a serious discrepancy between Griffith's curve and the water channel data. However, an examination of the original curve, Fig. 14 of reference 3, shows that there is a large spread in the data, which were used in determining the average curve. The water channel data fits within this spread.

The water table pressure distributions over the 15° wedge at Mach Numbers of 0.852, 0.97, 1.08, and 1.20 are plotted in Fig. 2 (the drag coefficients of Fig. 1 were determined from these pressure distributions). Guderley's theoretical result for flow over a 15° wedge at Mach Number 1.0 is shown for comparison. There is only a qualitative agreement with theory. The discrepancy is threefold: the sonic line is shifted forward of the shoulder, the center portion of the pressure distribution is essentially flat rather than having a strong pressure gradient, and the nose stagnation pressure is low.

The first two discrepancies can be treated together. The action of viscosity in a real case shifts the sonic line forward but does not affect the gradient. The flow about the shoulder in the water channel is equivalent to the flow of water over a free overfall. Rouse[4] has shown that the water height at the shoulder is less than critical ($M = 1$), the exact height being a function of the downstream conditions, and that the critical height is upstream of the shoulder. The height at the shoulder may be as little as 0.715 the sonic height. The critical point may be shifted toward the shoulder by raising the downstream pressure. Moreover, under certain conditions the flow height upstream of the real critical section may decrease appreciably. This would explain the decrease of pressure gradient and the upstream shift of the sonic line for the water channel data.

The last discrepancy, the loss of stagnation pressure, is an inertia effect, analogous to the time lag effect in high-speed aerodynamics. Height recovery near the stagnation point is effected in a short distance. At the higher speeds the time for recovery is so short that the water is unable to accelerate rapidly enough in the vertical direction to recover the total head depth. The head loss is dissipated by a series of wavelets emanating from the stagnation point. This loss is accentuated for a sharp-nose body by the difficulty of obtaining depth measurements near the sharp leading edge.

Any quantitative utilization of the hydraulic analogy for determining transonic pressure distributions would have to take into account the pressure loss at the stagnation point and the fixing of the sonic line at the proper position. The sonic line fix point does not pose the same problem for bodies with continuous slopes since pressure downstream of the sonic line is high, thus obviating the large drop in depth at the apparent fix point. This problem arises for blunt-based bodies or for bodies

where the sonic line occurs theoretically at a discontinuity in slope.

REFERENCES

[1] Crossley, Harry E., and Harleman, Donald R. F., *Studies on the Validity of the Hydraulic Analogy to Supersonic Flow*, M.I.T. Hydrodynamics Laboratory Technical Report No. 11, December, 1952.

[2] Laitone, E. V., and Nielsen, Helmer, *Transonic Flow Past Wedge Profiles by Hydraulic Analogy*, Journal of the Aeronautical Sciences, Vol. 21, No. 7, pp. 498–499, July, 1954.

[3] Griffith, Wayland, *Shock Tube Studies of Transonic Flow over Wedge Profiles*, Journal of the Aeronautical Sciences, Vol. 19, No. 4, pp. 249–257, April, 1952.

[4] Rouse, Hunter, *Fluid Mechanics for Hydraulics Engineers*, 1st Ed., pp. 323–324; McGraw-Hill Book Company, Inc., New York, 1938.

A Dust Method for Locating the Separation Point

A. M. O. Smith* and J. S. Murphy†

El Segundo Division, Douglas Aircraft Company, Inc., El Segundo, Calif.

October 17, 1954

THE PURPOSE OF THIS NOTE is to call attention to a relatively unknown, but simple and accurate, method of locating the separation point. The method is far more precise than the tuft method; it supplies a permanent record, and it appears more convenient to use than other precise methods. The senior author learned about the technique from personnel of the National Bureau of Standards, Washington, D.C.

The technique is as follows:

(a) Near the anticipated separation point smear a thin coat of oil on the surface to which dust may adhere. SAE 10 Oil is convenient. The film should be so thin that there is no tendency for the oil to flow.

(b) Downstream of the model, in the wake, introduce a suitable fine dust. Since the separated region contains reverse flow, some of the dust will blow forward and stick to the model—but only within the separated region. Talcum powder has proved satisfactory. Any other light powder would do; undoubtedly, common flour would be satisfactory.

* Supervisor, Design Research.

† Aerodynamics Engineer.

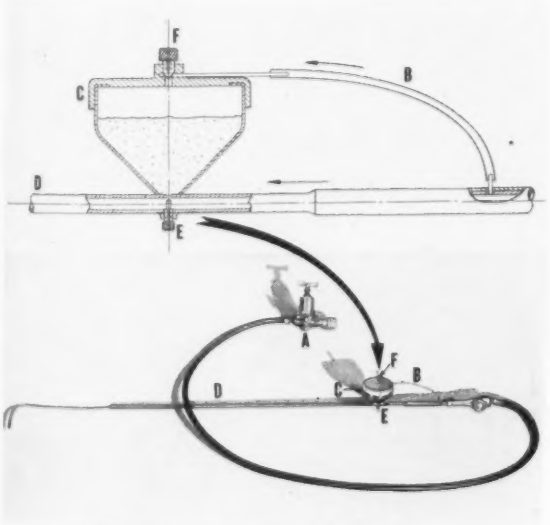

FIG. 1. A satisfactory talc dispenser.

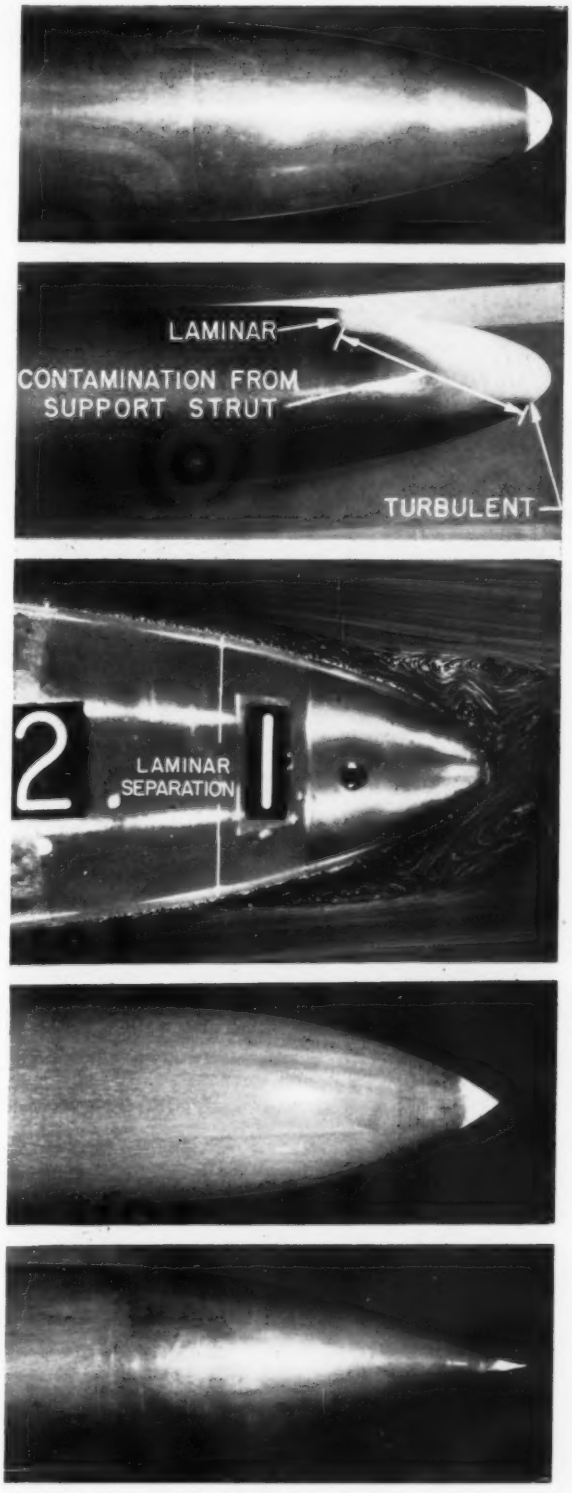

FIG. 2. Typical dust patterns.

One satisfactory talc dispenser designed for operation from a compressed air supply and suitable for a small wind tunnel is shown in Fig. 1. The air pressure and flow rate are controlled by a small regulator A which discharges through a hose to the

on-off button valve. The talc is held in a hopper C covered by a spring-loaded lid F. The talc is aspirated into tube D partly by the aspiration effect and partly by pressurization through line B. At E there is a pointed screw for adjusting the flow rate of the powder. The tip of the dispenser is $^3/_{16}$-in. copper tubing and therefore can be bent as needed for best application. As air pressures only slightly greater than tunnel static pressure are needed, flow from the dispenser does not interfere appreciably with the model flow field. The dispenser shown is about 4 ft. long.

Fig. 2 shows typical results as obtained on several tail fairings of a 60-in. long by 6-in. diameter body of revolution. Except for photographs (2) and (3) from the top, all represent turbulent separation. Photograph (2) shows a case of laminar separation. As the model was supported from below by a thin strut, the lower portion of the flow is turbulent. The purely turbulent and purely laminar regions are noted, together with a transition region between the two created by transverse contamination. The central picture, taken in the Douglas water channel is included because it shows well how the dust technique works. If dust is discharged in the wake near the right-hand margins of the picture, the strong eddying, circulatory motion will carry the powder to the forward limit of the reverse flow. The water channel and dust techniques for locating separation have been found to agree well.

The dust patterns do not produce a sharp boundary. On the present size models the region of transition between zero and full dust concentration covers about $^1/_8$ in., indicating that the separation point may not be absolutely stationary. However as the transition band is only about $^1/_8$ in. wide, the accuracy of the method is high.

Equations for the Chordwise Center of Pressure for the Basic Twist Distributions on Triangular Wings Having Supersonic Leading and Trailing Edges

R. N. Haskell,* J. J. Hosek,† and W. S. Johnson, Jr.†
Convair-Ft. Worth Division, General Dynamics Corporation
August 2, 1954

KAINER, REFERENCE 1, has presented equations for chordwise pressure distribution and spanwise load distribution for triangular wings having supersonic leading and trailing edges and constant, linear, parabolic, and cubic twist distributions. To utilize these results in aeroelastic studies, analytical expressions for the chordwise center of pressure are also desirable.

These equations are derived from

$$(c_n c\,\bar{X})_i = \int_{x_{LE}}^{x_{TE}} \bar{x}\left(\frac{\Delta p}{q}\right)_i dx$$

where $\bar{X}$ = distance of chordwise center of pressure from y axis. For the twisted wing the chordwise center of pressure is defined as:

$$\bar{X} = \sum_{i=0}^{3} (c_n c\bar{X})_i \Big/ \sum_{i=0}^{3} (c_n c)_i$$

The equations for $(c_n c\bar{X})_i$ are as follows:

$$(c_n c\bar{X})_0 = \frac{2a_0}{\pi \tan \epsilon \sqrt{m^2-1}} \left\{\left[\frac{(c_0/\gamma)\tan\delta + \bar{\eta}}{m_0}\right]^2 (m^2-t^2)(\theta_1+\theta_2) + 2\bar{\eta}^2\sqrt{m^2-1}\log\frac{1+\sqrt{1-t^2}}{t}\right\}$$

$$(c_n c\bar{X})_1 = \frac{4a_1 m^2\beta}{3\pi(m^2-1)^{3/2}} \left\{\left[\frac{(c_0/\gamma)\tan\delta + \bar{\eta}}{m_0}\right]^3 \left[2\sqrt{m^2-1}\,(1-t^2)^{3/2} - (\theta_1+\theta_2)\right] - \frac{\bar{\eta}^3(2-3m^2)}{m^2 t}\sqrt{(m^2-1)(1-t^2)} + \frac{\bar{\eta}^3(\theta_1-\theta_2)}{2m^3t^2}\left[3m^4 + t^2(2-3m^2)\right]\right\}$$

$$(c_n c\bar{X})_2 = \frac{2a_2 m\beta}{\pi(m^2-1)^{5/2}} \left\{\left[\frac{(c_0/\gamma)\tan\delta + \bar{\eta}}{m_0}\right]^4 \left\{\frac{t^2(1-2m^2)-3m^2}{2}\sqrt{m^2-1}\sqrt{1-t^2} + \frac{\theta_1+\theta_2}{4m^2}\left[m^6 + 2m^4 + m^4t^2(4m^2+2) - t^4(4m^4 - 5m^2 + 2)\right]\right\} + \frac{\bar{\eta}^4}{m^2}(m^2-1)^{5/2}\log\frac{1+\sqrt{1-t^2}}{t} - \frac{2m^2\bar{\eta}^4}{t^3}(\theta_1-\theta_2)\right\}$$

$$(c_n c\bar{X})_3 = \frac{2a_3 m^4\beta}{3\pi(m^2-1)^{7/2}} \left\{\left[\frac{(C_0/\gamma)\tan\delta + \bar{\eta}}{m_0}\right]^5 \left\{\frac{2}{5}\sqrt{m^2-1}\,(1-t^2)^{3/2}[t^2(14+21m^2)+4m^2+11] - \frac{3}{5}(3m^2+2)(\theta_1+\theta_2)\right\} + \frac{\bar{\eta}^5}{10m^2t}\sqrt{m^2-1}\sqrt{1-t^2}\left(\frac{15m^4+48m^2-8}{t^2} + \frac{90m^6 - 9m^4 + 68m^2 - 24}{m^2}\right) - \frac{3\bar{\eta}^5}{t^3}(4m^2+1)(\theta_1+\theta_2) + \bar{\eta}^5\left\{\frac{9m(m^2+4)}{4t^4} + \frac{3m(2m^2+3)}{2t^2} - \frac{3}{20m^5}(20m^6 - 35m^4 + 28m^2 - 8)\right\}(\theta_1-\theta_2)\right\}$$

All symbols are defined in reference 1 and t is evaluated at the trailing edge.

REFERENCE

[1] Kainer, J. H., *Equations for Loading on Triangular Wings Having Supersonic Leading and Trailing Edges Due to Various Basic Twist Distributions*, Journal of the Aeronautical Sciences, Vol. 20, No. 7, pp. 469–476, July, 1953.

* Senior Aerodynamics Engineer. † Senior Structures Engineers.

Conditions for the Appearance of Shock Waves in Steady Flows

Raymond Marchal
Ingénieur en Chef de l'Air, Professeur à l'Ecole Nationale Supérieure d'Aeronautique (Paris), Directeur Technique de la Société Nationale d'Etude et de Construction de Moteurs d'Aviation (Paris)

October 20, 1954

LET US CONSIDER the steady flow of a perfect gas issuing from an ideal centrifugal impeller delivering into a plane area located between two infinite planes ABA'B' and CDC'D'.

The stream lines are identical and can be deduced from each other by a rotation about the impeller's axis. Assuming the flow to be isentropic, the stream lines are determined by the conservation of the angular momentum rv_t, of the mass flow ρv_r, of the energy $v^2 + [2/(k-1)]a^2$, r denoting the distance to the center of the impeller, v_r and v_t the components of the velocity v along the radius vector r and the tangential direction, and a the sound speed.

Let m be the dimensionless number v_r/a. It can be verified by calculation that the circumstances of the flow differ greatly, at the outlet of the impeller, according as m_1 assumes a value m lower or higher than 1.

For the first case, the stream line is a spiral (AB_1 on the figure); the Mach Number decreases steadily to attain zero at infinity; v, and m also decrease to zero.

In the second case, the stream line is a curve with asymptote AB_2, v tends toward the limiting speed v_l corresponding to vanishing density; the pressure decreases to zero; v_r increases steadily, while m and the conventional Mach Number M increase without limit.

The stream lines have no inflection.

The cross section of a stream tube (between two stream lines) behaves as follows: along AB_2 the section is increasing with r; along AB_1, if the conventional Mach Number at the outlet of the impeller is less than 1, the section is permanently increasing, whereas if the Mach Number M_1 at the outlet of the impeller is above 1, the section first decreases to reach a minimum at the sonic throat, where $M = 1$, after which it increases.

In a perfect fluid, free from any friction against the walls, the only possibility of having a flow differing from those considered above results from the possible appearance of stationary shock waves. But such waves, according to symmetry, must be cylindrical about the axis. These waves are therefore oblique waves. It is well known that in the passage through such a wave the velocity component normal to the wave must jump from a supersonic to a subsonic value. Such a wave can only be conceived on the stream lines of the AB_2 type.

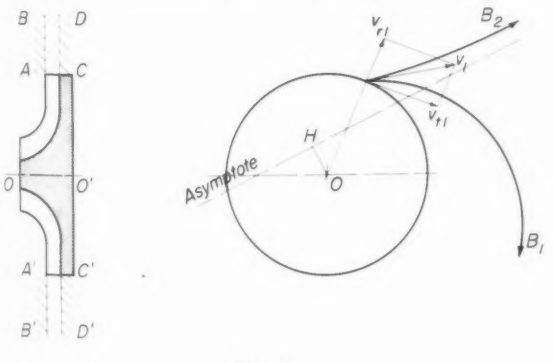

FIG. 1.

The fluid motion considered above is of the well-known type associated with a vortex-source.* The two types of stream lines correspond to the two possible types of this vortex-source motion, both defined outside of a limiting circle. The following properties are easily verified and do not seem to have been fully reported to date:

(a) The limiting circle corresponds to $m = 1$.

(b) The subtangent OH determining the position of the asymptote equals

$$v_t r/v_r$$

(c) The radius of curvature $\mathcal{R}$ of the trajectories is related to m by the relation

$$\mathcal{R} = r(v/v_t)\,(1 - m^2)$$

The number m, ratio of the velocity component normal to the isobar lines and the local speed of sound, possesses the following noteworthy properties:

(d) In the $m > 1$ field, the transition from a supersonic to a subsonic state can only be achieved through a shock wave.

(e) $m = 1$ is characteristic of the limiting line.

(f) Continuous variation from a supersonic to a subsonic state can only be observed in the $m < 1$ field.

It is quite natural to endeavor to extend these properties to any plane flow in which isobars are equally isochores and isovelocity—a condition often observed, for instance, when the stream lines issue from a common source, without crossing shock waves, or undergoing shocks of equal strength.

It is possible to check intuitively that the statements (d), (e), (f) are valid by replacing about a certain point the considered flow by a tangent vortex-source flow, determined by the knowledge of the partial derivatives of the pressure which, because of the above assumptions, implies the knowledge of the partial derivatives of the temperature, the specific mass, and the velocity.

For any plane flow, and considering intrinsic axes (x tangent, y normal, $\mathcal{R}$ radius of curvature of the stream line), we can write

$$\partial p/\partial y = \rho(v^2/\mathcal{R}) \tag{1}$$

$$\partial p/\partial x = -\rho v(\partial v/\partial x) \tag{1a}$$

Note that on the isobar $dp = 0$, or

$$(\partial p/\partial x)dx + (\partial p/\partial y)dy = 0$$

Denoting by α the angle between the stream line and the normal to the isobar facing the stream direction (positive normal)

$$dx/dy = -\tan\alpha$$

Thus

$$-(\partial p/\partial x)\tan\alpha + (\partial p/\partial y) = 0$$

hence,

$$\partial p/\partial x = \rho v^2/\mathcal{R}\tan\alpha \tag{2}$$

Then Eq. (1a) yields

$$\partial v/\partial x = v/\mathcal{R}\tan\alpha \tag{3}$$

The geometrical interpretation of Eq. (3) is as follows:

(g) Whenever the positive normal to the isobar surfaces is directed toward the trajectories' concavity, there is expansion and acceleration. In the opposite case there is compression and deceleration.

A flow of the type investigated in the opening paragraph shall be locally identical to our plane flow if it results from a vortex-source yielding, at the point under examination, the same $\mathcal{R}$ and α values. Now, $\mathcal{R}$ in a vortex-source flow is connected to the radius-vector r through the relation

$$r = \mathcal{R}\sin\alpha/(I - m^2) \tag{4}$$

* Courant, R., and Friedrichs, K. O., *Supersonic Flow and Shock Waves*, pp. 252–254; New York, 1948.

We can determine, then, the center 0 of the tangential vortex-source by plotting on the normal to the isobar the value of r given by Eq. (4). The mass flow D and the vortex intensity I are given by

$$D = 2\pi r\rho v_r = \pi\Re\rho v[\sin 2\alpha/(1 - m^2)]$$

$$I = (\Re v/2)\ [\sin 2\alpha/(1 - m^2)]$$

This generalization of the (d), (e), (f) properties, based upon the agreement between both flows up to the second order for the stream lines and up to the first order only for the isobar surfaces, offers the advantage of setting forth a characteristic number m, whose experimental measurement is possible in actual flows.

M. Pérès, member of the Académie des Sciences of Paris, has given the mathematical expression for m in the case of a compressible flow with velocity potential.

Denoting by u, v the first derivatives and by r, s, t, the second derivatives of the velocity potential $\varphi(x, y)$, he notes that the isobar, which is also isovelocity, is determined by

$$u(r\,dx + s\,dy) + v(s\,dx + t\,dy) = 0$$

The normal to the isobar is directed as the vector $(ur + vs)$, $(us + vt)$, whence the value for m^2 is given by

$$m^2 = \frac{[u(ur + vs) + v(us + vt)]^2}{a^2[(ur + vs)^2 + (us + vt)^2]} \tag{5}$$

$$\frac{1}{m^2} = \frac{a^2[r(ru^2 + 2suv + tv^2) + t(v^2t + 2suv + ru^2) + (s^2 - rt)(u^2 + v^2)]}{(ru^2 + 2suv + tv^2)^2}$$

By introducing the compressible potential equation

$$r + t = (1/a^2)(ru^2 + 2suv + tv^2)$$

it is found that

$$1/m^2 = 1 + M^2[(s^2 - rt)/(r + t)^2] \tag{6}$$

a simple expression for m.

M. Pérès has deduced from Eq. (6) another observation concerning the properties of the number m. For that purpose, he writes Eq. (6) in the form

$$1 - (1/m^2) = [M^2/(r + t)^2]\Delta \tag{7}$$

Δ denoting the Jacobian $rt - s^2$ of the transformation. $m - 1$ and Δ have the same sign and the boundary between two fields $m > 1$ and $m < 1$ of the flow is established along a singular line of the hodograph plane-flow plane correspondance. This line may be a so-called transition line in the flow plane or a limiting line in this plane. In case Δ changes sign passing through the infinity, we have to deal with a limiting line in the flow plane; but, then, there is an overlapping in the flow plane and such condition is physically impossible.

It is quite obvious, in a continuous flow, that we can only change from a supersonic to a subsonic state (or conversely with a field $m < 1$.

From a flow with $m > 1$, then necessarily supersonic, it will be impossible to return to a subsonic state, without first crossing either a shock wave or a transition line.

Matrix Method of Coupling Shear Flexibility and Rotatory Inertia in Bending Vibration

Marvin Stern
Design Specialist, Convair, San Diego, a Division of General Dynamics Corporation
October 22, 1954

Introduction

The influences of shear deformation and rotatory inertia on the bending vibration of beams have been recognized and have been treated in the literature.[1–3] Their effects have been especially well treated in the differential equation approach to the vibration problems.[3] These results have shown their influence on the vibration picture in their modification of the modal shapes and frequency spectrum and in their introduction of a second (and completely new) spectrum of natural frequencies.

For practical purposes, it is obviously advantageous to approximate a nonuniform beam by a system of discrete lumped masses. In addition, the matrix method has certain inherent assets. Some of these are:

(1) The utilization of "overall" structural influence coefficients.

(2) The possibility of capitalizing on well-developed algebraic methods.

(3) The adaptability to machine computation.

For the sake of these advantages, the matrix method has been extended here to include the additional effects of shear flexibility and rotatory inertia.

The introduction of the additional frequency spectrum found in the differential equation approach is clearly portrayed here. It is shown, however, that a beam of n lumped masses would have $2n$ natural modes and frequencies only if both the effects of shear and rotatory inertia are included. The inclusion of either effect alone, although influencing the frequency spectrum, still results in only n frequencies.

This result appears to be contrary to previous matrix attempts at the inclusion of rotatory inertia alone in the bending vibration analysis.[4,5] In effect, our results show that these previous attempts had resulted in matrix eigenvalue problems that may not have been reduced to their simplest forms.

(I) Cantilever Beam

We consider first a cantilever beam, divided into n discrete mass stations and vibrating at a natural frequency ω. The bending and shear deflections of the i'th mass point are given as the sums of the deflections at this point produced by loads applied at each station over the beam.

$$\left.\begin{aligned} y_i &= \sum_j a_{ij}p_j + \sum_j b_{ij}l_j \\ z_i &= \sum_j c_{ij}p_j \end{aligned}\right\} \tag{I.1}$$

where

y_i = bending deflection at i
z_i = shear deflection at i
a_{ij} = bending deflection at i due to unit force at j
b_{ij} = bending deflection at i due to unit moment at j

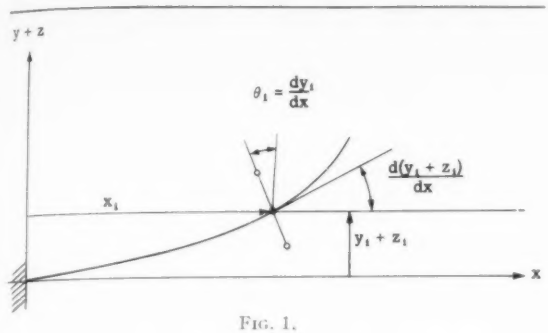

FIG. 1.

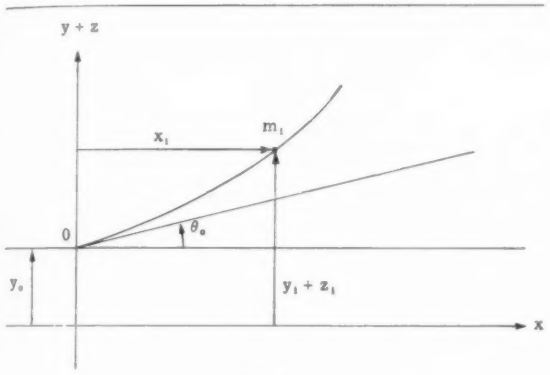

FIG. 2

c_{ij} = shear deflection at i due to unit force at j
p_j = inertia force at j
t_j = inertia moment at j

It is evident that

$$p_j = \omega^2 m_j (y_j + z_j)$$
$$t_j = \omega^2 I_j \varphi_j$$

where

m_j = mass at station j
I_j = rotatory inertia at station j
φ_j = bending angle (rotation angle of inertia segment) at station j

In matrix operator notation, Eqs. (I.1) are written

$$\begin{pmatrix} \eta \\ \zeta \end{pmatrix} = \omega^2 \begin{pmatrix} AD_m & AD_m & BD_I \\ CD_m & CD_m & 0 \end{pmatrix} \begin{pmatrix} \eta \\ \zeta \\ \theta \end{pmatrix} \qquad (I.2)$$

where

$$\eta = \begin{pmatrix} y_1 \\ y_2 \\ \vdots \end{pmatrix}, \quad \zeta = \begin{pmatrix} z_1 \\ z_2 \\ \vdots \end{pmatrix}, \quad \theta = \begin{pmatrix} \varphi_1 \\ \varphi_2 \\ \vdots \end{pmatrix}$$

$$A = (a_{ij}), \quad B = (b_{ij}), \quad C = (c_{ij})$$

$$D_m = \begin{pmatrix} m_1 & 0 \\ & m_2 \\ 0 & \ddots \end{pmatrix}, \quad D_I = \begin{pmatrix} I_1 & 0 \\ & I_2 \\ 0 & \ddots \end{pmatrix}$$

Applying standard difference interpolation formulas, we can express θ as a linear operator on η. (NOTE: The bending deflections, only, go into the determination of the rotations of inertia segments.) We express this relation as

$$\theta = E\eta$$

This reduces Eq. (I.2) to the following:

$$\lambda \begin{pmatrix} \eta \\ \zeta \end{pmatrix} = \begin{pmatrix} AD_m + BD_I E & AD_m \\ CD_m & CD_m \end{pmatrix} \begin{pmatrix} \eta \\ \zeta \end{pmatrix} \qquad (I.3)$$

where $\lambda = 1/\omega^2$.

Although we have now found a $(2n)^2$ dynamic matrix, we note the following cases:

Case (1) No Rotatory Inertia.—When $D_I = 0$, it is evident that the matrix in Eq. (I.3) has only n independent columns and is therefore only of rank n. The remaining eigenvalues correspond to n natural frequencies being infinite. These n modes are discarded by a simple addition in Eq. (I.3) yielding

$$\lambda\chi = [A + C]D_m\chi \qquad (I.4)$$

where $\chi = \eta + \zeta$ = total deflection.

We have thus found that when rotatory inertia is neglected, the problem reduces to n independent coordinates representing the total deflections and a frequency spectrum of n values.

Case (2) No Shear Flexibility.—When $C = 0$, $\zeta = 0$, Eq. (I.3) becomes simply

$$\lambda\eta = [AD_m + BD_I E]\eta \qquad (I.5)$$

This again is an eigenvalue equation with only n independent coordinates, the bending deflections.

We have thus derived the three matrix eigenvalue equations, Eqs. (I.3), (I.4), and (I.5), which represent the bending vibration problem where first the effects of rotatory inertia and shear flexibility have been included together and then each independently. It is found that only for the case where they are both included do we obtain a second frequency spectrum.

It has been shown[2] that, for a solid bar of rectangular cross section, the effect of shear flexibility is four times the rotatory inertia effect. With stressed-skin aircraft structures, this comparison can be expected to be even greater. For both practical and computational purposes then, it seems reasonable to calculate bending vibration modes and frequencies with the inclusion of shear flexibility alone.

(II) FREE-FREE BEAM

Following the model of reference (6) we derive the dynamic matrix with shear flexibility included, for the free-free beam. The deflection equations are

$$y_i - y_0 - x_i\varphi_0 = \sum_j a_{ij} p_j$$
$$z_i = \sum_j c_{ij} p_j$$

where the a_{ij} are the influence coefficients of the beam considered to be suspended as a cantilever at station 0. In matrix operator form, these equations are written

$$\chi - (1, \xi) \begin{pmatrix} y_0 \\ \varphi_0 \end{pmatrix} = \omega^2 [A + C] D_m \chi \qquad (II.1)$$

where

$$1 = \begin{pmatrix} 1 \\ 1 \\ \vdots \end{pmatrix} \qquad \xi = \begin{pmatrix} x_1 \\ x_2 \\ \vdots \end{pmatrix}$$

The conditions for the determination of the additional variables $\begin{pmatrix} y_0 \\ \varphi_0 \end{pmatrix}$ come from the imposition of the equilibrium of forces and moments:

$$\begin{pmatrix} 1^* \\ \xi^* \end{pmatrix} D_m \chi + \begin{pmatrix} m_0 & 0 \\ 0 & 0 \end{pmatrix} \begin{pmatrix} y_0 \\ \varphi_0 \end{pmatrix} = 0 \qquad (II.2)$$

where the asterisk indicates transpose.

Application of the operator $\begin{pmatrix} 1^* \\ \xi^* \end{pmatrix} D_m$ to Eq. (II.1) and insertion of the equilibrium condition (II.2) yields

$$-\begin{pmatrix} m_0 & 0 \\ 0 & 0 \end{pmatrix}\begin{pmatrix} y_0 \\ \varphi_0 \end{pmatrix} - \begin{pmatrix} 1^* \\ \xi^* \end{pmatrix} D_m(1, \xi)\begin{pmatrix} y_0 \\ \varphi_0 \end{pmatrix} = \omega^2 \begin{pmatrix} 1^* \\ \xi^* \end{pmatrix} D_m [A + C] D_m \chi \quad \text{(II.3)}$$

Noting the following definitions:

$$m_0 + 1^* D_m 1 = \sum_{i=0} m_i = M \qquad \text{(total mass)}$$

$$\xi^* D_m 1 = 1^* D_m \xi = \sum_{i=0} m_i x_i = S \text{ (first moment)}$$

$$\xi^* D_m \xi = \sum_{i=0} m_i x_i^2 = I \qquad \text{(second moment)}$$

we find Eq. (II.3) reduces to

$$-\begin{pmatrix} M & S \\ S & I \end{pmatrix}\begin{pmatrix} y_0 \\ \varphi_0 \end{pmatrix} = \omega^2 \begin{pmatrix} 1^* \\ \xi^* \end{pmatrix} D_m [A + C] D_m \chi$$

This equation, which represents the satisfaction of the equilibrium conditions (II.2), is solved for $\begin{pmatrix} y_0 \\ \varphi_0 \end{pmatrix}$. Insertion into Eq. (II.1) then yields n homogeneous equations in n unknowns.

$$\chi + \frac{\omega^2}{MI - S^2}(1, \xi)\begin{pmatrix} I & -S \\ -S & M \end{pmatrix}\begin{pmatrix} 1^* \\ \xi^* \end{pmatrix} D_m [A + C] D_m \chi = \omega^2 [A + C] D_m \chi$$

Rewriting this into the standard form of an eigenvalue equation,

$$\left[\mathbf{I} - \frac{1}{MI - S^2}(1, \xi)\begin{pmatrix} I & -S \\ -S & M \end{pmatrix}\begin{pmatrix} 1^* \\ \xi^* \end{pmatrix} D_m\right] \times [A + C] D_m \chi = \frac{1}{\omega^2}\chi$$

In a more condensed form, this can be written

$$G D_m [A + C] D_m \chi = \lambda \chi \qquad \text{(II.4)}$$

where

$$[D_m(A + C)D_m]^* = [D_m(A + C)D_m]$$

$$G^* = G = \left[D_m^{-1} - \frac{1}{MI - S^2}(1, \xi)\begin{pmatrix} I & -S \\ -S & M \end{pmatrix}\begin{pmatrix} 1^* \\ \xi^* \end{pmatrix}\right] = \left\{\frac{1}{m_i}\delta_{ij} - \frac{1}{MI - S^2}\left[I + M x_i x_j - S(x_i + x_j)\right]\right\}$$

The new $(n)^2$ dynamic matrix, whose diagonalization yields the required natural frequencies and modes, is

$$G D_m [A + C] D_m$$

References

[1] Rayleigh, *The Theory of Sound;* Macmillan, 1877.

[2] Timoshenko, S., *Vibration Problems in Engineering;* D. Van Nostrand, 1937.

[3] Traill-Nash, R. W., and Collar, A. R., *The Effects of Shear Flexibility and Rotatory Inertia on the Bending Vibrations of Beams,* Quarterly Journal of Mechanics and Applied Mathematics, Vol. VI, Part 2, 1953.

[4] Scanlan, R. H., *A Note on Transverse Bending of Beams Having Both Translating and Rotating Mass Elements,* Journal of the Aeronautical Sciences, Vol. 15, No. 7, p. 425, July, 1948.

[5] Fettis, H. E., *Effect of Rotary Inertia on Higher Modes of Vibration,* Journal of the Aeronautical Sciences, Vol. 16, No. 7, p. 445, July, 1949.

[6] Scanlan, R. H., and Rosenbaum, R., *Aircraft Vibration and Flutter;* Macmillan, 1951.

Equations for Loading on Triangular Wings Having Subsonic Leading Edges Due to Various Basic Antisymmetric Twist Distributions

R. N. Haskell and W. S. Johnson, Jr.

Senior Aerodynamics Engineer and Senior Structures Engineer, Respectively, Convair-Ft. Worth Division of General Dynamics Corporation, Ft. Worth, Tex.

November 8, 1954

Summary

Using the integral equations presented by Zienkiewicz,[1] for the antisymmetric boundary condition, load distributions are found for wings with local incidence proportional to t, t^2, and t^3.

Symbols

a_i = coefficients of power series expansion for the angle of attack
$b/2$ = wing semispan
b_i = constant coefficients, see Appendix B
c = local chord
c_{AV} = average chord = $c_R/2$
c_l = local chordwise lift coefficient
c_R = root chord
D = function of β and a_i
E = elliptic integral of second kind with modulus = $\sqrt{1 - m^2}$
F = function of m, K, and E
$H(s, t)$ = $\dfrac{(t - s)^k\sqrt{1 - s^2}}{s}$
$I_{q,\ n}$ = $\displaystyle\oint_1^m \frac{s^n\, ds}{\sqrt{1 - s^2}\,(s^2 - m^2)^{q\ +\ 1/2}}$ See Appendix C for values of $I_{3,\ 2}$ and $I_{3,\ 4}$
K = elliptic integral of first kind with modulus = $\sqrt{1 - m^2}$
M = free stream Mach Number
m = $\beta \tan \epsilon$, leading edge sweep parameter
m_0 = $\beta \tan \delta$, trailing edge sweep parameter
$\frac{\Delta_p}{q}$ = lifting pressure coefficient
q = free-stream dynamic pressure
s = t-like variable of integration
t = $\dfrac{\beta y}{x}$, the conical variable
t_{TE} = $\dfrac{m_0 y}{c_R \tan \delta + y}$, t evaluated at the trailing edge
x, y, z = rectangular coordinates, origin at the wing vertex, x-axis in the streamwise direction, z positive upward
$\bar{x}$ = distance of chordwise center of pressure from y axis
β = $\sqrt{M^2 - 1}$
δ = complement of trailing edge sweep angle, see Fig. 1
ϵ = complement of leading edge sweep angle, see Fig. 1
η = $y/(b/2)$, nondimensional span coordinate
λ = local wing incidence in radians

Analysis

General

For the antisymmetric boundary condition where local incidence, λ, is:

$$\left(\frac{\beta}{x}\right)^k \lambda = a_0 + a_1 t + a_2 t^2 + a_3 t^3 \ldots + a_k t^k, \qquad t > 0$$

$$= -a_0 + a_1 t - a_2 t^2 + a_3 t^3 \ldots \pm a_k t^k, \qquad t < 0$$

and

$$\lambda(x, y) = -\lambda(x, -y)$$

Zienkiewicz[1] has shown:

$$\frac{\Delta_p}{q} = \left(\frac{x}{\beta}\right)^k \left[\frac{1}{\sqrt{m^2 - t^2}} \sum_{i=0}^{(k/2)} b_{2i+1}\, t^{2i+1}\right] \qquad (1)$$

and

$$\left(\frac{\beta}{x}\right)^k \lambda = -\frac{\beta}{4k!}\oint_1^m H(s, t)\left(\frac{\partial}{\partial s}\right)^{k+1} \times \left[\frac{1}{\sqrt{s^2 - m^2}} \sum_{i=0}^{(k/2)} b_{2i+1} s^{2i+1}\right] ds \qquad (2)$$

If all the a_i are zero for $i = 0, 1, \ldots, k-1$ and $a_k \neq 0$, the polynomial will be called a pure kth degree polynomial and the corresponding twist will be called a pure kth degree twist. In what follows the terms linear, parabolic and cubic refer to pure first degree, pure parabolic, and pure cubic twist, respectively.

For any k, Zienkiewicz has shown that the redundant equations for determining the b_i in the case of pure twist are satisfied identically and that those remaining are just sufficient to determine the b_i.

Linear

This solution has been derived previously by other authors and is included herein only for completeness of presentation.

Parabolic

Let

$$\left(\frac{\beta}{x}\right)^2 \lambda = a_2 t^2, \qquad t > 0$$

$$= -a_2 t^2, \qquad t < 0$$

and Eq. (2) becomes

$$a_2 t^2 = -\frac{\beta}{4(2!)} \oint_1^m \frac{(t-s)^2 \sqrt{1-s^2}}{s} \frac{\partial^3}{\partial s^3} \times \left[\frac{1}{\sqrt{s^2-m^2}} (b_1 s + b_3 s^3)\right] ds \quad (3)$$

from which the two simultaneous equations are derived for the determination of b_1 and b_3:

$$3b_1(I_{2,4} - I_{1,2}) + b_3(6I_{0,2} - 7I_{1,4} + 3I_{2,6}) = 0$$

$$3b_1(I_{2,1} - I_{1,-1}) + b_3(6I_{0,-1} - 7I_{1,1} + 3I_{2,3}) = -\frac{8a_2}{\beta}$$

The resulting expressions for b_1 and b_3 are tabulated in Appendix B.

Cubic

Let

$$(\beta/x)^3 \lambda = a_3 t^3$$

and Eq. (2) becomes:

$$a_3 t^3 = -\frac{\beta}{24} \oint_1^m \frac{(t-s)^3 \sqrt{1-s^2}}{s} \frac{\partial^4}{\partial s^4} \times \left[\frac{1}{\sqrt{s^2-m^2}} (b_1 s + b_3 s^3)\right] ds \quad (4)$$

from which the four simultaneous equations for the determination of b_1 and b_3 are derived:

$$b_1[-5I_{3,2} + 6I_{2,0} - I_{1,-2}] + b_3[-5I_{3,4} + 12I_{2,2} - 9I_{1,0} + 2I_{0,-2}] = -\frac{8a_3}{\beta} \quad (5)$$

$$b_1[-5I_{3,5} + 6I_{2,3} - I_{1,1}] + b_3[-5I_{3,7} + 12I_{2,5} - 9I_{1,3} + 2I_{0,1}] = 0 \quad (6)$$

$$b_1[-5I_{3,4} + 10I_{3,6} + 6I_{2,2} - 12I_{2,4} - I_{1,0} + 2I_{1,2}] + b_3[-5I_{3,6} + 10I_{3,8} + 12I_{2,4} - 24I_{2,6} - 9I_{1,2} + 18I_{1,4} + 2I_{0,0} - 4I_{0,2}] = 0 \quad (7)$$

$$b_1[-15I_{3,7} + 10I_{3,5} + 18I_{2,5} - 12I_{2,3} - 3I_{1,3} + 2I_{1,1}] + b_3[-15I_{3,9} + 10I_{3,7} + 36I_{2,7} - 24I_{2,5} - 27I_{1,5} + 18I_{1,3} + 6I_{0,3} - 4I_{0,1}] = 0 \quad (8)$$

Eqs. (6) and (7) can be shown to hold identically, therefore Eqs. (5) and (8) are solved simultaneously for the unique solution for b_1 and b_3.

Span-Load Distribution

The span-load distribution is defined as:

$$\left(\frac{c_1 c}{c_{av}}\right)_i = \frac{1}{c_{av}} \int_{x_{LE}}^{x_{TE}} \left(\frac{\Delta_p}{q}\right)_i dx$$

and

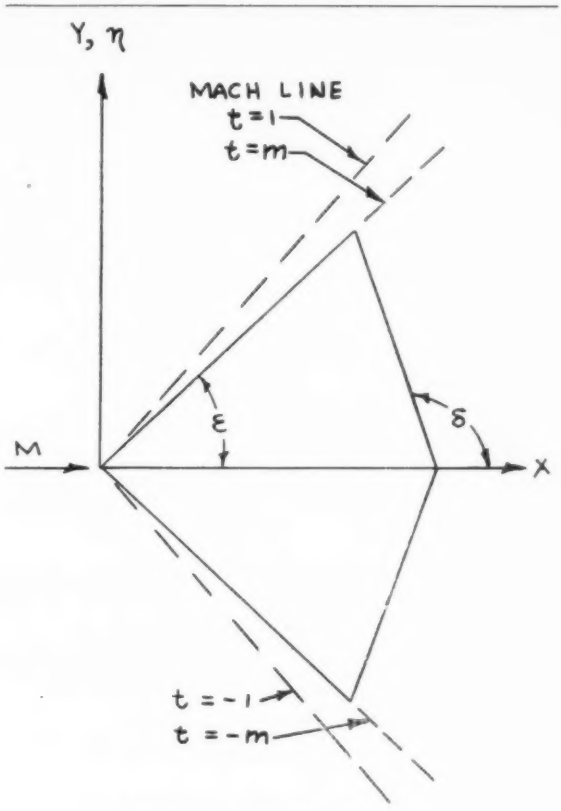

FIG. 1. Coordinates and notation.

$$\left(\frac{c_1 c}{c_{av}}\right)_{net} = \sum_{i=1}^{k} \left(\frac{c_1 c}{c_{av}}\right)_i$$

Chordwise Center of Pressure

The chordwise center of pressure is defined as:

$$(\bar{x}_i) = \frac{\int_{x_{LE}}^{x_{TE}} x \left(\frac{\Delta_p}{q}\right)_i dx}{\int_{x_{LE}}^{x_{TE}} \left(\frac{\Delta_p}{q}\right)_i dx}$$

and

$$(\bar{x})_{net} = \frac{\sum_{i=0}^{k} (\bar{x})_i \left(\frac{c_1 c}{c_{av}}\right)_i}{\sum_{i=0}^{k} \left(\frac{c_1 c}{c_{av}}\right)_i}$$

where x is the distance of the chordwise center of pressure from the y axis.

The expressions for $(\Delta_p/q)_i$, $(c_1 c/c_{av})_i$ and $\bar{x}_i$ are tabulated in Appendix A.

REFERENCE

[1] Zienkiewicz, H. K., *A Note on Generalized Conical Fields with Application to Lift on Twisted and Cambered Delta Wings with Subsonic Leading Edges*, English Electric Co., Ltd. Report No. L At 050, August, 1953. (ASTIA, AD 22135.)

(*Concluded on page 280*)

Appendix A

Load Equations for the Basic Antisymmetric Twist Distributions

1. Linear

$$\left(\frac{\Delta p}{q}\right)_1 = \left(\frac{x}{\beta}\right)\frac{b_1 t}{\sqrt{m^2 - t^2}}$$

$$\left(\frac{c_1 c}{c_{av}}\right)_1 = \frac{2b_1\beta\eta^2\sqrt{m^2 - t_{T.E.}{}^2}}{[c_R/(b/2)]\, m^2\, t_{T.E.}}$$

$$\left(\frac{\bar{x}}{b/2}\right)_1 = \frac{c_R/(b/2)\tan\delta + \eta}{2m_0\tan\epsilon}\left[m + \frac{t_{T.E.}{}^2}{\sqrt{m^2 - t_{T.E.}{}^2}}\log\frac{m + \sqrt{m^2 - t_{T.E.}{}^2}}{t_{T.E.}}\right]$$

2. Parabolic

$$\left(\frac{\Delta p}{q}\right)_2 = \left(\frac{x}{\beta}\right)^2\frac{b_1 t + b_2 t^3}{\sqrt{m^2 - t^2}}$$

$$\left(\frac{c_1 c}{c_{av}}\right)_2 = \frac{\beta\eta^2}{c_R/(b/2)m^2}\left[\frac{b_1\sqrt{m^2 - t_{T.E.}{}^2}}{t_{T.E.}{}^2} + \left(\frac{b_1 + 2m^2 b_2}{m}\right)\log\frac{m + \sqrt{m^2 - t_{T.E.}{}^2}}{t_{T.E.}}\right]$$

$$\left(\frac{\bar{x}}{b/2}\right)_2 = \frac{2(c_R/(b/2)\tan\delta + \eta)}{3m_0\tan\epsilon}\left\{\frac{\sqrt{m^2 - t_{T.E.}{}^2}\,[(m^2 + 2t_{T.E.}{}^2)b_1 + 3m^2 t_{T.E.}{}^2 b_2]}{mb_1\sqrt{m^2 - t_{T.E.}{}^2} + t_{T.E.}{}^2(b_1 + 2m^2 b_2)\log\dfrac{m + \sqrt{m^2 - t_{T.E.}{}^2}}{t_{T.E.}}}\right\}$$

3. Cubic

$$\left(\frac{\Delta p}{q}\right)_3 = \left(\frac{x}{\beta}\right)^3\frac{b_1 t + b_2 t^3}{\sqrt{m^2 - t^2}}$$

$$\left(\frac{c_1 c}{c_{av}}\right)_3 = \frac{2\beta\eta}{3c_R/(b/2)m^4}\left(\frac{c_R/(b/2)\tan\delta + \eta}{m_0}\right)^3\sqrt{m^2 - t_{T.E.}{}^2}\,[(2b_1 + 3m^2 b_2)t_{T.E.}{}^2 + m^2 b_1]$$

$$\left(\frac{\bar{x}}{b/2}\right)_3 = \frac{3}{8\tan\epsilon}\left(\frac{c_R/(b/2)\tan\delta + \eta}{m_0}\right)\times$$

$$\left\{\frac{m[(3b_1 + 4m^2 b_2)t_{T.E.}{}^2 + 2m^2 b_1]\sqrt{m^2 - t_{T.E.}{}^2} + t_{T.E.}{}^4(3b_1 + 4m^2 b_2)\log(m + \sqrt{m^2 - t_{T.E.}{}^2})/t_{T.E.}}{\sqrt{m^2 - t_{T.E.}{}^2}\,[(2b_1 + 3m^2 b_2)t_{T.E.}{}^2 + m^2 b_1]}\right\}$$

Appendix B

Table 1
Expressions for the b Coefficients

	$F\,b_1/D$
Linear	$m^2(1 - m^2)$
Parabolic	$m^3[2(1 - 2m^2)E - m^2(1 - 3m^2)K]$
Cubic	$2(15m^4 - 9m^2 + 2)I_{3,4} - 3m^2(9m^2 - 2)I_{3,2} + 2K - 4E$
	$F\,b_2/D$
Parabolic	$m^3[(m^2 + 1)E - 2m^2K]$
Cubic	$5m^2 I_{3,4}$
	F
Linear	$(2 - m^2)E - m^2K$
Parabolic	$2(m^4 - m^2 + 1)E - m^2(m^2 + 1)K$
Cubic	$3m^2(-135m^4 + 30m^2 - 8)(I_{3,2})^2 + (540m^6 - 240m^4 + 960m^2 - 160)(I_{3,2})(I_{3,4}) + (1035m^4 - 530m^2 + 120)(I_{3,4})^2 + 2(2E - K)(40 - 15m^2)I_{3,2} - 10(11E - 6K)I_{3,4}$
	D
Linear	$\dfrac{4a_1}{\beta}$
Parabolic	$\dfrac{16a_2}{3\pi\beta}$
Cubic	$\dfrac{8a_3}{\beta}$

Table 2
Numerical Values of the b_i Coefficients

	Linear	Parabolic		Cubic	
m	b_1/D	b_1/D	b_2/D	b_1/D	b_2/D
0.1	0.004988	0.000988	0.000480	0.00001838	0.00002427
0.2	0.019809	0.007708	0.003591	0.00027675	0.00037925
0.3	0.044085	0.024997	0.011102	0.00129747	0.0016694
0.4	0.077260	0.056353	0.023874	0.0036964	0.0045576
0.5	0.118648	0.103957	0.042086	0.0080898	0.0095402
0.6	0.167569	0.168894	0.065453	0.0149668	0.0169429
0.7	0.223297	0.251095	0.093465	0.0246952	0.0269278
0.8	0.285110	0.351214	0.125614	0.0375282	0.0395575
0.9	0.352332	0.467196	0.161572	0.0524396	0.0558255

Appendix C

Expressions for $I_{3,2}$ and $I_{3,4}$ Coefficients[1]

$$I_{3,2} = \frac{m^2(1 - 9m^2)K - (2 - 7m^2 - 3m^4)E}{15m^4(1 - m^2)^3}$$

$$I_{3,4} = \frac{(3 + 7m^2 - 2m^4)E - m^2(9 - m^2)K}{15m^2(1 - m^2)^3}$$

Buckling Loads for Beams of Variable Cross Section Under Combined Loads

B. E. Gatewood
Mechanics Department, USAF Institute of Technology, Wright-Patterson AFB, Ohio

October 6, 1954

THE AUTHOR[1] HAS PRESENTED curves for the buckling coefficient for columns of variable cross section for all taper ratios and for moment of inertia variation between constant and sixth power. This note presents curves for the lateral buckling coefficient for cantilever beams with the same variations as for the column case and gives interaction curves for buckling coefficient under combined lateral and compression loads on the beam. Timoshenko[2] has solved the lateral stability case for a beam with constant moment of inertia. Martin[3] has obtained interaction curves for the combined loading for the constant moment of inertia case and for the zero taper case with linear moment of inertia variation. Boley and Zimnoch[4] have indicated an approximate numerical procedure for the lateral stability case. DiMaggio, Gomza, Thomas, and Salvadori[5] have obtained an interaction curve for the constant moment of inertia case. Yoshihara[6] has solved the lateral stability case and obtained the interaction curve for a linear variation in width and thickness ($m = 4$ case below).

From Fig. 1, the taper ratio, the smaller moment of inertia variation, and the twisting stiffness variation are defined by, respectively,

$$\alpha = \frac{a}{a + L}, \quad I = I_1 \left(\frac{x}{a}\right)^m, \quad C = C_1 \left(\frac{x}{a}\right)^n \tag{1}$$

where for solid section $m = r + 3s$ with x^r the width variation and x^s the thickness variation. The variation of C is approximate for $r \neq s$, but this approximation is close for practical cases in which I is small compared with the moment of inertia about the 90° axis.

With the coordinate system of Fig. 1, the differential equations for the deflection y and the angle of twist θ are[2]

$$\begin{aligned} EI_1 x^m y'' + Pa^m y &= Qa^m (x - a)\theta, \\ GC_1 x^n \theta' &= Qa^m [y - (x - a)y'] \end{aligned} \tag{2}$$

with boundary conditions $y = 0$ at $x = a$, $y' = 0$ at $x = a + L$, $\theta = 0$ at $x = a + L$. This system can be solved by taking y as an infinite series in powers of x or $1/x$, depending upon whether

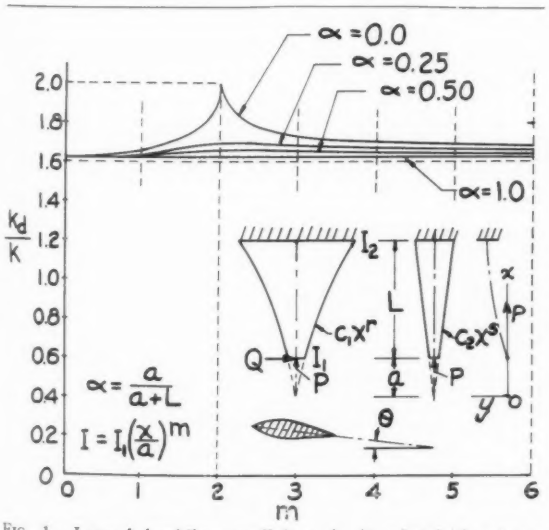

FIG. 1. Lateral buckling coefficient k_d in terms of column buckling coefficient k.

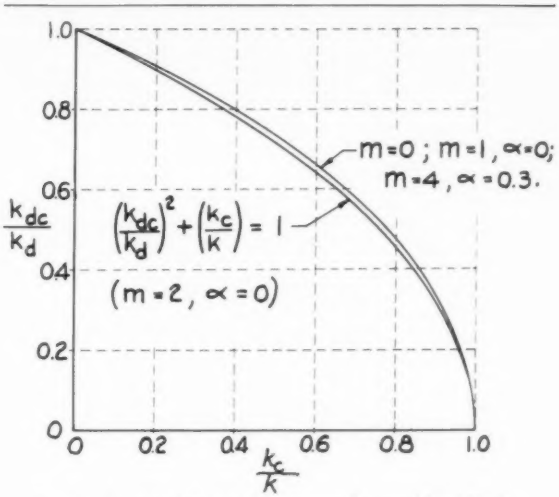

FIG. 2. Interaction buckling curves for combined loads.

$x = 0$ or $x = \infty$ is a regular singular point. With $P = 0$, the boundary conditions lead to a determinant for the lateral buckling coefficient. With assigned values to P, the determinant gives Q, whence on the interaction curve between the lateral buckling coefficient and column coefficient can be constructed.

By change of variables[6] in sequence

$$\begin{aligned} y &= (x - a)y_1, \qquad \theta = (P/Q)\theta_1 \\ t &= 1 - (a/x), \qquad dy_1/dt = U \end{aligned} \tag{3}$$

Eq. (2) becomes

$$t^2(1 - t)U'' + t[2 + (m - 6)t]U' + [-2 + 2(m - 3)t + p^2t^2(1 - t)^{m-3} + q^2t^4(1 - t)^{2m-6}]U = 0 \tag{4}$$

with boundary conditions $U = 0$ at $t = 0$, $tU' + [2 - p^2t^2(1 - t)^{m-3}]U = 0$ at $t = 1 - \alpha$, and

$$p^2 = Pa^2/EI_1, \qquad q = Qa^2/\sqrt{EI_1GC_1} \tag{5}$$

The determinant is

$$\sum_{n=0}^{\infty} [\alpha^{m-2}p^2(1 - \alpha)^2 - (n + 3)]a_n(1 - \alpha)^n = 0 \tag{6}$$

where

$$U = \sum_{n=0}^{\infty} a_n t^{n+1} \tag{7}$$

the a_n being determined from Eq. (4) in terms of m, p, and q.

Although Eq. (6) and the determinant derived directly from Eq. (2) can be shown to be the same, the two series are quite different in character and involve quite different recursion formulas. For some m and α, Eq. (6) converges rapidly and is easy to solve, while for other values of m and α the determinant from Eq. (2) is much shorter to use.

For the lateral instability case ($P = 0$) the buckling coefficient was found to vary with m and α in the same way as the buckling coefficient for the column case ($Q = 0$), which has been solved.[1] In fact, $k_d/k \cong 1.63$ for all α and m considered:

$$\begin{aligned} Q_{cr} &= (\pi^2/4)(k_d\sqrt{EI_2GC_2}/L^2) \\ \text{or} \\ Q_{cr} &= (2\pi^2)(k_d\sqrt{EI_1GC_1}/a^2) \end{aligned} \tag{8}$$

where k_d/k is given in Fig. 1 and k is given in Figs. 1 and 2 of reference 1. The two cases in Eq. (8) correspond to the two cases for k in reference 1.

For the combined load case, assign values to $(Q/P)\sqrt{EI_1/GC_1}$ and obtain p^2 from the determinant and hence q^2 from Eq. (5). If these values are divided by their respective peak values for each m and α, then an interaction curve can be drawn. Fig. 2

shows the results and also shows that the shape of the interaction curves are nearly independent of m and α and can be approximated closely by a parabola. In the Fig. 2, k is the buckling coefficient for column load alone, given in Figs. 1 and 2 of reference 1; k_d is the buckling coefficient for lateral load alone, given in Fig. 1; k_c and k_{d_c} are the respective column and lateral buckling coefficients for combined loads. All the curves, except around $m = 2$ and small α, lie on the $m = 0$ curve. Further, the $m = 0$ curve checks the results of references 3 and 5. Note that in the approximate interaction Eq. (15) of reference 5 the p and q should be interchanged. A perturbation method is used in reference 6 to get results that agree within a few per cent of results obtained here for $m = 4$.

Thus a conservative solution for the lateral buckling coefficient and for the combined loading case can be obtained directly from Figs. 1 and 2 of reference 1, as

$$k_d = 1.63\,k; \qquad (k_{d_c}/1.63k)^2 + (k_c/k) = 1 \qquad (9)$$

for all α and for m variation from constant to sixth power.

References

[1] Gatewood, B. E., *Buckling Loads for Columns of Variable Cross Section*, Journal of the Aeronautical Sciences, Vol. 21, No. 4, pp. 287–288, April, 1954.

[2] Timoshenko, S., *Theory of Elastic Stability*, pp. 245–246, McGraw-Hill Book Company, Inc., New York, 1936.

[3] Martin, H. C., *Elastic Instability of Deep Cantilever Struts Under Combined Axial and Shear Loads at the Free End*, Proceedings of the First U. S. Congress of Applied Mechanics, pp. 395–402, 1951.

[4] Boley, B. A., and Zimnoch, V. P., *Lateral Buckling of Nonuniform Beams*, Journal of the Aeronautical Sciences, Vol. 19, No. 8, pp. 567–588, August, 1952.

[5] DiMaggio, F., Gomza, A., Thomas, W. E., and Salvadori, M. G., *Lateral Buckling of Beams in Bending and Compression*, Journal of the Aeronautical Sciences, Vol. 19, No. 8, pp. 574–576, August, 1952.

[6] Yoshihara, Hideo, *On the Lateral Buckling of a Tapered Cantilever Beam*, Unpublished report, September, 1954.

Further Comments on "Note on Boundary-Layer Transition in Supersonic Flow"[1]

A. H. Lange and R. E. Lee

U. S. Naval Ordnance Laboratory, White Oak, Silver Spring, Md.

October 17, 1954

THE STRONG EFFECT of an expansion on boundary-layer transition in supersonic flow had been observed on cone cylinders and hollow cylinders with outside leading edge bevels and had been reported in reference 1.

A systematic experimental study of this effect was carried out subsequently. Transition on an open-nose truncated cone-cylinder (cone half angle = 10°) was determined from schlieren pictures at $M = 2.15$ in the NOL Aeroballistics Wind Tunnel No. 1. The conical part of the model, which was originally 8 in. long, was shortened in 2-in. steps and the leading edge resharpened in each case.

Fig. 1 shows the results. Transition Reynolds Number is based on free-stream velocity, kinematic viscosity, and on wetted length along the body contour. Transition Reynolds Numbers up to ~2.5 times larger than those observed on a constant pressure surface were obtained. The effect begins to deteriorate when the cone Reynolds Number R_{cone} (R based on cone length) reaches the transition Reynolds Number of the constant pressure surface (see the auxiliary curve R_{cone} vs. a). The boundary layer behind the shoulder appears to be more stable even than a boundary layer starting at a leading edge, as evidenced by the fact that the transition Reynolds Number observed is more than twice the constant pressure transition Reynolds Number.

Tests reported in reference 2 show that the skin friction on a cone-cylinder body is under certain circumstances actually less than the skin friction on a carefully shaped parabolic body (NACA RM 10) due to the effect discussed above. This possibility was first mentioned in reference 1.

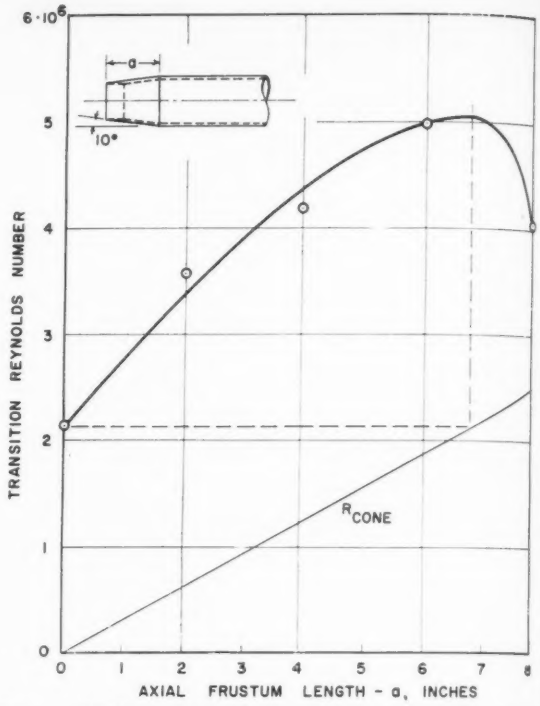

FIG. 1 AVERAGE TRANSITION REYNOLDS NUMBER VS. FRUSTUM LENGTH ON AN OPEN — NOSE TRUNCATED CONE-CYLINDER, M = 2.15

References

[1] Lange, A. H., and Lee, R. E., *Note on Boundary Layer Transition in Supersonic Flow*, Readers' Forum, Journal of the Aeronautical Sciences, Vol. 21, No. 1, p. 58, January, 1954.

[2] Hilton, J. H., and Czarnecki, K. R., *An Exploratory Investigation of Skin Friction and Transition on Three Bodies of Revolution at a Mach Number of 1.61*, NACA TN No. 3193.

An Approximate Relationship Between Small Radius Ratio Turbine Passage Geometry and Radial Pressure Variation

J. P. Fraser*

Knolls Atomic Power Laboratory, General Electric Company, Schenectady, N.Y.†

November 12, 1954

THE PROCEDURE TO BE briefly summarized was undertaken to give a first approximation to the deviation from a "vortex" radial pressure distribution in a nonvortex stage. To this end, incompressible and lossless flow are assumed. The relationships developed take into account passage geometry of nozzle and bucket at all axial stations. It is believed that this approach will assist in the approximate layout of nonvortex turbine stages having a radius ratio approaching unity.

Essentially the entire flow is treated as one filament. Free-vortex radial pressure is "corrected" by finding the "centroid"

* This work was done while the writer was in the Fluid Mechanics Section, Large Steam Turbine Division, General Electric Co., Schenectady, N. Y.

† Operated for the U.S. Atomic Energy Commission on Contract No. W-31-109 Eng-52.

of flow at each axial position and relating the correction to vortex radial pressure distribution to the radial curvature of the path of the flow centroid. Solution is effected when radial equilibrium is satisfied at all axial positions.

The radial momentum equation in axisymmetric coordinates is

$$\frac{1}{\rho}\frac{\partial P}{\partial r} = \frac{v^2}{r} - w\frac{\partial u}{\partial z} - u\frac{\partial u}{\partial r} \tag{1}$$

If attention is confined to stages having cylindrical sidewalls, the last term is second order and may be omitted in an approximate treatment.

The concept of an effective flow path is introduced. The radial location of this flow "centroid" is defined by

$$r_c = \frac{\int_{r_i}^{r_0} q_{ax} r\, dr}{\int_{r_i}^{r_0} q_{ax}\, dr} \tag{2}$$

where q_{ax} = axial flow per unit radius and the entire flow is treated as one flow filament. The effective radial velocity of the filament $(r_0 - r_i)$ is written

$$u = w_{avg.}\frac{\partial r_c}{\partial z} \tag{3}$$

Then

$$\frac{\partial u}{\partial z} = w_{avg.}\frac{\partial^2 r_0}{\partial z^2} + \frac{\partial w_{avg.}}{\partial z}\frac{\partial r_c}{\partial z} \tag{4}$$

By talking of "average" conditions over the radial height of the flow annulus, Eq. (1) with Eq. (4) substituted takes the dimensionless form

$$\Delta P = 4(1 - \tau_i)\,[v_{avg.}^2 - w_{avg.}^2 r_c'' - w_{avg.} w_{avg.}' r_c'] \tag{5}$$

where ΔP = pressure difference from tip to root and primes indicate derivative with respect to the nondimensional axial distance, z. P_0, stage pressure drop; V_0, the theoretical velocity corresponding to P_0; and r_p, the average radius are the units of pressure, velocity, and length used to nondimensionalize Eq. (1). τ represents dimensionless radius. Eq. (5) is the key to solution of the stage pressure distribution. The first term in parentheses represents an approximate vortex pressure difference; the second and third terms represent corrections taking into account radial flow.

The application of Eq. (5) is illustrated by setting up a solution for flow through a hypothetical nozzle. Assume that the pressure varies linearly with radius. That is, nondimensionally,

$$P(z) = M(z) + N(z)\,(\tau - 1) \tag{6}$$

The pressure at the outer wall is given by

$$P_0(z) = M(z) + N(z)\,(1 - \tau_i) \tag{7}$$

or

$$P_0(z) = M(z) + (1/2)\,\Delta P(z) \tag{8}$$

Solving for $N(z)$ between Eqs. (5), (6), (7), and (8),

$$N(z) = 2[v_{avg.}^2 - w_{avg.}^2 r_c'' - w_{avg.} w_{avg.}' r_c'] \tag{9}$$

Eq. (9) gives radial pressure gradient. The second and third terms correct vortex radial pressure distribution for radial flow.

The next step is the injection of nozzle passage geometry into Eq. (9). Assume that the nozzle is untwisted or the average nozzle flow angle is given by

$$\sin\alpha = G(z) \tag{10}$$

Also assume

$$S(z) = \tau F(z) \tag{11}$$

where $S(z)$ is the unblocked circumference divided by pitch radius.

$G(z)$ and $F(z)$ can be readily evaluated, approximately at least, from the nozzle layout.

Assuming incompressible flow, let the nondimensional flow be

$$Q = \frac{Flow}{\rho r_p V_0} \tag{12}$$

By continuity,

$$w_{avg.} = \frac{Q}{2(1 - \tau_i)F(z)} \tag{13}$$

and

$$v_{avg.}^2 = \left[\frac{Q}{2(1 - \tau_i)F(z)}\right]^2 \frac{1 - G(z)^2}{G(z)^2} \tag{14}$$

Substituting Eqs. (13) and (14) into Eq. (9),

$$N(z)_{nozzle} = 2\left[\frac{Q}{2(1 - \tau_i)F}\right]^2 \left[\frac{1 - G^2}{G^2} - r_c'' + \frac{F'}{F} r_c'\right] \tag{15}$$

Now using Eqs. (2) and (10), one can write

$$r_c(z) = \frac{G(z)\int_{\tau i}^{\tau_0} V(z)\tau^2\, d\tau}{G(z)\int_{\tau i}^{\tau_0} V(z)\tau\, d\tau} \tag{16}$$

Now

$$V(z) = \sqrt{1 - P(z)} \tag{17}$$

or, using Eq. (6),

$$V(z) = \sqrt{1 - M(z) - N(z)\,(\tau - 1)} \tag{18}$$

Pitch line pressure distribution is given by

$$M(z) = 1 - \frac{w_{avg.}^2}{G(z)^2} \tag{19}$$

where

$$w_{avg.}(z) = \frac{Q}{2(1 - \tau_i)F(z)} \tag{13}$$

By substituting Eq. (18) into Eq. (16),

$$r_c(z) = \frac{\int_{\tau i}^{\tau_0} \sqrt{1 - M(z) - N(z)\,(\tau - 1)}\,\tau^2\, d\tau}{\int_{\tau i}^{\tau_0} \sqrt{1 - M(z) - N(z)\,(\tau - 1)}\,\tau\, d\tau} \tag{20}$$

The solution to nozzle flow must satisfy Eqs. (15) and (20) for radial equilibrium.

The two equations applicable to bucket flow, which are analogous to Eqs. (15) and (20) for the nozzle, can be developed in terms of stage vector geometry and bucket passage geometry.

Solution of Eqs. (15) and (20) for the nozzle and the corresponding pair of equations for the bucket can be solved conveniently by a process of iteration. $r_c(z)$ is found from Eq. (20) using values of $N(z)$ corresponding to vortex flow. The derivatives r_c'' and r_c' are calculated which lead to corrected values of $N(z)$ using Eq. (15). The process is continued until the radial path of the "centroid" is a continuous curve satisfying boundary conditions at the entrance and exit of the stage.

On the Determination of Local Heat-Transfer Coefficients for Bodies with Pressure Gradient in Supersonic Flow

Irving Korobkin
U.S. Naval Ordnance Laboratory, White Oak, Silver Spring, Md.
October 11, 1954

IN EXPERIMENTAL HEAT-TRANSFER INVESTIGATIONS for supersonic flow, local heat-transfer coefficients are usually evaluated from two independent sets of measurements—one set made to determine recovery temperatures and the second set made to

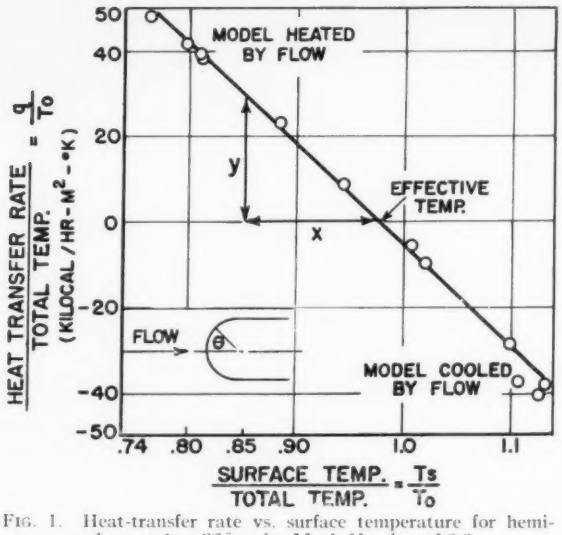

FIG. 1. Heat-transfer rate vs. surface temperature for hemisphere at $\theta = 32°$ and a Mach Number of 3.3.

determine heat-transfer rates. For a body such as a flat plate or a cone with a constant surface temperature and no pressure gradient, the local heat-transfer coefficient h is determined from the following equation:

$$h = q/(T_r - T_S) \tag{1}$$

where q is the time rate of heat transfer per unit surface area, T_S is the body surface temperature, and T_r is the recovery or adiabatic wall temperature. Because of the absence of any pressure gradient, the recovery temperature is constant along the body and is usually measured early in the experiment. The heat-transfer coefficients are determined in accordance with Eq. (1) after tests on heat-transfer rates have been made, and these coefficients generally agree with the correlations obtained for incompressible flow.

For the case of a body with a pronounced pressure gradient such as a cylinder or sphere, the recovery temperature is not a constant but varies along the body surface. Because of this fact Eckert and Livingood[1] point out that the recovery temperature is no longer a significant parameter for the determination of supersonic heat-transfer coefficients if one desires agreement with incompressible values. The recovery temperature in Eq. (1) must be replaced by an effective recovery temperature $T_{r_{ff}}$, which is determined at any particular point by maintaining the entire body at a uniform temperature and changing the constant temperature level until the local heat-transfer rate is zero at the point under consideration. It is evident that an accurate experimental determination of $T_{r_{ff}}$ along the entire body presents more difficulty than the measurement of recovery temperatures.

For some recent heat-transfer measurements on a hemisphere in supersonic flow (unpublished), the author has been able to obtain both heat-transfer data that are in fair agreement with incompressible theory and an estimate of $T_{r_{ff}}$ from only one type of measurement, by using an extension of the data reduction method described in reference 2. The local heat-transfer rates were measured all along the hemisphere, which was maintained at a constant surface temperature at various temperature levels for heat transfer to and from the body. The local heat-transfer rates at each point on the body were then plotted against surface temperature as indicated in Fig. 1. The point of intersection of the data curve and the line of zero q/T_0 gives a direct estimate of the effective temperature. Furthermore, for any temperature such as $T_S/T_0 = 0.85$ in Fig. 1, the heat-transfer coefficient can be determined by merely calculating the ratio of length y to length x. The case illustrated involved about an 80°C. difference between the maximum and minimum levels of surface temperature for a total temperature T_0 of about 15°C. and a tunnel supply pressure of 1 atmosphere, and a straight line fit the actual data points quite well. This result indicates that the heat-transfer coefficient is practically constant over the investigated range of temperatures and can be determined from the slope of the line. The method looks promising, and is being applied to data obtained in the Mach Number range of 2 to 5.

REFERENCES

[1] Eckert, E. R. G., and Livingood, J. N. B., *Method for Calculation of Laminar Heat Transfer in Air Flow around Cylinders of Arbitrary Cross Section (Including Large Temperature Differences and Transpiration Cooling)*, NACA Report No. 1118, 1953.

[2] Slack, E. G., *Experimental Investigation of Heat Transfer through Laminar and Turbulent Boundary Layers on a Cooled Flat Plate at a Mach Number of 2.4*, NACA TN No. 2686, April, 1952.

Second-Order Pressure Law for Two-Dimensional Compressible Flow

Wallace D. Hayes*
Princeton University, Princeton, N.J.
November 10, 1954

SYMBOLS

U	=	free-stream velocity
M	=	free-stream Mach Number
Γ	=	second-order flow parameter
κ	=	$\Gamma M^4(1 - M^2)^{-1}$
ϕ	=	U^{-1} times perturbation velocity potential, linear solution
ϕ_1	=	same as ϕ, but complete second-order solution
ϕ_2	=	same as ϕ, but a particular inhomogeneous solution
$f(x)$	=	body shape function
x, y	=	Cartesian coordinates
ξ, η	=	reduced coordinates
ψ	=	stream function in reduced coordinates
Φ	=	reduced velocity potential
K	=	"similitude" parameter

INTRODUCTION

THE FIRST-ORDER terms in the pressure on a two-dimensional body in a uniform subsonic or supersonic flow at a given Mach Number may be related to those for a geometrically similar body at a reference value of the Mach Number by means of the well-known Prandtl-Glauert similarity laws. The reference value of the Mach Number is generally chosen to be 0 for subsonic flow and $\sqrt{2}$ for supersonic flow. The mean-surface assumption is automatically satisfied for two-dimensional linearized flow; hence the result is more specific than the usual functional behavior deduced from similitude considerations, and in subsonic flow specifies a direct proportionality of the first-order terms in the pressure with $\tau/\sqrt{1 - M^2}$. Here the thickness ratio τ is to be replaced by the camber ratio or angle of attack where appropriate, and $\sqrt{1 - M^2}$ is to be replaced by $\sqrt{M^2 - 1}$ in supersonic flow. The purpose of the present note is to derive a similar law for the second-order terms in the pressure evaluated on the body, showing that these terms are proportional to $\tau^2(1 - M^2)^{-2}\{\Gamma M^4 + 2(1 - M^2)\}$, where Γ is a dimensionless thermodynamic parameter evaluated in the undisturbed flow. For a perfect gas with constant ratio of specific heats, $\Gamma = (\gamma + 1)/2$.

The writer obtained this result shortly after the VIII International Congress of Theoretical and Applied Mechanics at Istanbul in August, 1952, where he heard a brief presentation of a contribution of Professor Isao Imai.[1] At the time he believed he had merely reproduced Imai's results, and only an informal note

* Associate Professor of Aeronautical Engineering. At the time this note was originally prepared the writer was Scientific Liaison Officer with the Office of Naval Research, U.S. Embassy, London, England.

was prepared.[2] However, as Dr. Milton Van Dyke has pointed out to the writer, his result differs basically from any of Imai's, and separate publication is indicated.

This result may be seen to be related to the classic expression of Busemann for the second-order expression for the pressure on a body in two-dimensional supersonic flow with a single wave system. An integrated form of this result was obtained earlier by Kaplan,[3] who gave the same expression for the lift of an airfoil of arbitrary symmetrical shape.

Preliminary Discussion

For purposes of orientation it is helpful to list the second-order effects which appear in the problem of determining the pressure on a two-dimensional body from a knowledge of the geometry of the body. These are the following:

A—The Axial Velocity-Slope Effect. The lateral velocity component, which must be determined as a boundary condition from the slope of the body, is equal to this slope times the actual axial velocity. The effect of the perturbation axial velocity on this boundary condition formulation is a second-order effect.

B—The Boundary Displacement Effect. In a linear theory boundary conditions may be satisfied on the plane. If the advantages of the mean surface approximations are not to be discarded, in a more complete theory account must be taken of the fact that these boundary conditions are actually to be satisfied on the body itself instead of on the plane, and the effect of this displacement is a second-order effect.

C—The Second-Order Terms Effect. Once correct boundary conditions have been established they must be applied to a differential equation for solution. Second-order terms in the differential equation itself give a second-order effect in the solution.

D—The Second-Order Pressure Effect. The solution to the differential equation yields the axial velocity. Presuming that it is the perturbation pressure which is of interest, its expression in terms of the velocity components has a term which is of the second order.

E—The Pressure Displacement Effect. In a linear theory the pressure would be evaluated on the plane, while it is of physical interest on the surface of the body itself. The effect of this displacement in the point at which the pressure is evaluated is a second-order effect.

There does, of course, exist interaction between these basic second-order effects, but such interaction is of the third order and is properly excluded in a second-order theory. Thus these second-order effects may be considered completely superimposable in a second-order development. Since disturbance effects in two-dimensional flow are principally important locally, it might be thought that the two displacement effects, *B* and *E*, should cancel and together give only a third-order effect; this does not turn out to be the case, except in the special case of supersonic flow with a single wave family. However, the two displacement effects and the second-order pressure effect (*B*, *D*, *E*), together with a part of the second-order terms effect which may be designated as C_B, do cancel and give together a third-order effect for the pressure. The second-order term effect with C_B removed may be termed C'.

Since the rotation engendered by shock waves is of the third order and properly neglected in a second-order theory, the existence of a velocity potential is assumed.

Basic Analysis

The symbols x and y represent the axial and lateral coordinates, respectively, and $U\phi$ represents the perturbation velocity potential. The subscript 1 refers to the complete second-order solution. The quantity Γ is introduced, defined by

$$\Gamma = a^{-1}(\partial \rho a/\partial \rho)_s \tag{1}$$

to replace $(\gamma + 1)/2$ usually used for a perfect gas; this permits extension of the results to an arbitrary single-phase fluid.

The equation for the velocity potential may be written

$$\phi_{1yy} + (1 - M^2)\phi_{1xx} = \Gamma M^4(\phi_x^2)_x + M^2[\phi_y^2 + (1 - M^2)\phi_x^2]_x \tag{2}$$

to include second-order terms. The boundary conditions to be satisfied are

$$\phi_1 = 0 \tag{3a}$$

at infinity, and

$$\phi_{1_y} = \tau f'(x)\,(1 + \phi_x) \tag{3b}$$

to be evaluated on the body surface

$$y = \tau f(x) \tag{3c}$$

A subsidiary first-order equation is that the body surface may be expressed as the value of a suitably defined stream function evaluated on the plane

$$y = \int_{-\infty} \phi_y\, dx \tag{4}$$

From this point on a separate analysis is indicated for the cases of subsonic and supersonic flow.

Subsonic Flow Analysis

The change of variables is made

$$\xi = x \tag{5a}$$

$$\eta = y\sqrt{1 - M^2} \tag{5b}$$

whereby the potential equation takes the form

$$\phi_{1\xi\xi} + \phi_{1\eta\eta} = \kappa(\phi_\xi^2)_\xi + M^2(\phi_\xi^2 + \phi_\eta^2)_\xi \tag{6}$$

where

$$\kappa = \Gamma M^4(1 - M^2)^{-1} \tag{7}$$

The boundary condition on the body takes the form

$$\phi_{1\eta} = \tau(1 - M^2)^{-1/2} f'(\xi)\,(1 + \phi_\xi) \tag{8}$$

and the subsidiary first-order expression for the body coordinate

$$\eta = (1 - M^2)\int_{-\infty} \phi_\eta\, d\xi = (1 - M^2)\psi \tag{9}$$

evaluated on the plane $\eta = 0$. The quantity ψ is a stream function conjugate to the harmonic function ϕ.

Before expressing the solution it is convenient to define ϕ as the solution to the linear problem with the mean surface approximation and ϕ_2 as the solution of the equation with boundary conditions

$$\phi_{2\xi\xi} + \phi_{2\eta\eta} = (\phi_\xi^2 + \phi_\eta^2)_\xi \tag{10a}$$

$$\phi_2 = 0 \quad \text{at infinity} \tag{10b}$$

$$\phi_{2\eta} = \phi_\xi\phi_\eta \quad \text{on} \quad \eta = 0 \tag{10c}$$

The solution $\phi\phi_\xi$ to equation (10a) found by Van Dyke does not satisfy boundary condition (10c).

The solution for the derivatives of ϕ_1, the complete second-order potential, may now be expressed

$$\phi_{1\eta} = \underset{\text{A}}{\phi_\eta} + \underset{\text{B}}{\phi_\eta\phi_\xi} - \underset{\text{C}'}{(1 - M^2)\psi\phi_{\eta\eta} - (\kappa/2)\eta(\phi_\xi\phi_\eta)_\eta} + (1 + \kappa/2)\,(\phi_{2\eta} - \phi_\xi\phi_\eta) \tag{11a}$$

$$\phi_{1\xi} = \underset{\text{A}}{\phi_\xi} - \underset{\text{D}}{(1/2)\,(1 - M^2)\,(\phi_\xi^2 + \phi_\eta^2)} - \underset{\text{E}}{(1 - M^2)\psi\,\phi_{\xi\eta}} - (\kappa/2)\eta\,(\phi_\xi\phi_\eta)_\xi + (1 + \kappa/2)\,\phi_{2\xi} \tag{11b}$$

The fact that $\phi_{1\eta\xi} = \phi_{1\xi\eta}$ may be readily checked, and the Laplacian of ϕ_1 is

$$\phi_{1\xi\xi} + \phi_{1\eta\eta} = \underset{\text{C}_B}{-(1 - M^2)\,(\phi_\xi^2 + \phi_\eta^2)_\xi} + \underset{\text{C}'}{(1 + \kappa/2)\,(\phi_\xi^2 + \phi_\eta^2)_\xi} + \underset{\text{C}'}{(\kappa/2)\,(\phi_\xi^2 - \phi_\eta^2)_\xi} \tag{12}$$

which checks the basic Eq. (6). On the body the pressure may be expressed

$$-(1/2)Cp = \underset{E}{\phi_{1\xi}} + (1 - M^2)\underset{D}{\phi_{\eta\xi}} + (1/2)(1 - M^2)(\phi_\xi^2 + \phi_\eta^2)$$
$$= \phi_\xi + (1 + \kappa/2)\,\phi_{2\xi} \qquad (13)$$

evaluated on the plane $\eta = 0$. In the equations (11) to (13) above certain of the terms are labeled to indicate with which second-order effect they are connected. In order to reduce the boundary condition on the body to a form independent of the Mach Number and the thickness ratio the transformation is made

$$\phi_1 = \tau(1 - M^2)^{-1/2}\Phi_1; \quad \phi_2 = \tau^2(1 - M^2)^{-1}\Phi_2 \qquad (14)$$

With the definition for the "similitude" parameter

$$K = \tau(1 - M^2)^{-3/2}\{\Gamma M^4 + 2(1 - M^2)\} \qquad (15)$$

the linear boundary condition takes the form

$$\Phi_\eta = f'(\xi) \qquad \text{on} \qquad \eta = 0 \qquad (16)$$

and the second-order pressure coefficient the form

$$-\frac{\sqrt{1 - M^2}}{2\tau}\,C_p = \Phi_\xi + \frac{1}{2}\,K\,\Phi_2 \qquad (17)$$

In the linear theory of a subsonic two-dimensional airfoil the lift or antisymmetric part of the solution and the thickness or symmetric part of the solution are distinct and do not interact. The second-order effects due to either of these parts are symmetric and give no lift. The interaction second-order effects between these two parts are antisymmetric and do contribute to the lift on the foil. In this connection the solution for this interaction effect must be chosen to satisfy the Kutta condition on the trailing edge of the foil. As might have been expected, the nature of the usual leading-edge singularity does not improve by the addition of the second-order terms; the lift integral still converges, however, and this singularity is not particularly any more of a difficulty in second-order theory than in the linear theory. The conditions on the plane in front of or in back of the airfoil follow the theory without difficulty.

Confidence in the soundness of the application of these second-order results to airfoils for which the solutions contain certain singularities is lent by the result of Kaplan,[3] who showed that the result holds for the total lift of an arbitrary symmetrical airfoil, and by the successes of Lighthill's method[4] of rendering solutions uniformly valid. Kaplan's procedure did not involve the singularities of linear theory. Van Dyke[5] has pointed out the agreement between the results of this paper and those previously obtained in special cases, and has promised to show how subsonic solutions can be rendered uniformly valid near stagnation points.

If the second-order effects (B, C_B, D, E) are removed from the theory, the same results are obtained. In other words, if the only second-order effects included are the axial velocity-slope effect and part of the second-order terms effect (A, C'), using the mean-surface approximation and the linear pressure formula, and altering the potential Eq. (2) to the fictitious form

$$\phi_{1yy} + (1 - M^2)\phi_{1xx} = \Gamma M^4(\phi_x^2)_x + [\phi_y^2 + (1 - M^2)\phi_x^2]_x \qquad (18)$$

the correct second-order pressure result is obtained.

Supersonic Flow Case

A similar analysis may be made in the supersonic case in which $1 - M^2$ is negative, by substituting $\sqrt{M^2 - 1}$ for $\sqrt{1 - M^2}$ where appropriate. The results are in accord with those for the subsonic case.

A general two-dimensional supersonic flow is composed of two wave families, which physically must be considered to arise from bodies on either side of the flow which is of interest. The pressure on one body due to the presence of the other is usually more strongly influenced by first-order wave effects which are not taken into account in this theory than by the second-order effects discussed here. Only in special cases is this untrue, such as in a relatively narrow channel without strong singularities in the slope distribution. Thus the value of this second-order theory must be considered to be very much restricted in practice in the general supersonic case.

With a single wave family, the solution is immediate and identical with the second-order result of Busemann.

Relation to Transonic Similitude

With a given body shape the pressure expression including all second-order effects is similar under a transformation which preserves the "similitude" parameter K. This result does not yield a similitude in the usual sense, as it is restricted to the single quantity pressure, as evaluated only on the body surface. The result is more valuable than a similitude in that it specifies a definite proportionality, rather than just a functional behavior. However, the quantity K may be used in place of the classic form of the von Kármán transonic similitude parameter to correlate pressure results in transonic flow. Van Dyke has informed the author that K appears to compete quite well for this purpose with the form of the transonic similitude parameter treated by Spreiter.[6] It would appear to be difficult to establish a theoretical justification for this use of K, however, as the theory here presented is really an extension of the linear theory and does not include any mechanism to allow for such typically transonic phenomena as shock waves on the body or a bow wave in front of the body.

References

[1] Imai, I., *Extension of von Kármán's Transonic Similarity Rule*, J. Ph. Soc. Japan, Vol. 9, 103–108, 1954.

[2] Hayes, W. D., *Second-order Two-Dimensional Flow Theory and Imai's Similitude*, British A.R.C., No. 15, 722, F.M. 1877.

[3] Kaplan, C., *Effect of Compressibility at High Subsonic Velocities on the Lifting Force Acting on an Elliptic Cylinder*, NACA TN 1118 or Rep. 834, 1946.

[4] Lighthill, M. J., *A Technique for Rendering Approximate Solutions to Physical Problems Uniformly Valid*, Phil. Mag., Vol. 40, 1179–1201, 1949. See also Aero. Quart., Vol. 3, 193–210, 1951, and *General Theory of High Speed Aerodynamics*, Section E, Princeton, 1954.

[5] Van Dyke, M. D., *The Second-Order Compressibility Rule for Airfoils*, Journal of the Aeronautical Sciences, Vol. 21, 647–648, 1954.

[6] Spreiter, J. R., *Theoretical Prediction of Pressure Distributions on Nonlifting Airfoils at High Subsonic Speeds*, NACA TN 3096, 1954. See also Journal of the Aeronautical Sciences, Vol. 21, 70–72, 1954.

Brachistocronic Maneuvers of a Constant Mass Aircraft in a Vertical Plane

Placido Cicala and Angelo Miele

Professor, Politecnico di Torino, Italy, and Research Assistant Professor of Aeronautical Engineering, Polytechnic Institute of Brooklyn, Aerodynamics Laboratory, Freeport, L. I., New York, Respectively

December 18, 1954

Symbols

D = drag, lbs.
D_L = $\partial D/\partial L$ = partial derivative of drag with respect to lift, calculated at constant altitude and constant velocity
g = acceleration of gravity, ft.sec.$^{-2}$
h = altitude, ft.
L = lift, lbs.
t = time, secs.
T = thrust, lbs.
V = velocity, ft.sec.$^{-1}$
W = weight, lbs.
θ = path inclination, positive for climbing flight

Subscripts

1 = initial conditions
2 = final conditions

Superscripts

$'$ = derivative with respect to altitude (e.g., $V' = dV/dh$)

Introduction

THE STUDY OF THE CLIMBING TECHNIQUES for minimum time and for minimum fuel consumption has received considerable

attention in recent years. Because of the mathematical difficulties associated with this category of problems, various simplifications were introduced into the equations of the motion. For the papers of references 1 to 9 the following assumptions were explicitly or implicitly used: (1) the small angle between the vectors thrust and velocity is neglected; (2) the weight of the aircraft is assumed constant; (3) the curvatures and the squares of the path inclination are considered negligible with regard to their effects on that part of the drag which depends on the lift; (4) the thrust and the specific fuel consumption are assumed functions of velocity and altitude only; (5) the aerodynamic lag is disregarded—i.e., the aerodynamic forces are calculated as in steady flow; and (6) only flight paths contained in a vertical plane are considered.

The hypotheses (2) and (3) have a particular importance insofar as the equation of the motion on the normal to the flight path is consequently approximated with $L = W = \text{const.}$ and the drag is analytically reduced to a function of velocity and altitude only. It follows that the aforementioned variational problems consist in general in finding the extremals of integrals of the form[1]

$$\int_{h_1}^{h_2} A(V, \theta, h)\, dh \tag{1}$$

subject to a nonholonomic subsidiary condition of the type

$$B(V, V', \theta, h) = 0 \tag{2}$$

which results from the equations of the motion, the polar, and the expressions of the aerodynamic forces. The same integrals may be reduced to the equivalent scheme[1]

$$\int_{h_1}^{h_2} [C(V, h) + V'E(V, h)]\, dh \tag{3}$$

Because of the difficulties arising from the analytical nature of the problem, earlier investigations were carried out with techniques other than the general methods of the Calculus of Variations. In references 1 and 3 the minimal problem was solved using Green's theorem and the special properties of the function

$$\omega(V, h) = (\partial C/\partial V) - (\partial E/\partial h) \tag{4}$$

It was shown that in general the optimum path is composed of three arcs: an initial arc of equation $\theta = \pm\pi/2$; a central arc of equation $\omega = 0$; and a final arc of equation $\theta = \pm\pi/2$, the dive or zoom character of the two end arcs depending on the boundary conditions of the problems. In reference 2 the same problem was solved with a graphic-analytic method based on the concept of energy height ($h_e = h + V^2/2g$).

In more recent times an indirect variational attack to the problem was attempted in references 5, 6, and 7. These approaches, however, were limited to the form (3) of the integral written as

$$\int_{he_1}^{he_2} F(V, h_e)\, dh_e \tag{5}$$

following a transformation of coordinates from the (V, h) plane to the (V, h_e) plane. The solution consequently obtained is correct for the free boundary value problem (V_1, V_2 free) but incomplete for the fixed end-points problem (V_1, V_2 given) insofar as in general the boundary conditions are not satisfied. As a matter of fact, because of the formal independence of the integrand function of dV/dh_e, the order of the Euler equation associated with the integral (5) reduces to zero.

Scope of the Present Research

The object of the present note is twofold: (1) to prove that indirect variational methods may supply the complete solution of the problem and in particular justify the dive or zoom character of the end arcs of the optimum path and (2) to formulate the necessary conditions for the extremum in a more general way by lifting the restriction (3) used in all the previous papers. The equation of the motion on the normal to the flight path is consequently written in its exact form.

The main advantage of the present approach lies in the fact that it leads to continuous solutions while the results of all the previous theories indicated discontinuities in dV/dh at the points where the curve of equation $\omega = 0$ intersects the patterns of equation $\theta = \pm\pi/2$. Only the brachistocronic problem is here treated, the minimum fuel consumption problem being mathematically analogous.

Necessary Conditions for the Existence of the Extremum

The fundamental equations of the motion of the aircraft on the normal and on the tangent to the flight path are the following*[1]

$$G \equiv \Psi[1 + (VV'/g)] - [1/(V \sin\theta)] = 0 \tag{6}$$

$$L/W = \alpha + \beta(\cos\theta - 1) + \gamma(V^2/g)\theta' \sin\theta \tag{7}$$

where

$$\Psi = W/[V(T - D)] \tag{8}$$

The thrust T is assumed a function of the type $T = T(h, V)$. Because of the polar and the expressions of the aerodynamic forces, the drag may be conceived as a function $D = D(h, V, L)$ of altitude, velocity, and lift. The effects of the Mach and Reynolds Numbers on D are taken into consideration.

The time necessary to fly an aircraft from one altitude h_1 to another h_2 is given by

$$t = \int_{h_1}^{h_2} \frac{dh}{V \sin\theta} = \int_{h_1}^{h_2} \Psi\left(1 + \frac{VV'}{g}\right) dh \tag{9}$$

The value of the integral (9) is determined if two functions $V(h)$ and $\theta(h)$ are prescribed. These two functions, however, are not mutually independent, insofar as they must satisfy an equation of the type

$$G(h, V, V', \theta, \theta') = 0 \tag{10}$$

which results by introducing in the first member of Eq. (6) the expressions for $T = T(V, h)$, $D = D(V, h, L)$, and $L = L(V, \theta, \theta')$, the last one being supplied by Eq. (7). As occurs in many mechanical problems, Eq. (10) is a *nonintegrable* differential expression or *nonholonomic* condition. The use of Lagrange multipliers is therefore indispensable.[10]

The brachistocronic problem is now formulated† as follows: "to determine the two unknown functions $V(h)$ and $\theta(h)$ which make the integral (9) stationary and satisfy the subsidiary condition (10) at any point of the flight path."

If the first form of the integral (9) is used, the optimum path is to be found as the extremal of the integral

$$I = \int_{h_1}^{h_2} \left(\lambda G + \frac{1}{V \sin\theta}\right) dh = \int_{h_1}^{h_2} \left[\frac{1 - \lambda}{V \sin\theta} + \lambda\Psi\left(1 + \frac{VV'}{g}\right)\right] dh \tag{11}$$

where $\lambda = \lambda(h)$ is a variable Lagrange multiplier.

By varying V and θ, the following two Euler equations are derived.

$$V(\lambda\Psi)' + g[(1 - \lambda)/(V^2 \sin\theta)] - \lambda(g + VV')(\partial\Psi/\partial V) = 0 \tag{12}$$

$$(\gamma\lambda\Psi V^2 D_L)' + \{g[(1 - \lambda)/V](\cos\theta/\sin^2\theta)\} + \lambda\Psi D_L(\beta g - \gamma V^2\theta' \cot\theta) = 0 \tag{13}$$

An inspection of Eqs. (10), (12), and (13) shows that this differential system is of order four. As a consequence four boundary conditions may be imposed. For instance, the values of the velocity (V_1, V_2) and of the path inclination (θ_1, θ_2) may be prescribed at the altitudes h_1 and h_2 if the variational problem is of fixed end-points type.

* The coefficients α, β, and γ are introduced in order to simplify the derivation of the solution under particular approximations. The general case is represented by $\alpha = \beta = \gamma = 1$.

† It is immaterial to use the first or the second form of the integral (9) in the solution of the minimal problem. The Lagrange multipliers corresponding to each of these two possibilities differ by a numerical constant only.

Integration of Euler's Equations

The integration of the differential system constituted by Eqs. (10), (12), and (13) is to be performed by approximate methods in the most general case.

Under particular circumstances, however, the problem may be simplified.

Required Lift Independent of Path Inclination and Curvature

For this case ($\alpha = 1, \beta \to 0, \gamma \to 0, L \to W$), Eq. (13) reduces to

$$(1 - \lambda) \cos\theta/\sin^2\theta = 0 \tag{14}$$

which means that the optimum path is composed of arcs of equation $\cos\theta = 0$ ($\theta = \pm\pi/2$) and arcs of equation $\lambda = 1$.

It is to be noted that for $\lambda = 1$ Eq. (12) yields

$$(\partial\Psi/\partial V) - [(V/g)(\partial\Psi/\partial h)] = 0 \tag{15}$$

In this way the results of references 1, 2, and 3 are found again by means of the indirect methods of the Calculus of Variation. It is to be noted that the assumption $L = W$ has changed the analytical nature of the problem insofar as only two boundary conditions may now be imposed to the flight path—i.e., the values of the velocity (V_1, V_2) at the altitudes h_1 and h_2 in the case of a fixed end-points problem.

Negligible Induced Drag

For $\alpha \to 0, \beta \to 0, \gamma \to 0, L \to 0$, Eqs. (14) and (15) are still formally true, with the additional simplification that the D function to be introduced in the expression for Ψ is the zero-lift drag of the aircraft. This case may be of some interest for turbojet powered aircraft at low tropospheric altitudes.

References

[1] Miele, A., *Problemi di Minimo Tempo nel Volo Non-Stazionario degli Aeroplani*, Atti della Accademia delle Scienze di Torino, Classe di Scienze Matematiche, Fisiche e Naturali, Vol. 85, pp. 41–52, 1950–1951.

[2] Lush, K. J., *A Review of the Problem of Choosing a Climb Technique with Proposals for a New Climb Technique for High Performance Aircraft*, Aeronautical Research Council, R.M. 2557, 1951.

[3] Miele, A., *Soluzioni Generali di Problemi di Ottimo in Volo Non-Stazionario*, L'Aerotecnica, Vol. 32, No. 3, pp. 135–142, 1952.

[4] Miele, A., *Traiettorie Ottime di Volo degli Aeroplani Azionati da Turboreattori*, L'Aerotecnica, Vol. 32, No. 4, pp. 206–219, 1952.

[5] Kelly, L., *Optimum Climb Technique for a Jet-Propelled Aircraft*, The College of Aeronautics, Cranfield, Report No. 57, April, 1952.

[6] Rutowski, E. S., *Energy Approach to the General Aircraft Performance Problem*, Journal of the Aeronautical Sciences, Vol. 21, No. 3, pp. 187–195, March, 1954.

[7] Garbell, M. A., *Optimum Climbing Techniques for High-Performance Aircraft*, Garbell Aeronautical Series, No. 8, 1953.

[8] Miele, A., *On the Nonsteady Climb of Turbojet Aircraft*, Journal of the Aeronautical Sciences, Vol. 21, No. 11, pp. 781–783, November, 1954.

[9] Kaiser, X. X., *The Climb of Jet-Propelled Aircraft. Part I—Speed Along the Path in Optimum Climb*, Ministry of Supply, RTP/TIB Translation GDC/15/148T, April, 1944.

[10] Courant, R., and Hilbert, D., *Methods of Mathematical Physics*, Vol. I, Interscience Publishers, Inc., New York, 1953.

[11] Cicala, P., and Miele, A., *Evoluzioni Brachistocrone di un Aereo*, Atti della Academia delle Scienze di Torino, Classe di Scienze Mathematiche, Fisiche e Naturali (in publication).